Mechanisms Controlling Kv Channel Surface Density in Cardiac Myocytes

by

Sarah Marie Schumacher

A dissertation submitted in partial fulfillment
of the requirements for the degree of
Doctor of Philosophy
(Pharmacology)
in The University of Michigan
2011

Doctoral Committee:

Associate Professor Jeffrey Randall Martens, Chair
Professor Ronald W. Holz
Professor José Jalife
Professor Benedict R. Lucchesi
Associate Professor Anatoli N. Lopatin

To my family

ACKNOWLEDGEMENTS

I would like to first extend my sincerest gratitude to my research mentor, Dr. Jeffrey R. Martens. The time I have spent in his laboratory has shaped me both professionally and personally. His drive and dedication to science serves as a model that I strive towards every day. The past few years have been extremely rewarding for me due to his patience, continual mentoring, and devotion to my professional development. I would not be where I am today without his guidance.

I would also like to acknowledge my thesis committee members, Dr. Ronald Holz, Dr. Jose Jalife, Dr. Benedict Lucchesi, and Dr. Anatoli Lopatin. I have been extremely lucky to have a committee that not only acted as thesis advisors, but also as collaborators and mentors.

I would like to thank the numerous members of the Martens laboratory, present and former. Particularly, I would like to thank Kristin Arendt, Paul Jenkins, Dyke McEwen, Jeremy McIntyre, Katherine Ryland, Laurie Svoboda, Kristin van Genderen, Eileen Vesely, Liz Williams, and Lian Zhang. Your guidance, mentorship, research assistance, feedback, and friendship have left me with many good memories.

Special thanks to the collaborators I have worked with in my time spent in graduate school: the José Jalife laboratory, including Michelle Milstein, Luqia Hou, Aneeqa Ahmad, Guadalupe Guerrero-Serna, and Viviana Zlochiver for advice and technical support. I would also like to acknowledge my funding from the Molecular and

Integrative Physiology Training Program, Inaugural Cardiovascular Predoctoral Fellowship, and Pharmaceutical Manufacturers Association (PhRMA) Predoctoral Fellowship in Pharmacology and Toxicology.

I would like to show appreciation to my parents, Gary and Lynn, as well as my sister Lara, for their love and support through the years. I would also like to show appreciation to my in-laws Stephen, Sandy, and Michelle for their support. I would also like to thank all of my friends for their encouragement over the years. Finally I would like to thank my husband, Michael for his patience, encouragement, and devotion. Your love and unconditional support have been so important to me throughout graduate school. I could not have done it without you. Thank you all so much.

TABLE OF CONTENTS

LIST OF FIGURES

CHAPTER 1

ION CHANNEL TRAFFICKING: A NEW THERAPEUTIC HORIZON FOR ATRIAL FIBRILLATION

PREVALENCE AND TREATMENT OF ATRIAL FIBRILLATION

Atrial fibrillation (AF) is the most common sustained cardiac arrhythmia affecting an estimated 2.2 million adults in the in the United States.[1] AF is caused by the rapid and irregular activation of the atria by electrical sources outside the normal sinus node, and can be classified as paroxysmal, persistent, or long-standing persistent.[2] The occurrence of atrial fibrillation increases dramatically with age, affecting less than 1% of individuals under age 50 to approximately 10% of individuals over age 80.[1, 3] Importantly, over the past two decades the age standardized death rate (per 100,000 in the US) has increased from 27.6 to 69.8.[4] Therefore, AF presents a significant increasing health risk with an untold burden for healthcare costs.

The combination of inefficient atrial contraction and irregular ventricular rate can lead to serious complications. AF related deaths are due primarily to the increased risk of stroke and heart failure. AF is associated with a nearly 5-fold increase in the risk of embolic stroke with nearly one fourth of all strokes in patients over 80 attributable to AF.[5, 6] This

---

Part of Chapter 1 is published as **Schumacher SM**, **Martens JR**. (2010). Ion channel trafficking: a new therapeutic horizon for atrial fibrillation. Heart Rhythm. Sep;7(9):1309-15. For copyright release, please see Appendix I.

increased rate of stroke is due to the rapid, uncoordinated atrial rhythm that leads to inefficient contraction of the atria, resulting in the pooling of blood in the atria and promotion of thrombo-emboli formation. The presence or absence of several other risk factors significantly contributes to the risk of stroke, such as recent cardiac failure, hypertension, age, diabetes, or a history of stroke or transient ischemic attack (TIA).[7, 8] In addition to an increased risk of stroke, atrial thrombo-emboli can propagate to regions other than the brain, such as the kidneys, mesenteric circulation, or the heart itself where they may induce myocardial infarction. AF also participates reciprocally with several comorbid conditions including congestive heart failure, thyrotoxic heart disease, and hypertension.[9]

Current therapy for AF is aimed at rate control or rhythm control.[10] In rate control, the goal is to maintain the ventricular rate within a physiological range by slowing atrioventricular conduction. In rhythm control, treatment aims to restore normal sinus rhythm through pharmacological cardioversion or through electrical cardioversion or catheter ablation. Catheter ablation is considered a 2nd-line treatment for AF with published success rates of 22-85%. Higher success rates are often seen for patients with paroxysmal AF.[2, 11-13] While approximately half of these patients remain asymptomatic, nearly 30% require a second procedure and 10-25% require additional pharmacological therapy in order to maintain normal sinus rhythm post ablation therapy.[14, 15] However, the long-term effectiveness of this technique remains to be fully determined.[16, 9]

Pharmacological cardioversion makes use of antiarrhythmic drugs targeting cardiovascular ion channels to achieve normal sinus rhythm control in the treatment of AF.[17-20] Pharmacological cardioversion has an advantage over catheter ablation in that it

is not invasive, however it has been reported to be less effective.[21] If class I or III antiarrhythmic agents are administered within the first 24 hours of onset of AF, the reported success rate is 47-84%; however, this drops sharply for AF that persists longer than 48 hours in that the antiarrhythmic therapy can only achieve cardioversion in 15-30% of patients.[22]

COMPOSITION OF THE ATRIAL ACTION POTENTIAL

Atrial action potentials result from the coordinated opening and closing of voltage-gated ion channels in the myocyte membrane.[23, 24] The atrial action potential is initiated by rapid depolarization induced by a large inward sodium current I_{Na} through the cardiac-specific sodium channel Nav1.5.[23, 24] This influx of Na^+ constitutes phase 0 and depolarizes the cell from the threshold membrane potential of approximately -70mV to the area of +40mV. Partial repolarization is then mediated by the transient outward K^+ current I_{to}, mediated by a combination of Kv1.2, Kv4.2, and Kv4.3.[23, 24] Rapid inactivation of I_{to} and the activation of an inward L-type Ca^{2+} current I_{Ca}, produce the notch (phase 1) and plateau (phase 2) of the action potential. Time-dependent activation of a series of delayed rectifier currents, the ultra-rapid I_{Kur} (Kv1.5), the rapid I_{Kr} (Kv2.1 and Kv11.1, or hERG), and the slow I_{Ks} (Kv7.1 or KvLQT1) components, mediate cellular repolarization (phase 3).[23, 24] Hyperpolarization of atrial myocytes to the resting membrane potential of -90 mV is then achieved through the I_{K1} inward rectifier current (Kir2.x) and the muscarinic K^+ current I_{KACh} (Kir3.1/3.4) (phase 4).[23, 24] The atrial action potential is thus shaped by the ensemble average of these ion channels. The balance between inward and outward currents during the plateau and repolarization phase of the

atrial action potential determines the action potential duration (APD). APD is a measure of the time from depolarization to recovery of excitability and thereby determines both the effective refractory period (ERF) and susceptibility to reentry.

ELECTRICAL AND STRUCTURAL REMODELING DURING AF

Atrial fibrillation is a progressive disorder wherein the duration of the arrhythmia advances electrical and structural adaptations that further the susceptibility of the myocardium to re-entrant circuits. Electrical remodeling is evident from the decreased APD and depression of the plateau of the atrial action potential. During AF, atrial myocytes fire at a rate of 400-600 beats per minute (bpm), compared to the resting heart rate of 60 bpm or a rate of 180-200 bpm during peak exercise. Increased atrial rate leads to a negative metabolic balance, associated with decreased pH and Po_2 and increased oxidative stress. The α1c subunit of the L-type Ca^{2+} channel is reversibly inhibited by clinically relevant decreases in Po_2, therefore altered oxidative state contributes to the ~60-70% decrease in I_{Ca} observed within 24 hours of rapid atrial pacing and in permanent AF.[25] In addition to an altered oxidative state, increased atrial rate leads to elevated intracellular Ca^{2+} levels via entry through L-type calcium channels with each beat.[26] As an adaptive mechanism to decrease the threat to cell viability posed by Ca^{2+} loading, atrial myocytes inactivate L-type Ca^{2+} channels through voltage-dependent and Ca^{2+} concentration-dependent mechanisms.[27] Decreased I_{Ca}, which under normal conditions drives the positive plateau voltage and contributes to action potential duration, constitutes a portion of the electrical remodeling observed in AF. Electrical remodeling is also characterized by a 50-60% decrease in the I_{to} and I_{Kur} components of repolarization.[25]

Such a decrease would be expected to prolong atrial APD, however these alterations are countered by an increase in the outward K^+ currents I_{K1} and I_{KACh}.[25] The summation of these alterations in atrial currents produces the attenuated plateau phase and decreased APD that characterize electrical remodeling during AF.

Structural remodeling is first exhibited by the redistribution of heterochromatin in the nucleus to resemble the homogenous pattern characteristic of embryonic and neonatal myocytes.[28, 29] Subsequently, myolysis and glycogen deposition are evident in a population of atrial myocytes that are projected to undergo apoptosis.[30] While the mechanism of sarcomeric degradation has not been fully elucidated, attention has been drawn to the calpain class of calcium-activated neutral proteases. Calpain activation provides a link between the calcium overload induced by increased atrial rate and the molecular changes observed during AF. For instance, in a number of cases the decrease in atrial ionic current is accompanied by a decrease in channel protein, not mRNA.[30] The activity of calpain in the degradation of membrane-associated as well as cytoskeletal proteins would disrupt excitation-contraction coupling and may significantly underlie the mechanisms of electrical and structural remodeling in atrial myocytes. Effective block of pacing induced structural remodeling by calpain inhibitors gives further credence to this model.[31] Structural remodeling may also be the result of ischemic stress and stretch-induced adaptive and maladaptive processes in the atrial myocardium; however, these processes and the timeline of their involvement remain to be fully elucidated.

PHARMACOLOGICAL TREATMENT OF ATRIAL FIBRILLATION

Three main classes of antiarrhythmic drugs are indicated for the treatment of abnormal rhythms such as atrial fibrillation. Class Ia, b, and c compounds block the inward Na^+ current with intermediate, fast, and slow association and dissociation, respectively. These compounds, including quinidine, procainamide, disopyramide, flecainide, and propafenone among others are used in the prevention of paroxysmal atrial fibrillation. Class III compounds such as amiodarone, dronedarone, sotalol, ibutilide, dofetilide, and E-4031 are K^+ channel blockers important for rhythm control in the treatment of AF. Class IV Ca^{2+} channel blockers verapamil and diltiazem are used to prevent recurrence of paroxysmal AF and attain ventricular rate control. Despite the existence of multiple antiarrhythmic drugs with varying targets for the treatment of AF, there is currently no drug in clinical use that does not exhibit significant negative side effects. While many of these side effects are linked to non-selective block of Kv channels in the atrium and ventricles, others, such as amiodarone, cause hepatotoxicity, peripheral neuropathy, and pulmonary toxicity, among others.[32, 33] Several compounds, including quinidine and flecainide, are no longer used in the clinic due to the increased risk for torsade de pointes associated with long-term treatment with these compounds.[18, 32] Class III antiarrhythmic compounds that block atrial potassium channels also exhibit an increased risk for pro-arrhythmia in the ventricles upon prolonged exposure of higher doses.[19, 32] Therefore, a common negative side effect for antiarrhythmic drug therapy is proarrhythmia in the ventricles due to non-selective ion channel block and/or overlapping expression of ion channels in both the atria and ventricles.

Recently, there has been a shift in both academia and industry to target atrial specific currents in order to terminate AF and maintain normal sinus rhythm while avoiding proarrhythmic risk in the ventricles. One of the main targets in this research effort is the voltage-gated potassium channel Kv1.5 that underlies the I_{Kur} current. Importantly, I_{Kur} is selectively reported only in the human atria[17, 20, 34, 35] where it contributes to repolarization and participates in the control of action potential duration. In the human atria, Kv1.5 is a predominant channel mediating repolarization and alterations in its expression level have been demonstrated in pathophysiological states such as persistent and paroxysmal AF and chronic pulmonary arterial hypertension.[17, 36] More specifically, there is a marked reduction in Kv1.5 channel protein expression in these pathophysiological states,[37,38, 39] perhaps as an endogenous compensatory mechanism. Given the atrial specific expression of Kv1.5 and its known alterations in cardiovascular disease, it is no surprise that the development of Kv1.5-specific blockers has been a target of both academic and industrial research efforts for the treatment of AF.[32, 40, 41] While several compounds have been developed, these antiarrhythmic drugs have been limited by a lack of channel or tissue selectivity, or by poor bioavailability.

Over the past fifteen years research in both industry and academia has focused on developing small-molecule inhibitors of Kv1.5 for the treatment of AF. Three different mechanisms have been employed, including drugs for direct pore block of the channel, allosteric modulation, and use-dependent open channel block, resulting in numerous publications and patents.[32] Two compounds, AVE0118 and AVE1231, were bisaryls developed by Aventis Pharma/Sanofi-Aventis. While these compounds were not Kv1.5-specific, demonstrating inhibition of Kv1.5, Kv1.3, Kv2.1, and Kv4.3 with less

effectiveness for blocking hERG, they exhibited both atrial selectivity and efficacy and were developed for clinical trials.[23, 32, 42-44] The Kv1.5 selective blocker DPO-1, developed by Merck, increased atrial APD without altering ventricular function, but failed to demonstrate sufficient oral bioavailability.[32] The clinical development of several potent Kv1.5 blockers generated by Icagen was also plagued by poor bioavailability.[45] Cardiome/Astellas Pharma developed vernakalant hydrochloride (RSD1235) as a use-dependent blocker of Kv1.5; however, its clinical efficacy was hampered by a potent block of Nav1.5 at resting membrane potentials.[46-49] Therefore, there remains an unmet need for the development of safe new compounds with both atrial selectivity and clinical efficacy for the long-term treatment of AF.

New therapeutic strategies that focus on the regulation of ion channel surface density are emerging from basic research at the bench (Figures 1.1 and 1.2).[50, 51] Traditional antiarrhythmic drugs target the ion permeability of channels; however, as highlighted above this approach has not yet yielded a satisfactory outcome. There are two ways to decrease I_{Kur}, through a direct effect on the conductance properties (classically pore block) of channel subunits or through alterations in surface density of the protein. The concept of drugs modulating ion conductance and/or surface density of channels is not new. For example, the antiarrhythmic agents ketoconazole and fluoxetine have been shown to reduce hERG density by at least 50% following 48 hours of treatment,[52-55] whereas pentamidine and probucol reduce cell-surface hERG without affecting ion conductance.[55-58] Research into the therapeutic potential of antiarrhythmic drugs that alter channel trafficking has primarily focused on hERG. Alterations in hERG mediated I_{Kr}, whether drug-induced or a result of the over 200 naturally occurring

mutations of this channel, may induce or contribute to the development of long QT syndrome. In particular, long QT syndrome type II which results from retention of misfolded hERG in the quality control pathways of the ER.[59, 60] Nearly 70% of these mutant channels can be rescued to the plasma membrane by antiarrhythmic drugs such as E4031.[59, 61] These drugs likely act to stabilize misfolded protein through facilitation of quality control machinery in the ER such as Hsc70 and Hsp90 that have been shown to exist in a macromolecular complex with hERG and facilitate its maturation and export from the ER.[60, 62] Arsenic trioxide, on the other hand, interferes with the hERG-chaperone complexes thereby decreasing surface channel.[63] Thus far research has focused primarily on hERG folding and maturation with little investigation into the molecular mechanisms regulating anterograde trafficking from the ER to the plasma membrane. In addition to interfering with hERG trafficking through inhibition of hERG-chaperon complexes, arsenic trioxide has been demonstrated to increase cardiac calcium currents and $I_{K\text{-}ATP}$ via different cellular processes.[63, 64] Researchers have also discovered that oxidative stress decreases forward connexin trafficking by disrupting microtubule association of EB1.[65] Together, these studies give credence to the idea that antiarrhythmic drugs may be developed to manipulate specific ion channel trafficking pathways as a novel therapeutic approach for treating cardiac arrhythmias.

GENERAL TRAFFICKING MECHANISMS

The steady-state cell surface density of proteins is determined by the balance between the anterograde and retrograde trafficking pathways. Anterograde trafficking ensues only after proper synthesis and processing in the endoplasmic reticulum and golgi,

including quality control mechanisms, glycosylation, and post-translation modification (Figure 1.1).[66] Retrograde movement initiates with endocytosis after which internalized proteins can follow multiple routes to different intracellular fates (Figure 1.1).[67] One well-recognized fate is the targeting of internalized proteins to lysosomes or proteasomes followed by degradation (Figure 1.1). Alternatively, trafficking through recycling endosomes allows proteins to return to the plasma membrane and protects them from degradation (Figure 1.1).[68] Sorting at early endosomes to Rab-GTPase specific compartments is now established as an important event determining the intracellular fate of internalized proteins.[69-71] Another important component of the endocytic machinery regulating protein surface levels is the coordinated movement of molecular motors. In general, protein trafficking is highly coordinated between long-range events, involving the microtubule-based kinesin and dynein motors, and short-range events using unconventional myosin motors.[72-75] There is a significant and growing body of literature about ion channel trafficking from synthesis to sorting to degradation in multiple tissues and cells systems that has been reviewed previously.[76-80] Our discussion will center mainly on recent work focused on the acute modulation of ion channel density at the plasma membrane in the heart where relatively little is known about protein trafficking.

KV1.5 CHANNEL TRAFFICKING IN ATRIAL MYOCYTES

While the precise mechanisms regulating plasma membrane localization and targeting of Kv1.5 in atrial myocytes have not been fully elucidated, several key components and steps are now known. The formation of functional Kv1.5 begins in the endoplasmic reticulum (ER) where tertiary folding is coupled to formation of the

quaternary structure through tetramerization of the T1 domain in the amino terminus of this channel.[81] The first transmembrane segment (S1) of Kv1.5 has also been implicated in the co-assembly of homo- and heterotetrameric K^+ channels.[82] ER to Golgi trafficking of Kv1.5 is facilitated by a "VXXSN" forward trafficking signal located in the C-terminus of the channel.[83, 84] In addition to forward trafficking signals, ER to Golgi trafficking of many Kv channels is dependent upon interactions with accessory subunits such as the KvBeta subunits, K^+ channel associated protein KChAP, and the K^+ channel interacting protein KChIP.[76] Despite interaction with the N-terminus of Kv1.5, KChAP does not alter the current properties or current density of the channel and therefore is not necessary for plasma membrane trafficking.[85]

In addition to protein folding/assembly and subunit composition, post-translational modification can play a crucial role in determining the plasma membrane levels of functional Kv1.5.[86-95] Kv1.5 contains putative PKC and PKA phosphorylation sites; however, direct PKC- or PKA-mediated phosphorylation of channel has not been demonstrated. Association of Src tyrosine kinase with two, repeated Src homology 3 (SH3) domains in the N-terminus of Kv1.5 leads to direct phosphorylation the channel and a significant decrease in current density.[96] N-linked glycosylation of human Kv1.5 at serine 292 is important for determining the voltage-dependence of activation and current density of the channel.[97, 98] In addition to phosphorylation and glycosylation, Kv1.5 has been shown to undergo S-acylation.[87] S-acylation occurs via the reversible linkage of fatty acids to target proteins through a thioester bond to a cysteine residue. Kv1.5 contains two N- and four C-terminal cysteine residues that can undergo S-acylation, and pharmacological inhibition of this modification results in the intracellular accumulation

and proteasomal degradation of Kv1.5.[87] As S-acylation was found to occur prior to glycosylation in the biosynthetic pathway of Kv1.5, and pharmacological intervention led to a significant decrease in current density, this post-translational modification may play an important role in the cell surface trafficking of properly assembled Kv1.5.[87]

At the plasma membrane, localization to specific membrane microdomains and association with scaffolding proteins into macromolecular signaling complexes may contribute to the stability and biological function of Kv1.5.[98-104] Golgi to plasma membrane trafficking of Kv1.5 involves targeting to calveolar-lipid raft membrane microdomains.[102] Disruption of lipid rafts through depletion of their component cholesterol and sphingolipids alters the biophysical properties of the channel. While the Kv4.2 subunit that is not targeted to lipid raft microdomains was unaltered, depletion led to a hyperpolarizing shift in both the voltage dependence of activation and inactivation of Kv1.5.[105] Targeting of Kv1.5 to lipid rafts involves interactions with caveolin-1, as evidenced by the depolarizing shift in the voltage dependence of activation and inactivation observed upon its expression.[105] Cell surface levels of Kv1.5 are also determined through interaction with the PDZ domain-containing proteins SAP97, alpha-actinin-2, and PSD95.[98, 99, 101, 104, 106-109] SAP97, a membrane associated guanylate kinase (MAGUK), is localized in lipid rafts and contains numerous protein interaction motifs including SHK and guanylate kinase (GUK)-like domains that may serve as nucleation sites for the formation of macromolecular signaling complexes for the regulation of Kv1.5.[98] PSD95, which associates with Kv1.5 via a T1/core region of the channel, may also play a critical role in the localization of Kv1.5 to specific membrane microdomains as evidenced by its role in the clustering of the NMDA receptor and Kv1.4 in neurons.[109]

Alpha-actinin-2, a member of the spectrin gene superfamily, also interacts with Kv1.5 through the T1/core region of the channel and direct knockdown of alpha-actinin-2 via antisense oligonucleotides alters channel current density.[94, 103, 110]

Despite association with scaffolding proteins, Kv1.5 has been shown to undergo dynamic trafficking at the plasma membrane through constitutive internalization and recycling.[111] Internalization of Kv1.5 occurs via a dynein-mediated, microtubule dependent pathway to perinuclear endosomal compartments with a t1/2 of approximately 11 minutes at physiological temperature.[111, 112] Following internalization, sorting of Kv1.5 into specific, rab-dependent endocytic compartments determines the intracellular fate of the channel. Specifically, association of Kv1.5 with Rab 4- or Rab 11-containing endocytic vesicles is associated with recycling of the channel back to the plasma membrane, whereas association with Rab 7-containing vesicles denotes channel degradation.[111-113] In addition, ubiquitin modification of Kv1.5 has been described in agreement with data implicating the proteasome in channel degradation.[50, 87, 114-116] As the molecular machinery and endogenous regulatory mechanisms controlling Kv1.5 surface density begin to emerge, one new therapeutic horizon is the extrinsic manipulation of Kv1.5 surface levels (Figure 1.2).

SUMMARY

Atrial fibrillation (AF) is a common cardiac arrhythmia with potentially life-threatening complications. Drug therapies for treatment of AF that seek long-term maintenance of normal sinus rhythm remain elusive due in large part to proarrhythmic ventricular actions. Kv1.5, which underlies the atrial specific I_{Kur} current, is a major

focus of research efforts seeking new therapeutic strategies and targets. Difficulty in attaining clinical efficacy and safety through atrial selective block and increasing evidence of pleiotropic effects of pharmacological agents has led to the emergence of channel trafficking as a novel therapeutic target for the treatment of AF. The underlying mechanism of these pleiotropic effects and the molecular machinery and endogenous regulatory mechanisms selectively controlling Kv1.5 surface density must be elucidated to determine the therapeutic potential of extrinsic manipulation of Kv1.5 surface levels.

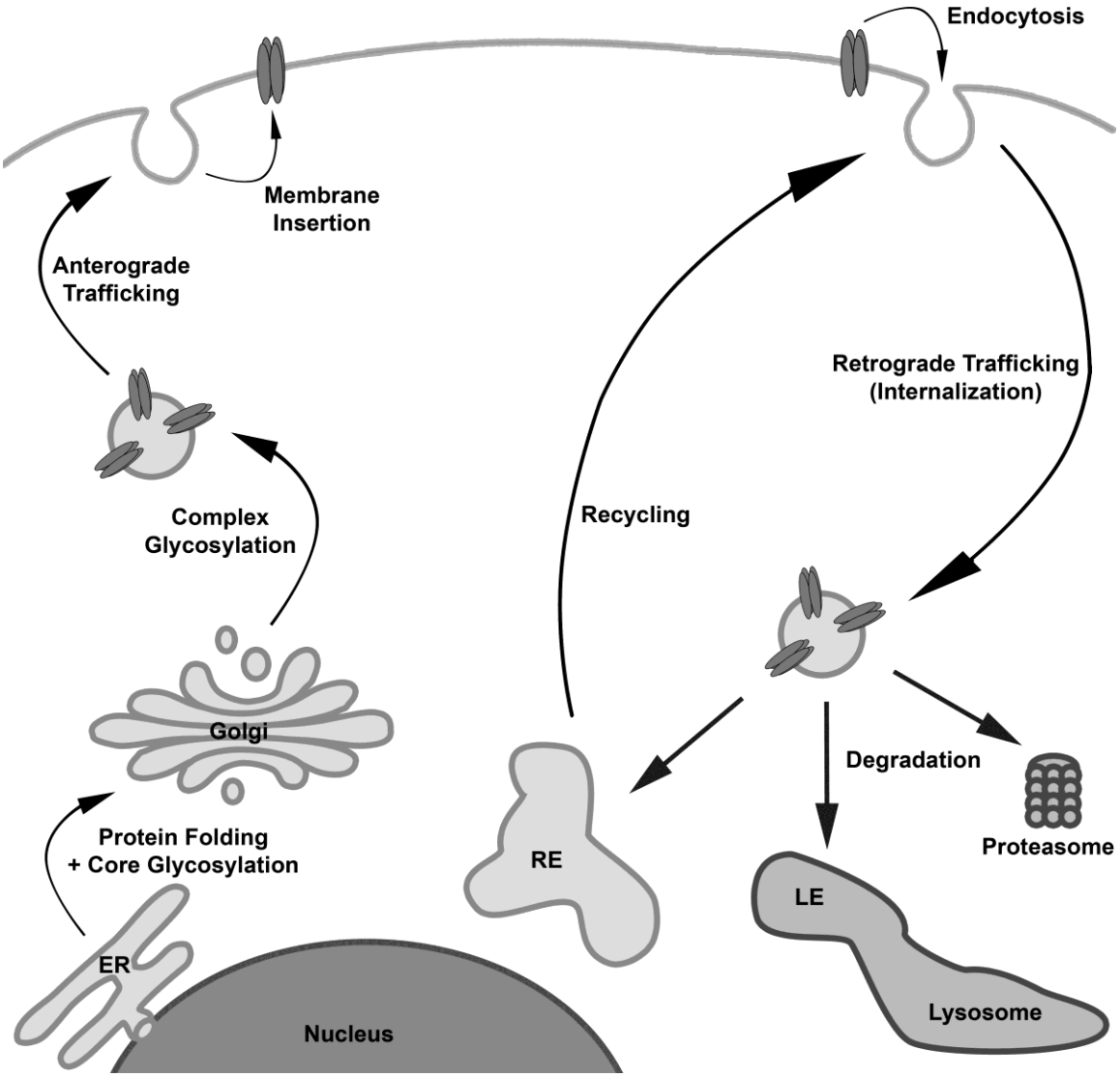

Figure 1.1 Potential therapeutic intervention points in the trafficking of membrane.

Each arrow represents a regulatory step in the trafficking of membrane proteins that could serve as a potential therapeutic target for modulating steady-state cells surface levels of ion channels. The left half of this figure represents an area where much work has been done in the hERG field for the treatment of LQTS and other arrhythmias. The right half represents and exciting developing field for the regulation of Kv1.5 membrane levels in the treatment of atrial fibrillation. Endoplasmic Reticulum (ER); Recycling Endosome (RE); Late Endosome (LE).

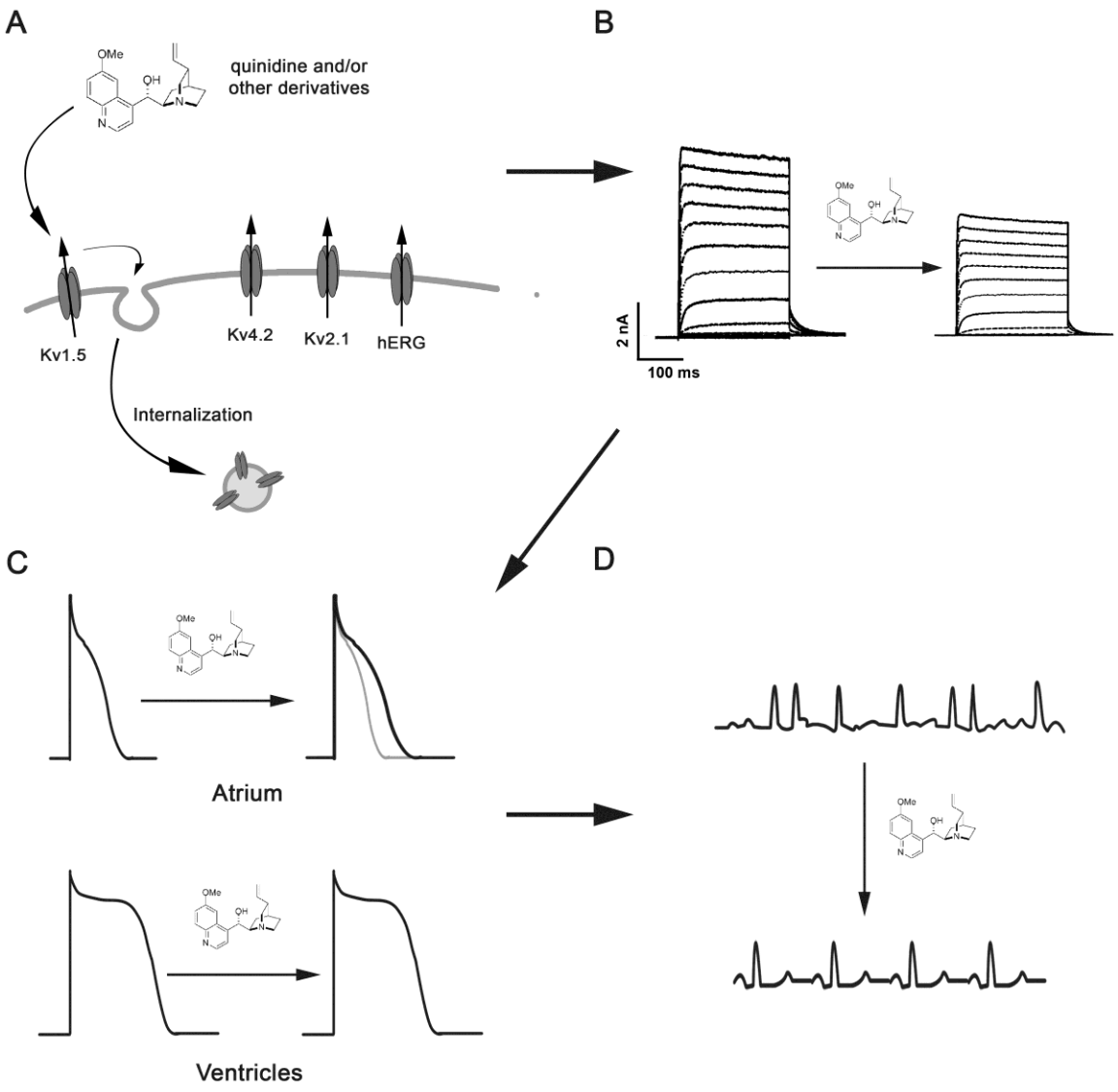

Figure 1.2 Antiarrhythmic drug-induced internalization of atrial specific Kv1.5 as a novel therapeutic target for AF.

(A) Drug-induced internalization is specific to the atrial potassium channel Kv1.5. **(B)** Kv1.5 specific internalization results in a decrease in I_{Kur} density. **(C)** Decreased I_{Kur} may result in an increase in atrial, not ventricular, action potential duration. **(D)** Increased atrial action potential duration may terminate atrial fibrillation and restore normal sinus node rhythm control.

CHAPTER 2

ANTIARRHYTHMIC DRUG-INDUCED INTERNALIZATION OF THE ATRIAL SPECIFIC K+ CHANNEL, KV1.5

ABSTRACT

Conventional antiarrhythmic drugs target the ion permeability of channels, but increasing evidence suggests that functional ion channel density can also be modified pharmacologically. Kv1.5 mediates the ultrarapid potassium current (I_{Kur}) that controls atrial action potential duration. Given the atrial specific expression of Kv1.5 and its alterations in human atrial fibrillation, significant effort has been made to identify novel channel blockers. In this study, treatment of HL-1 atrial myocytes expressing Kv1.5-GFP with the class I antiarrhythmic agent quinidine, resulted in a dose-, and temperature-dependent internalization of Kv1.5, concomitant with channel block. This quinidine-induced channel internalization was confirmed in acutely dissociated neonatal myocytes. Channel internalization was subunit-dependent, activity-independent, stereospecific, and blocked by pharmacologic disruption of the endocytic machinery. Pore block and channel internalization partially overlap in the structural requirements for drug binding.

Chapter 2 is published as **Schumacher SM**, McEwen DP, Zhang L, Arendt KL, Van Genderen KM, **Martens JR**. (2009). Antiarrhythmic drug-induced internalization of the atrial-specific k+ channel kv1.5. Circ Res. Jun 19;104(12):1390-8. For copyright release, please see Appendix I.

Surprisingly, quinidine-induced endocytosis was calcium-dependent and therefore unrecognized by previous biophysical studies focused on isolating channel-drug interactions. Importantly, while acute quinidine-induced internalization was reversible, chronic treatment led to channel degradation. Together, these data reveal a novel mechanism of antiarrhythmic drug action and highlight the possibility for new agents that selectively modulate the stability of channel protein in the membrane as an approach for treating cardiac arrhythmias.

INTRODUCTION

Atrial fibrillation (AF) is the most common cardiac arrhythmia, and a major risk factor for increased stroke, heart failure, and cardiovascular morbidity. The preferred therapy for AF is sustained sinus rhythm control; however, the efficacy of currently-used antiarrhythmic drugs is diminished by adverse side effects resulting from a lack of ion channel selectivity and nonspecific ventricular activity [117, 118]. Due to the frequency of AF and its associated morbidity, development of atrial-specific therapies is a major focus of both industrial and academic research efforts [40, 41].

Kv1.5 (KCNA5) has emerged as a promising pharmacologic target for treatment of AF. In humans, Kv1.5 is selectively expressed in atrial myocytes where it mediates the ultrarapid delayed rectifier current (I_{Kur}) that contributes to cellular repolarization and controls action potential (AP) duration [67, 119]. Although significant effort has been made to identify novel blockers of Kv1.5, compounds with both atrial selectivity and clinical efficacy remain elusive and highlight the need for new potential therapeutic strategies or targets.

Conventional antiarrhythmic drugs generally target the ion permeability of channels. Increasing evidence, however, suggests that functional ion channel density can be modified pharmacologically in that a drug may both directly block an ion channel and indirectly disrupt normal protein trafficking [51]. In fact, one report shows that nearly half of hERG channel pore-blockers tested also decrease anterograde delivery of the channel to the cell surface [120]. In addition, two reported cases of disrupted protein trafficking leading to drug-induced prolongation of the cardiac AP highlight that this pleiotropic drug action can modulate cardiac excitability [63, 64]. Research into the therapeutic value for antiarrhythmic agents that affect channel trafficking has focused almost exclusively on hERG channel blockers that stabilize misfolded channels and rescue hERG trafficking mutants. To date, no studies have addressed the potential properties of antiarrhythmic drugs to acutely modulate surface density of functional channels that exist on the cardiac myocyte membrane. Here we report, for the first time, a novel paradigm for antiarrhythmic pharmacology in the control of the cell surface stability of Kv1.5 in atrial myocytes and present a new mechanism for the inhibition of ion current through drug-stimulated endocytosis of channel protein.

RESULTS

The Antiarrhythmic Drug, Quinidine, Stimulates Rapid Kv1.5 Internalization in HL-1 Atrial Myocytes.

Multiple antiarrhythmic drugs have been shown to inhibit Kv1.5, including the class I antiarrhythmic drug quinidine, which, like many Kv channel inhibitors, causes an activity-dependent, open-channel block of Kv1.5 (Figure 2.2A). The present study was

designed to investigate the potential pleiotropic effects of antiarrhythmic agents on Kv1.5 using this well characterized drug as a prototype [121]. Our studies were initiated in the HL-1 immortalized mouse atrial myocyte cell line in which we previously demonstrated that Kv1.5 undergoes constitutive internalization and recycling to maintain steady-state ion channel surface levels [111]. Using an extracellular GFP epitope-tagged Kv1.5 construct that mimicked wild type channel function, we discovered that quinidine triggered Kv1.5 internalization concomitant with block of channel current (Figure 2.1A, Figure 2.2). Exposure to increasing concentrations of quinidine stimulated a dose-dependent increase in internalized Kv1.5 with a corresponding loss of surface protein (Figure 2.1B). This quinidine-induced internalization culminated in an 80 ± 13% ($n = 143$; $p < 0.001$) increase over constitutive channel endocytosis at 100 μmol/L quinidine ($EC_{50} \approx 1$ μmol/L). Quinidine-induced internalization of Kv1.5 was rapid and achieved a maximum within 10 min of treatment (Figure 2.2E). Electrophysiology experiments confirmed that 10 min quinidine treatment represents steady-state channel block (Figure 2.2D). Together, these data indicate that the rate-limiting step for this process is equilibration of quinidine across the cell membrane. Following 10 min vehicle treatment, the level of internalized Kv1.5 is minimal and consistent with constitutive endocytosis as previously reported[111] (Figure 2.1A). Importantly, at the 10 min time point quinidine-stimulated internalization was statistically greater compared to control ($p < 0.001$) and could be reliably separated from constitutive endocytosis and was therefore used, unless otherwise stated, in our later studies.

We also measured a temperature-dependence for the quinidine-induced internalization of Kv1.5 (Figure 2.1C). The drug-induced internalization was greater than

two-fold higher at the physiological temperature of 37˚C compared to room temperature (80 ± 13% (n = 143) at 37˚C versus 45 ± 11% (n = 130) at 25˚C; $p < 0.001$). Importantly, the EC_{50} values were identical and only the extent of quinidine-induced internalization was temperature-dependent. It is noteworthy, that previous biophysical studies measuring pore-block with quinidine were performed at room temperature where the effects of internalization would be inadvertently reduced.

One potential concern regarding our internalization assay is that the treatment with primary antibody prior to initiating internalization could cause an antibody-induced artifact. To negate this possibility we generated a Kv1.5 construct in which GFP was replaced with pHluorin, a GFP variant whose fluorescent properties are sensitive to the pH of the immediate environment [122]. Internalization of cell surface channel to endosomes with acidic pH quenches the pHluorin signal as measured by reduced fluorescence. Internalized channel was protected from photobleach and its perinuclear localization revealed by neutralization with ammonium chloride (Figure 2.3B). Using live-cell imaging of HL-1 cells expressing Kv1.5-pHluorin, we found no difference in the time course, extent, or subcellular localization of quinidine-induced internalized channel compared to results from our antibody-labeling internalization assay (Figure 2.3A). Together, these results suggest that antiarrhythmic drugs may modulate retrograde trafficking of Kv1.5 as a mechanism contributing to their inhibition of outward K^+ current.

Constitutive and Quinidine-induced Internalization of Kv1.5 is Conserved in Native Dissociated Mouse Myocytes.

We investigated the validity of the quinidine effect in native dissociated mouse myocytes. The live-cell internalization assay was performed on acutely dissociated neonatal mouse myocytes expressing Kv1.5-GFP to probe for alterations in Kv1.5 distribution upon quinidine treatment. Using this technique, we found levels of constitutive and quinidine-induced channel internalization similar to those observed in the HL-1 model (Figure 2.4A). This drug-induced internalization culminated in an 84 ± 19% ($n = 45$) ($p < 0.001$) increase over constitutive channel endocytosis at 100 μmol/L quinidine ($n = 52$), with a corresponding decrease in surface levels (Figure 2.4B). These data confirm that the endogenous machinery and mechanistic requirements for constitutive and quinidine-induced Kv1.5 internalization are conserved in native cardiac tissue.

Specificity of Quinidine-induced Internalization.

We investigated the subunit specificity by measuring quinidine effects on internalization of two other prominent cardiovascular potassium channels, Kv4.2 and Kv2.1, expressed in HL-1 cells. Although ion permeability of both channels is blocked by quinidine (IC_{50} of 10 μmol/L and 20 μmol/L quinidine, respectively) [123, 124], neither Kv4.2 nor Kv2.1 internalized in response to any drug concentration tested over the time course studied (Figure 2.5A, Figure 2.6 and 2.7). Despite differences in surface levels of channel, the surface to total protein ratio for each subunit did not differ from Kv1.5 (Figure 2.6A and 2.7B), indicating that the absence of quinidine-induced internalization is not due to a lack of surface channel. In addition, Kv4.2 was found to undergo constitutive endocytosis

similar to Kv1.5 (Figure 2.6B), indicating that detection of internalized channels is not problematic at the low expression levels observed with Kv4.2 and that the lack of quinidine-induced internalization is not due to an inability of the channel to access the endocytic pathway. Interestingly, we observed that Kv2.1 was sequestered in plaque-like clusters in agreement with previous reports in native atrial, but not ventricular, myocytes [125]. This finding further validates that the molecular machinery for channel localization is intact in the HL-1 atrial myocyte model (Figure 2.7A). Together, these data demonstrate a subunit-dependence for the quinidine-induced internalization of Kv1.5.

Quinidine-induced internalization occurred at resting membrane potentials suggesting that the drug-induced trafficking effects may be conductance-independent. To address this possibility, we measured internalization of the pore-dead mutant Kv1.5-W472F, which efficiently traffics to the myocyte membrane but is incapable of conducting current [126]. For both the mutant and wild-type controls, the quinidine-induced internalization resulted in an approximately 90 ± 20% ($n = 90$) ($p < 0.001$) increase over constitutive endocytosis, with no difference observed in the EC_{50} value (Figure 2.5B). These data confirm that the quinidine-induced internalization of Kv1.5 is independent of channel ion conductance.

Structural Requirements of Quinidine-induced Internalization.

To further examine specificity and gain possible insight into the pharmacophore responsible for drug-induced internalization of Kv1.5, we tested quinine, the diastereomer of quinidine that also causes a dose-dependent block of Kv1.5 current [127, 128]. We found that, contrary to quinidine, a maximal concentration of quinine was not

able to enhance Kv1.5 internalization above constitutive levels (Figure 2.5C). Quinine was, however, capable of inducing significant, dose-dependent block of Kv1.5 that was reversible upon drug washout (Figure 2.8). The inability of quinine to induce channel internalization, despite effective pore block, demonstrates that quinidine-induced internalization of Kv1.5 is stereospecific.

The subunit-dependence and stereospecificity of quinidine-induced internalization of Kv1.5 indicates a reliance of this internalization on the structure of the channel. To determine whether the protein structural requirements for quinidine-induced internalization were the same as those for pore block, we used the live-cell internalization assay to investigate the effect of quinidine on several mutants of Kv1.5. Kv1.5-T480A contains a single point mutation in the putative binding site for quinidine, resulting in a greater than 90% reduction in sensitivity to open-channel blockers of Kv1.5 [42, 129]. We found that, as with pore block, quinidine-induced internalization was abolished with the T480A mutation (Figure 2.9A). To further probe the amino acid requirements, we expanded our alanine-scanning mutagenesis to include three additional amino acid residues (Ile-508, Leu-510, and Val-512) which are considered part of the highly conserved antiarrhythmic drug binding site within Kv channels [42, 129]. We found that as reported for channel block, quinidine-induced internalization was abolished by the Kv1.5-I508A mutation. Surprisingly, however, unlike channel block, internalization was near wild-type for both Kv1.5-L510A and Kv1.5-V512A (Figure 2.9B). Additionally, we tested Kv1.5-P532L, a naturally occurring mutation reported to cause a significant rightward shift in the dose response curve for quinidine block of channel current [130]. We observed a similar decrease in sensitivity to quinidine-induced channel internalization

with a shift in the EC_{50} from approximately 1 μmol/L for wild-type channel to 104 μmol/L for Kv1.5-P532L ($n \geq 90$) (Figure 2.9C). These data show that quinidine is acting directly on the channel and not through off-target effects that may influence trafficking. Importantly, these data also indicate that antiarrhythmic drugs may both block channel current and disrupt protein endocytosis concurrently to alter the functional ion channel density in the cell membrane and that these two effects share partial overlap in the structural requirements for drug binding, but the necessary amino acids are not identical.

Channel Internalization is Prevented by Disruption of Endocytic Machinery.

Our previous studies demonstrated that constitutive Kv1.5 internalization occurs via a microtubule-dependent, dynein-mediated endocytic pathway [111]. To further address specificity and determine if quinidine-induced internalization shares a similar mechanism, we used pharmacological and dominant-negative methods to disrupt the endocytic machinery prior to measuring quinidine-stimulated Kv1.5 internalization. Dynasore, a cell-permeant, potent small molecule inhibitor of dynamin, prevents the budding and pinching off of endocytic vesicles [131, 132], and has been used in neurons to block synaptic vesicle endocytosis [133]. Acute pretreatment with this pharmacologic inhibitor abolished quinidine-induced internalization of Kv1.5 in atrial myocytes (Figure 2.10A). We also observed a nearly 100% increase in surface levels of Kv1.5 over untreated controls indicating that Dynasore prevents constitutive endocytosis of the channel (Figure 2.10B, C). Another major component of the endocytic machinery is the microtubule-dependent retrograde motor complex consisting of dynein and dynactin

connected by the adaptor protein p50-dynamitin [134, 135]. Previously, we and others reported that overexpression of p50-dynamitin, which results in the uncoupling of the retrograde motor complex from its cargo to disrupt retrograde trafficking, blocked constitutive Kv1.5 endocytosis [111, 112]. In our current studies, we found that p50-dynamitin overexpression also blocked quinidine-induced internalization with a corresponding increase in surface levels similar to the inhibition measured with Dynasore (Figure 2.11). These data indicate that quinidine-induced internalization of Kv1.5 occurs via a microtubule-dependent, dynein-mediated pathway as previously demonstrated for constitutive endocytosis.

Quinidine-induced Internalization is Calcium-dependent.

To further investigate the mechanisms controlling quinidine-induced internalization, we tested the calcium dependence of this process. The biophysical properties of Kv1.5 pore-block by quinidine have been previously characterized [121, 128]. Our survey of the literature revealed that all of these electrophysiological studies included a calcium-chelating agent in the pipette solution to isolate the drug-channel interaction. Since several intracellular trafficking pathways are known to be calcium-dependent [136], inclusion of a calcium-chelating agent could inhibit the endogenous or drug-induced trafficking pathways. To investigate this possibility, we performed whole-cell patch-clamp recordings on cells stably expressing Kv1.5 both in the presence and absence of the calcium-chelating agent, BAPTA, in the pipette solution. In response to a single depolarizing pulse from -80mV to +60mV, perfusion of cells for 10 min with 6 μmol/L quinidine reduced the peak current and accelerated the time course of inactivation under both conditions. Surprisingly, however, exclusion of BAPTA resulted in a much larger

effect on peak current and revealed a significant calcium-dependent decrease. This decrease in Kv1.5 current in the absence of BAPTA was observed over a range of voltages (Figure 2.13). Further, in the absence of BAPTA in the pipette solution, the dose-response for quinidine was significantly leftward shifted with a 3-fold decrease in the IC_{50} (IC_{50} = 13 μmol/L + BAPTA and 3.5 μmol/L – BAPTA) (n = 5) (Figure 2.12B). Conversely, this calcium-dependent decrease in current density did not occur with 20 μmol/L quinine, the diastereomer of quinidine (Figure 2.14). This is in agreement with our finding that quinine did not induce channel internalization. Together, these data provide functional evidence for quinidine-induced channel internalization through a calcium-dependent mechanism.

To determine if these functional measurements are supported by fluorescence imaging data, we measured the quinidine-induced internalization of Kv1.5 in the presence of the cell-permeant compound BAPTA-AM to chelate intracellular calcium. Using this method, pretreatment with 10 μmol/L BAPTA-AM completely blocked quinidine-induced internalization of Kv1.5 with a corresponding increase in surface levels (Figure 2.12C). These results were nearly identical to those determined after endocytic disruption with Dynasore and p-50 dynamitin (Figure 2.10C and Figure 2.11). Together, these data demonstrate that quinidine-induced internalization is calcium-dependent and therefore unrecognized by previous biophysical studies focused on isolating channel-drug interactions.

Differential Effects of Acute Versus Chronic Treatment with Quinidine.

Previously we reported that, following constitutive internalization, a population of Kv1.5 originating on the atrial myocyte cell surface recycled back to the plasma membrane [111]. Electrophysiologically, we showed that quinidine-induced block of Kv1.5 current is reversible upon drug washout. Upon quinidine-stimulation, internalized Kv1.5 also co-localized with the early endosomal marker EEA1 (data not shown). Therefore, we measured the intracellular fate of the quinidine-induced, internalized Kv1.5 upon drug washout. Using a modified form of the recycling assay developed previously within our laboratory, and HL-1 cells transiently expressing Kv1.5-GFP, we found that a population of Kv1.5 undergoing quinidine-induced internalization recycled back to the plasma membrane with the same time constant as constitutive recycling (τ =29.06 min and 25.72 min, respectively) (Figure 2.15A). This channel recycling also occurred on a time scale nearly identical to recovery from current block [121]. This suggests that the rate limiting step for recovery of Kv1.5 current is not quinidine dissociation from channel and indicates that quinidine is acting on the internalization pathway and not on the recycling pathway. Recycled channel levels 60 minutes post quinidine-induced internalization were approximately 33% greater than those post constitutive endocytosis (Figure 2.16A). This difference is most likely attributed to an increased pool of internalized Kv1.5 available for recycling following drug treatment. To clarify this difference, we labeled surface channel 60 minutes post washout of both constitutive endocytosis and quinidine-induced internalization, and found no difference in steady-state cell surface levels of channel (Figure 2.16B). Importantly, over the time course studied, we detected no loss in

total protein, as measured by total GFP fluorescence, indicating that there was no detectable channel degradation (Figure 2.15A inset).

In a clinical setting, however, antiarrhythmic agents are administered chronically, over long periods of time [18, 137-139]. To investigate a potential long-lasting effect of chronic quinidine on the dynamic trafficking of Kv1.5, we treated HL-1 cells stably expressing Kv1.5 with a clinically relevant concentration of 10 μmol/L quinidine. Total Kv1.5 protein levels were assessed by Western blot at 0, 12, and 48 hours of quinidine exposure, and were reduced by 13% and 43% at 12 and 48 hours, respectively ($n = 9$; $n = 21$, respectively; $p < 0.01$ at 48hr) (Figure 2.15B). Immunocytochemistry revealed a corresponding decrease in surface Kv1.5 (Figure 2.16C) that was significant at 12 hours of quinidine treatment. As expected, these data indicate that Kv1.5 internalization precedes the loss of total channel protein and likely reflects a delay in the cellular time course for the onset of protein degradation. Importantly, the decrease in total Kv1.5 protein at 48 hours of chronic quinidine treatment was blocked by the mild proteasome inhibitor, ALLN, but not the lysosomal inhibitor, leupeptin (Figure 2.15C). Together, these data reveal that acute quinidine treatment leads to channel internalization that is reversible upon drug washout, whereas chronic quinidine treatment leads to channel degradation.

DISCUSSION

Recently, we demonstrated an unexpected dynamic trafficking of Kv1.5 at the atrial myocyte plasma membrane and a role for recycling in the maintenance of steady-state ion channel surface levels [111]. Here, we report a previously unrecognized

mechanism of antiarrhythmic drug action in the acute modulation of surface channel density. Using quinidine, an antiarrhythmic agent which has both class Ia actions [140, 141] and class III actions in mammalian atrium and ventricle, we demonstrate that channel blockers can both inhibit ion conductance and regulate the stability of the channel protein within the membrane. These pleiotropic actions, which may be independent, have important implications for antiarrhythmic drug therapy as well as drug safety testing.

The manipulation of ion channel trafficking pathways, particularly those that target functional channels existing in the myocyte membrane represents an alternative and potentially beneficial new therapeutic strategy. There is a clear need for the development of new, longer-term antiarrhythmic drugs to successfully maintain normal atrial sinus rhythm without risking the occurrence of potentially life-threatening, proarrhythmic ventricular side effects. The inhibition of I_{to} current, through block of Kv4.2/Kv4.3 channels in the atria and ventricle, is a frequent side effect of putative Kv1.5-selective agents. Our data demonstrate that quinidine-induced internalization of Kv1.5 is dose-, and temperature-dependent and, although it inhibited current, did not stimulate internalization of Kv2.1 or Kv4.2 channels. Ultimately, the development of new compounds and their efficacy to selectively modulate trafficking pathways is dependent on the ability to separate the pleiotropic actions and to isolate the pharmacophore responsible for block and/or internalization. In the current study, several lines of evidence indicate that these two processes may be separable. For instance, quinidine-induced internalization was voltage- and activity-independent in that it occurs at resting membrane potentials during immunocytochemistry and when cells are voltage clamped at -80 mV during electrophysiology measurements (Figures 2.1 and 2.12). In

contrast, open channel block of Kv1.5 was voltage- and activity-dependent (Figure 2.2). In addition, there are several pieces of data in this study in which pore block occurred without channel internalization. As mentioned above, both Kv4.2 and Kv2.1 exhibit significant quinidine-mediated current block, however neither underwent drug-induced internalization, despite constitutive endocytosis of Kv4.2 nearly identical to Kv1.5 (Figure 2.6). Importantly, drug-induced internalization of Kv1.5 was stereospecific in that quinine, the diastereomer of quinidine, caused current block of Kv1.5, but was incapable of inducing channel internalization even at a maximal dose (Figure 2.5). Interestingly, alanine-scanning mutagenesis of the conserved Kv channel drug binding site showed that not all residues were conserved for both pore block and channel internalization (Figure 2.9). To facilitate the development of new antiarrhythmic drugs that selectively modulate channel density, future detailed structure-activity studies are required to identify the essential features within the channel and as part of the drug molecule responsible for quinidine's multiple activities. The mechanism of drug-induced internalization most likely involves a conformational change in the channel protein; however, not all of the mutagenesis results in this study can be reconciled with the model that drug block and drug-induced internalization can be separated. For example, if one considers the effects of the T480A mutation, which occurs within the pore helix and diminishes both block and internalization, compared to our results that drug-induced internalization occurs when cells are clamped at -80 mV, it is difficult to envision how quinidine can reach a binding site in the conduction pathway to initiate internalization if the cytoplasmic gate of Kv1.5 is firmly closed. An alternative strategy is the identification of the molecular machinery and further elucidation of the proteins involved

in channel targeting, such as the dynein motor complex (Figure 2.11), which may reveal novel, selective auxiliary therapeutic targets. Nonetheless, this study highlights the potential for development of new agents which can selectively affect either ion conduction and/or ion channel trafficking pathways as a new means to gain therapeutic specificity.

The potential for drugs to modulate surface density also raises important issues for drug safety screening. It is well known that non-antiarrhythmic drugs can have proarrhythmic liabilities through the off-target inhibition of ion channels in the heart. This issue has received considerable attention from pharmaceutical companies and regulatory agencies that now mandate cardiac ion channel testing as part of drug safety profiling. Attention to the potential problem of non-antiarrhythmic drugs affecting both pore-block and channel trafficking originated with work related to the hERG channel [51]. Data presented in this manuscript advance this concept to include the atrial specific target Kv1.5 and extend this concern to the acute regulation of surface density. Current safety screens focus almost entirely on a drug's capacity to block ion conductance. The calcium-dependence of quinidine-induced internalization of Kv1.5 is important when considering the *in vivo* effects of this drug and most likely many others. Our results demonstrate that use of compounds that deplete free intracellular calcium block a major component of quinidine action on Kv1.5. This calcium-dependent component is responsible for a significant fraction of the quinidine-mediated decrease in current density and can explain the leftward shift in the EC_{50} for quinidine from 13 μmol/L in the biophysical studies including BAPTA to 3.5 μmol/L in the absence of BAPTA (Figure 2.12B). However, it is important to note that the free calcium concentration is likely very

high in our electrophysiological experiments performed in the absence of any calcium buffer, while large changes in free calcium are not expected in immunocytochemistry experiments. In addition, the two experiments were performed at different temperatures; therefore, the two conditions may not be identical. It is also possible that what is marked as calcium-dependent channel internalization (Figure 2.12A) is a mix of fast block and channel internalization. However, separation of these two mechanisms is complicated by our finding that the rate-limiting step for the onset of drug action is equilibration across the membrane and both block and internalization recover upon washout of the drug. Nevertheless, this work implies that antiarrhythmic agents such as quinidine, which affect channel trafficking pathways, may show greater efficacy and potency in the *in vivo* condition where calcium-dependent pathways are uninhibited. Screens for pore block may simply miss channel trafficking effects and dramatically underestimate drug actions.

Another issue that may compound these concerns is the acute versus chronic effects of altering channel surface density. Our results show that chronic quinidine treatment results in a significant decrease in Kv1.5 channel protein by diverting channel from a recycling to degradation pathway. Recent work suggests that a fraction of internalized Kv1.5 enters proteasomal compartments [87]. This is supported by data in this manuscript showing that inhibition of the proteasomal degradation machinery prevented the chronic quinidine-induced decrease in total Kv1.5. The time course of recovery from this repression may precipitate drug-withdrawal side effects while long-term suppression of channel expression may contribute to remodeling of heart tissue. The alternative is that chronic suppression may overcome current antiarrhythmic drug limitations of acute cardioversion and result in the benefit of maintained rhythm control. Nonetheless,

together these data give further credence to concerns regarding the comprehensiveness of current ion channel drug safety tests.

In summary, this report reveals a novel mechanism of antiarrhythmic drug action in the modulation of surface channel density. Results of this study highlight the possibility for development of new agents that selectively modulate ion conduction and/or the stability of channel protein in the membrane as an alternative or complementary strategy for treating atrial fibrillation and other potential cardiac arrhythmias.

EXPERIMENTAL PROCEDURES

Materials

Kv1.5-GFP and Kv1.5-mCherry constructs were generated from human Kv1.5 as previously described [111]. Polyclonal anti-GFP, monoclonal anti-V5, and Alexa Fluor secondary antibodies were from Invitrogen (Carlsbad, CA). Polyclonal Anti-DsRed antibody was obtained from BD Biosciences Clontech (Palo Alto, CA). Anti-troponin I was obtained from Millipore (Billerica, MA). Horseradish peroxidase-conjugated secondary antibodies were from Zymed (San Francisco, CA). HL-1 cells were a generous gift from Dr. William Claycomb (Louisiana State University Health Sciences Center, New Orleans, LA). Dynasore was a generous gift from Dr. Tomas Kirchhausen (Department of Cell Biology, Harvard Medical School and the CBR Institute for Biomedical Research, Inc. Boston, Massachusetts). Quinidine and quinine from Sigma (St. Louis, MO) were dissolved in DMSO and diluted 1:1000 into culture medium. All vehicle was DMSO 1:1000 in culture medium equivalent to drug addition.

Western Blot

HL1 cells were harvested in PBS containing Complete® protease inhibitors (Roche Applied Science, Indianapolis, IN) and lysed in SDS-PAGE sample buffer. Proteins were then separated by SDS-PAGE on a NuPAGE, Novex 4-12% Bis-Tris gel (Invitrogen), transferred to nitrocellulose, and probed with the indicated primary antibody for 1 hr at 4°C. Blots were then incubated with secondary antibodies conjugated to horseradish peroxidase (1:5000) and visualized using the Western Lightning enhanced chemiluminescent reagent according to the manufacturer's protocol (Perkin- Elmer Life Sciences, Wellesley, MA). Images were captured using the EpiChemi3 Darkroom (UVP, Inc., Upland, CA).

Immunocytochemistry

For analyzing fluorescence data, background fluorescence was subtracted for each cell, prior to normalizing surface or internalized signal to the total GFP fluorescence of that cell. Normalized values for drug treated conditions were then expressed as percent of vehicle or, in some cases, normalized to maximal drug response. These values were calculated by the following equations. λ = wavelength at which the data were collected; λ_1 = fluorophore 1, λ_2 = fluorophore 2.

For % Vehicle:

$$100 \times \left\{ \left(\frac{(\text{Internalized}_{[\text{drug}]\,\lambda 1} - \text{Background}_{[\text{drug}]\,\lambda 1})}{(\text{GFP}_{[\text{drug}]\,\lambda 2} - \text{Background}_{[\text{drug}]\,\lambda 2})} \right) \Big/ \left(\frac{(\text{Internalized}_{[\text{vehicle}]\,\lambda 1} - \text{Background}_{[\text{vehicle}]\,\lambda 1})}{(\text{GFP}_{[\text{vehicle}]\,\lambda 2} - \text{Background}_{[\text{vehicle}]\,\lambda 2})} \right) \right\}$$

For % Max Internalization: 100 ×

$$\left(\frac{\left\{ \left(\frac{(\text{Internalized}_{[\text{drug}]\lambda 1} - \text{Background}_{[\text{drug}]\lambda 1})}{(\text{GFP}_{[\text{drug}]\,\lambda 2} - \text{Background}_{[\text{drug}]\,\lambda 2})} \right) - \left(\frac{(\text{Internalized}_{[\text{vehicle}]\lambda 1} - \text{Background}_{[\text{vehicle}]\lambda 1})}{(\text{GFP}_{[\text{vehicle}]\,\lambda 2} - \text{Background}_{[\text{vehicle}]\,\lambda 2})} \right) \right\}}{\left\{ \left(\frac{(\text{Internalized}_{[\text{drug}]\text{max}\,\lambda 1} - \text{Background}_{[\text{drug}]\text{max}\,\lambda 1})}{(\text{GFP}_{[\text{drug}]\text{max}\,\lambda 2} - \text{Background}_{[\text{drug}]\text{max}\,\lambda 2})} \right) - \left(\frac{(\text{Internalized}_{[\text{vehicle}]\,\lambda 1} - \text{Background}_{[\text{vehicle}]\lambda 1})}{(\text{GFP}_{[\text{vehicle}]\,\lambda 2} - \text{Background}_{[\text{vehicle}]\,\lambda 2})} \right) \right\}} \right)$$

Immunocytochemistry was performed as previously described [111]. Briefly, 48 hr post transfection, HL-1 cells transiently expressing Kv1.5-GFP were live cell stained with a polyclonal anti-GFP antibody (1:500) in 2% goat serum for 30 min on ice to minimize internalization of membrane proteins. For surface labeling, cells were then incubated with goat anti-rabbit Alexa Fluor secondary antibody (1:500) in 2% goat serum for 30 min on ice, fixed with 4% paraformaldehyde for 10 min on ice, and mounted with ProLong Gold anti-fade reagent (Invitrogen). For labeling surface and internalized protein following live-cell staining with anti-GFP, cells were treated with vehicle or drug for the specified amount of time prior to incubation with secondary antibody. Cells were then incubated with goat anti-rabbit Alexa Fluor 405 antibody (1:200) in 2% goat serum for 30 min on ice to saturate remaining surface channel populations, fixed with 4% paraformaldehyde for 10 min on ice, permeabilized with 0.1% Triton X-100 in 2% goat serum for 10 min on ice, incubated with goat anti-rabbit Alexa Fluor 647 antibody (1:500) in 2% goat serum for 30 min on ice, and mounted with ProLong Gold. Images of transfected cells displaying fluorescent signals were acquired on an Olympus Flouview 500 confocal microscope with a 60 by 1.35 N.A. oil objective. Signal intensities were

adjusted so that the maximal pixel intensities were at least half saturation. Images were obtained by taking a series of images every 0.5 μm through the cell (generally 3–4 μm) and combining the images into a composite stack. To minimize effects of overexpression on Kv1.5-GFP localization, we analyzed only cells with low to mid levels of expressed protein. Images were analyzed with ImageJ software (NIH, Bethesda, MD), and statistics were performed with Prism 5 software from GraphPad Prism Software (San Diego, CA). The resolution obtained in these imaging experiments was 512 by 512 pixels with a z resolution of 0.5μm for each filter set. Regarding the laser configuration, Alexa Fluor 405 was excited using a 405nm laser diode, reflected off of an SDM 490nm dichroic mirror, and passed through a BA 430-460nm bandpass filter. Kv1.5-GFP was excited using a 488nm laser, reflected off of an SDM 560nm dichroic mirror, and passed through a BA505-525nm bandpass filter. Alexa Fluor 594 was excited using a 543nm laser and passed through a BA560IF bandpass filter. Alexa Fluor 647 was excited using a 633nm laser and passed through a BA660IF bandpass filter. Fluorescent signals of compressed Z-stacks were quantified using NIH ImageJ software (NIH, Bethesda, MD). To determine specific fluorescence, the background signal from neighboring untransfected cells was subtracted from the total fluorescence for all quantified signals. Surface and internalized Kv1.5 fluorescent signals were then normalized to total Kv1.5-GFP fluorescence for each cell.

Recycling Assay: The recycling assay was performed as previously described with the following modifications [111]. 48 hr post-transfection, HL-1 cells transiently expressing Kv1.5-GFP were live-cell stained with an anti-GFP antibody (1:500) for 30 min on ice.

Following this incubation, the cells were returned to 37°C for 10 minutes with vehicle or drug, removed, and stained with goat anti-rabbit Alexa Fluor 594 secondary antibody (1:200) for 30 min on ice to saturate remaining surface channels. Cells were then returned to 37°C for the indicated times, removed, and incubated with goat-anti-rabbit Alexa Fluor 405 (1:500) for 30 min on ice to detect the recycled channel population. Additionally, cells were fixed and permeabilized as described above and internalized channel was detected with goat-anti-rabbit Alexa Fluor 647 (1:500) for 30 min on ice before mounting with ProLong Gold.

Live-cell Imaging

Kv1.5-pHluorin was generated by replacing the extracellular GFP tag with the pH sensitive variant of GFP, pHluorin. 48 hr post transfection HL-1 cells transiently expressing Kv1.5-pHluorin were imaged in a heated perfusion chamber using an Olympus FluoView 500 confocal microscope. Both the chamber and perfusion solutions were maintained at 37°C throughout the experiment. Cells were perfused with Liebovitz's medium from Gibco (Carlsbad, CA) pH7.4 or Liebovitz's medium containing 0.1%DMSO for 10 minutes, followed by quinidine treatment for 10 minutes. Images were collected using Olympus FluoView 500 (every 2.5 minutes at 1% laser intensity) and quantified as described above.

Electrophysiology

For electrophysiological studies, recordings were performed on HL-1 cells stably expressing Kv1.5-pHluorin and whole-cell voltage clamp experiments were performed as

described previously [142]. The intracellular pipette solution contained (in mmol/L): Potassium aspartate 110, KCl 20, NaCl 8, HEPES 10, K_2ATP 4, $CaCl_2$ 1, and $MgCl_2$ 1, either in the presence or absence of 10 mmol/L K_2BAPTA; and was adjusted to pH 7.2 with KOH. The bath solution contained (in mmol/L): NaCl 110, KCl 4, $MgCl_2$ 1, $CaCl_2$ 1.8, HEPES 10, and glucose 1.8; and was adjusted to pH 7.35 with NaOH. All currents were normalized to the peak current measured at +60 mV for each cell tested. All experiments were performed at room temperature.

Neonatal Myocyte Isolation and Electroporation

Cardiomyocytes from neonatal mice were isolated and cultured according to methods adapted from Zlochiver, et al [143]. Briefly, hearts from 1-3 day-old mice were removed and collected in Ca^{2+}- and Mg^{2+}-free Hank's balanced salt solution (HBSS) from Gibco. Finely minced cardiovascular tissue was digested in 0.05% trypsin (Invitrogen) and 0.001% pancreatin (Sigma) at 37°C in consecutive 10 min steps. Supernatant cells suspensions were collected in an equal volume of medium M199 (Lonza BioWhittaker, Basel, Switzerland), containing 10% fetal bovine serum (FBS) from Gibco, 20 units/mL penicillin, 20 μg/mL streptomycin. Following 8 digestion steps, collected cell suspensions were centrifuged at 800 rpm for 5 min and the supernatant was aspirated and discarded. The dissociated tissue was then resuspended in 10 mL medium and filtered through a 70 μm mesh filter into a 100mm tissue culture dish. Fibroblasts were depleted through 2 hour preplating at 37˚C with 5% CO_2. Myocytes were collected off the dish by gentle agitation, filtered through a 40 μm mesh filter, and spun down for 1 min at 4,000 rpm. Myocytes were then resuspended in 100μL Nucleofector solution from Amaxa

(Gaithersburg, MD) and 2.5 μg of the desired DNA, per reaction. This solution was then transferred to an Amaxa-certified cuvette, inserted into the cuvette holder of an Amaxa biosystems Nucleofector II, and program G-09 was run. 500μL of pre-warmed medium was then added to the solution in the cuvette and the myocytes were plated onto collagen-coated coverslips in medium containing Bromodeoxyuridine (Sigma) and Fungizone (Gibco) and incubated in a humidified tissue culture incubator for 36-48 to allow protein expression.

Statistical Analysis

Statistics were performed using GraphPad Prism 5 Software (San Diego, CA). All data are expressed as the mean ± SEM of n cells. Comparisons between groups were made using a Student's *t* test (paired or unpaired) or One-way ANOVA as indicated. Values of $p<0.05$ were considered significant.

ACKNOWLEDGEMENTS

We thank Dr. Benedict Lucchesi (University of Michigan) for his insight and discussion regarding this work, and Dr. Tomas Kirchhausen (Harvard Medical School) for the generous gift of Dynasore.

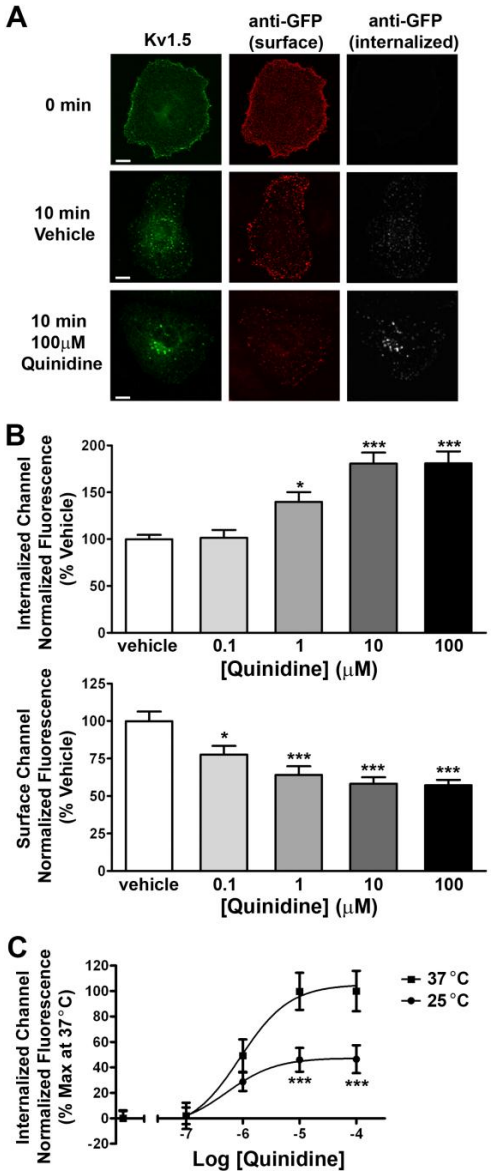

Figure 2.1 Quinidine stimulates internalization of Kv1.5 in a dose- and temperature-dependent manner.

(A) Representative images of Kv1.5-GFP overexpressed in HL-1 cells, showing total GFP signal (left), surface channel as detected by surface labeling with anti-GFP followed by goat anti-rabbit Alexa Fluor 405 (middle), and internalized channel detected by labeling with goat anti-rabbit Alexa Fluor 647 (right), at 0min (top), 10min at 37°C with vehicle (0.1% DMSO) (middle), and 10min at 37°C with 100 μmol/L quinidine (bottom). **(B)** Quantification of internalized (top) and surface (bottom) Kv1.5 following treatment with increasing concentrations of quinidine for 10min at 37°C. **(C)** Comparison of dose response for Kv1.5-GFP internalization following quinidine treatment for 10min at room temperature (25˚C) and 37˚C (EC_{50} = 900 nmol/L at 37˚C). Scale bars = 10 μm. * indicates $p < 0.05$; *** indicates $p < 0.001$ as determined by one-way ANOVA with Tukey post-test.

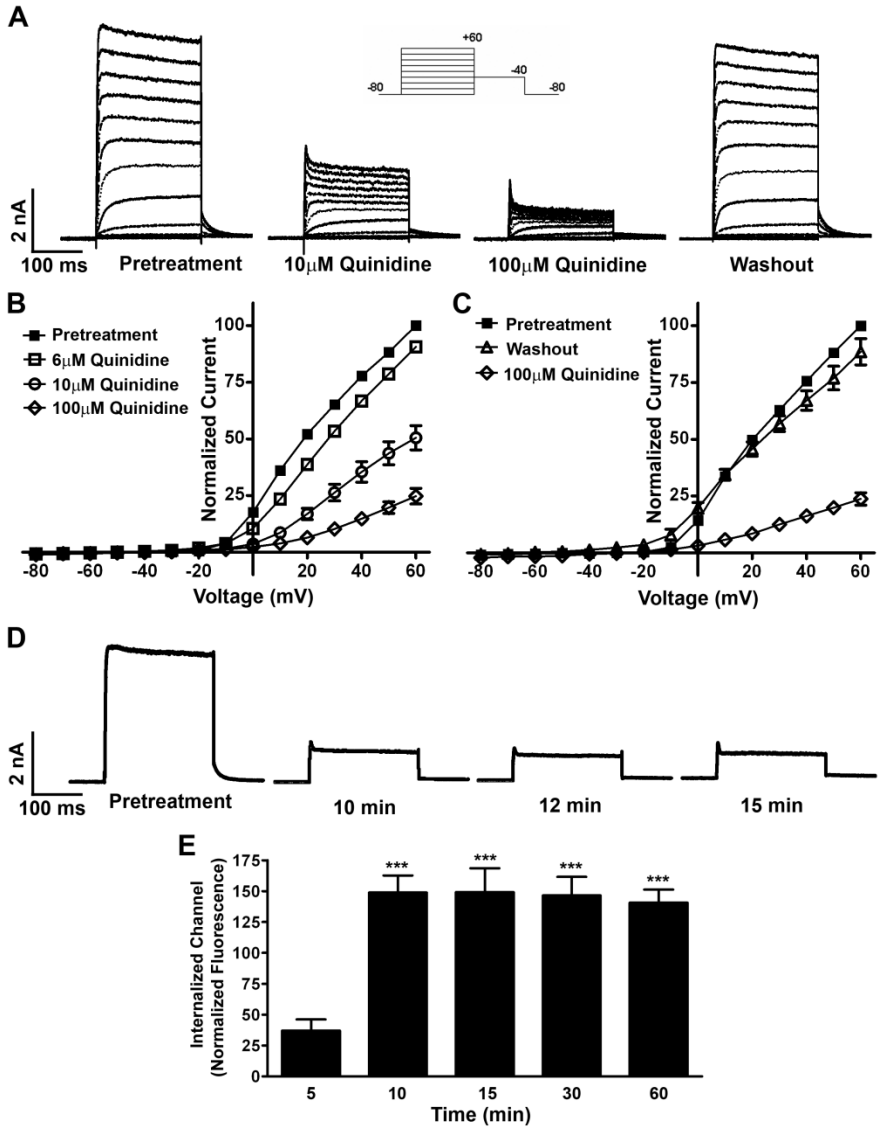

Figure 2.2 Quinidine treatment causes a reversible, dose-dependent open-channel block of Kv1.5.

(A) Whole-cell voltage clamp experiments were performed on HL-1 cells stably expressing Kv1.5-pHluorin. Recordings were taken prior to and following 10 min perfusion with 1, 6, 10, or 100μmol/L quinidine and following 20 min of drug washout. Representative traces for sequential dosing of a single cell are shown. **(B)** Cells were treated as above and I-V curves were generated for cells prior to treatment and following 10 min perfusion with 6, 10, and 100μmol/L quinidine. **(C)** I-V curves are shown for cells prior to treatment, and following 100μmol/L quinidine, and 20 min washout of quinidine. **(D)** A single depolarizing pulse to +60mV was applied as described in methods. Representative traces are shown for a single cell prior to and following 10, 12, and 15 min perfusion with 100 μmol/L quinidine. **(E)** Quantitation of internalized Kv1.5-GFP (overexpressed in HL-1 cells) in response to 10 μmol/L quinidine for 5, 10, 15, 30, or 60 min at 37˚C. *** indicates $p < 0.001$ as determined by one-way ANOVA with Tukey post-test.

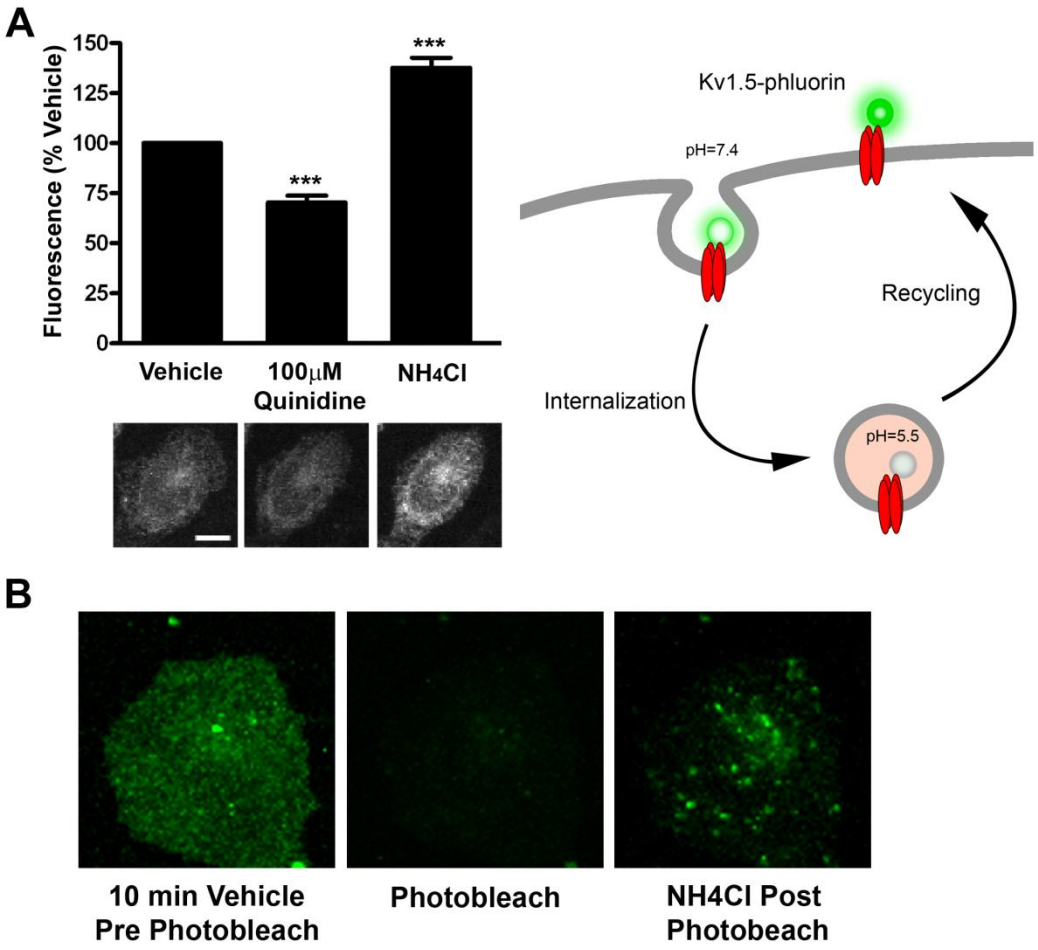

Figure 2.3 Quinidine-induced internalization is independent of antibody labeling.

(A) Quantification of surface Kv1.5-pHluorin following perfusion at 37˚C for 10 min with 0.1% DMSO followed by 10 min with 100μmol/L quinidine and a brief pulse with 50 mmol/L NH_4Cl. Representative images for each of these conditions are shown. **(B)** HL-1 cells expressing Kv1.5-pHluorin were perfused for 10 min with vehicle as described above. Remaining cell surface Kv1.5-pHluorin was photobleached at high laser intensity, followed by rapid application of NH_4Cl, to reveal foci of intracellular, endosomal Kv1.5-pHluorin. Scale bar = 20μm. *** indicates $p < 0.001$ as determined by one-way ANOVA with Tukey post-test.

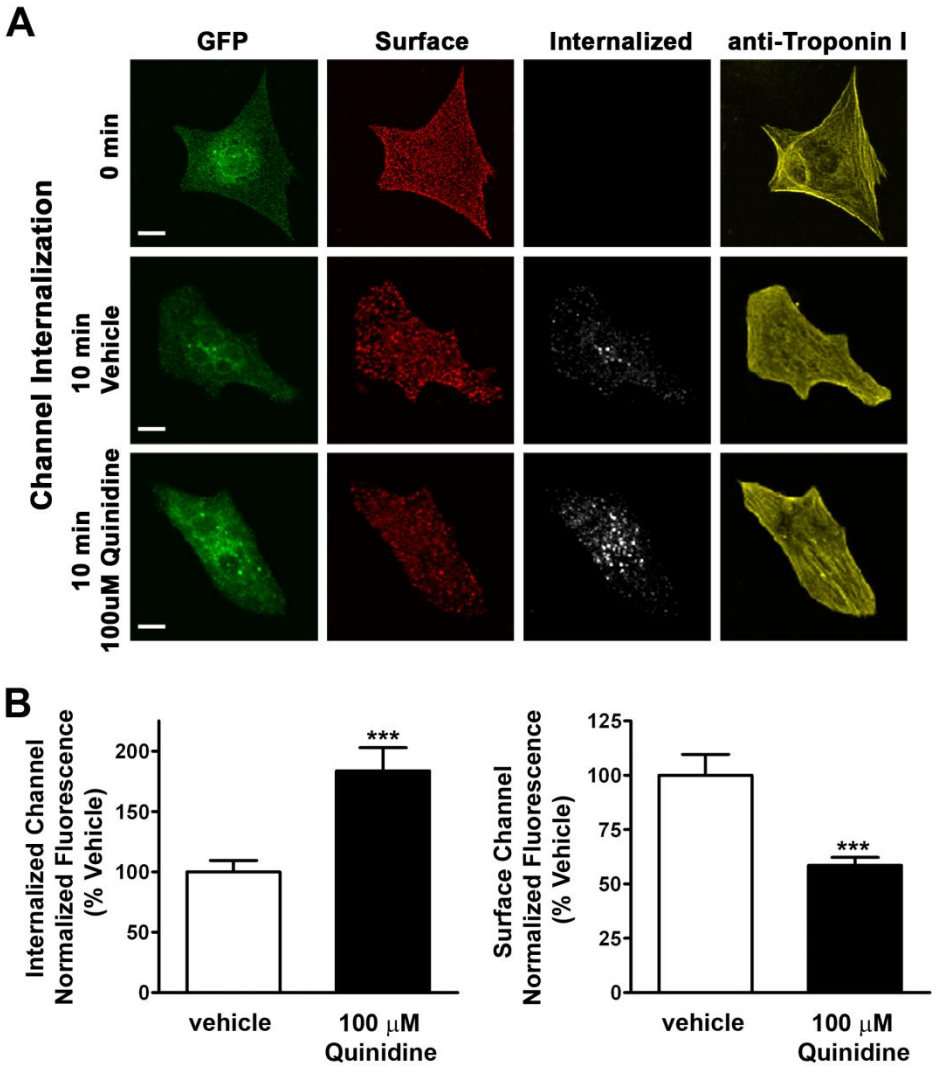

Figure 2.4 Constitutive and quinidine-induced internalization occur in native mouse myocytes.

(A) Representative images of acutely dissociated neonatal mouse myocytes transiently expressing Kv1.5-GFP by electroporation showing total GFP signal (left), surface channel (left middle), internalized channel (right middle), and anti-troponin (right) signal, at 0min (top), 10min at 37°C with vehicle (middle), and 10min at 37°C with 100 μmol/L quinidine (bottom). Scale bars = 10 μm. **(B)** Quantification of internalized (left) and surface (right) Kv1.5 following treatment with 100 μmol/L quinidine for 10min at 37°C. *** indicates $p < 0.001$ as determined by unpaired t-test.

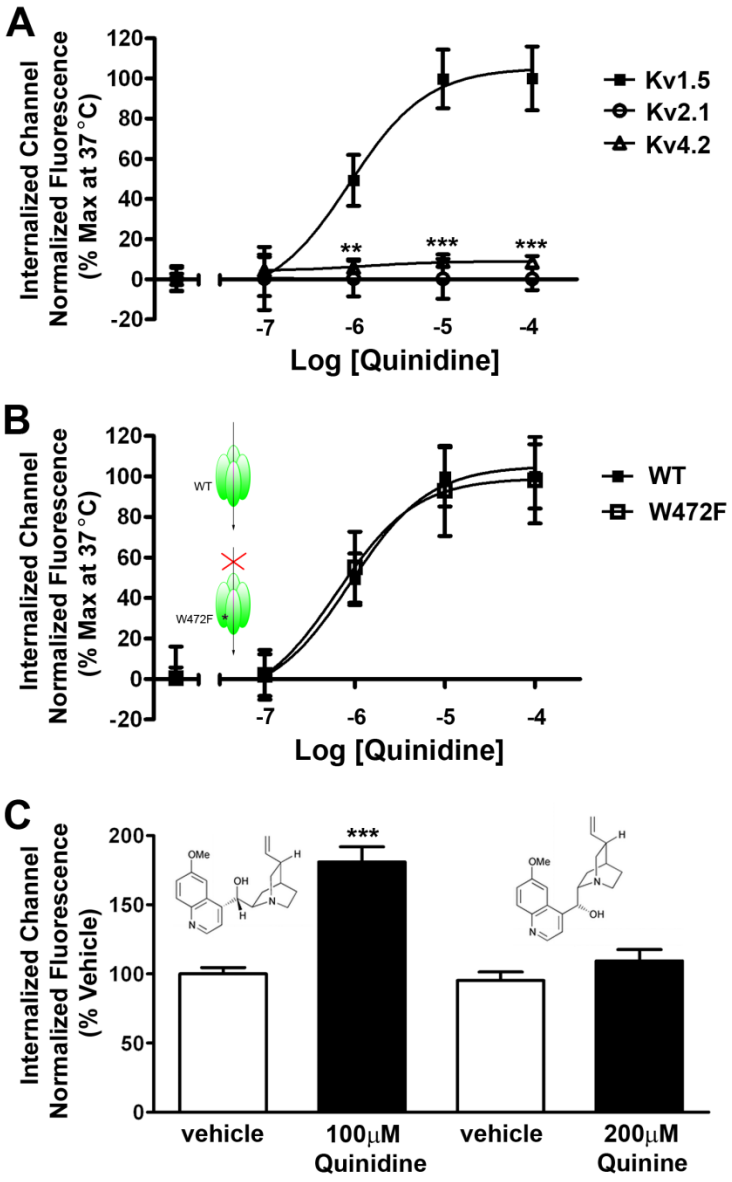

Figure 2.5 Quinidine-induced internalization is subunit-dependent, activity-independent, and stereospecific.

Dose-response for HL-1 cells expressing Kv4.2-GFP or Kv2.1-GFP **(A)** or Kv1.5-W472F **(B)** treated with increasing concentrations of quinidine for 10min at 37°C. ** indicates $p < 0.01$; *** indicates $p < 0.001$ as determined by one-way ANOVA with Tukey post-test. **(C)** Quantification of internalized Kv1.5 following treatment with 100 μmol/L quinidine or 200 μmol/L quinine, the diastereomer of quinidine, for 10min at 37°C. *** indicates $p < 0.001$ as determined by student's unpaired t-test.

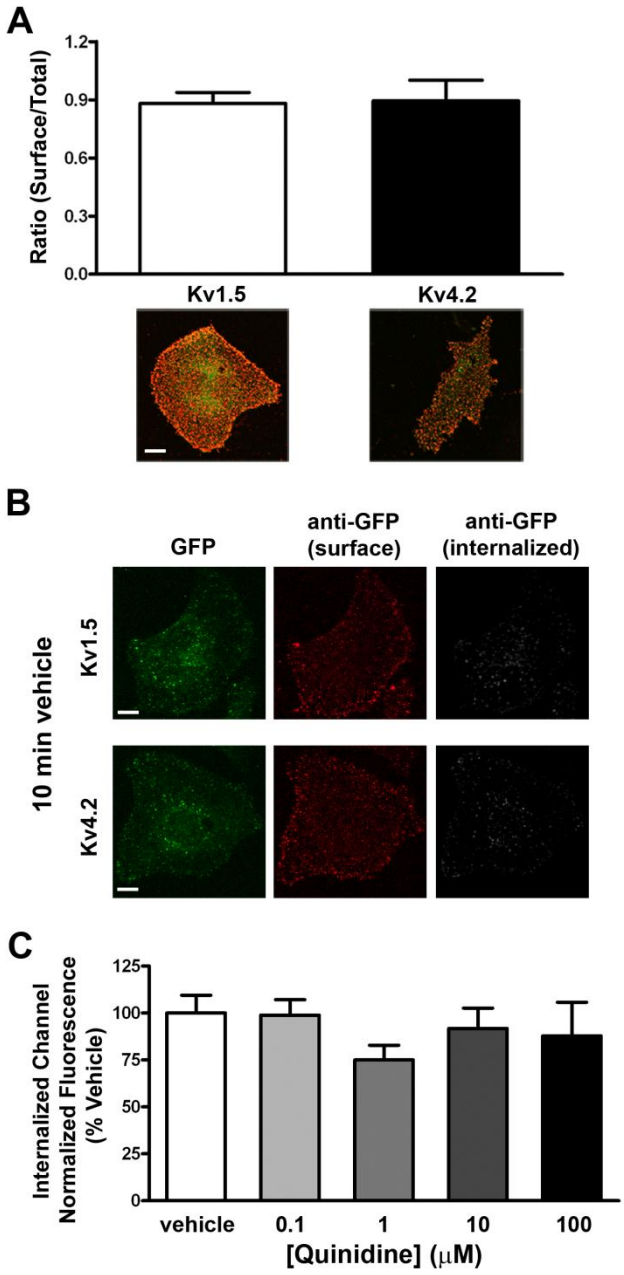

Figure 2.6 Surface to total protein ratio is similar for Kv1.5 and Kv4.2.

HL-1 cells overexpressing Kv1.5-GFP or Kv4.2-GFP were **(A)** surface-labeled and the ratio of surface (red) to total protein (green) was quantified. Representative images are shown for both channel subunits. **(B)** Representative images of Kv1.5-GFP (top) or Kv4.2-GFP (bottom) showing total GFP signal (left), surface channel as detected by surface labeling with anti-GFP followed by goat anti-rabbit Alexa Fluor 405 (middle), and internalized channel detected by labeling with goat anti-rabbit Alexa Fluor 647 (right), after 10min at 37°C with vehicle (0.1% DMSO). **(C)** Quantification of internalized Kv4.2 following treatment with increasing concentrations of quinidine for 10min at 37°C. Scale bar = 10μm.

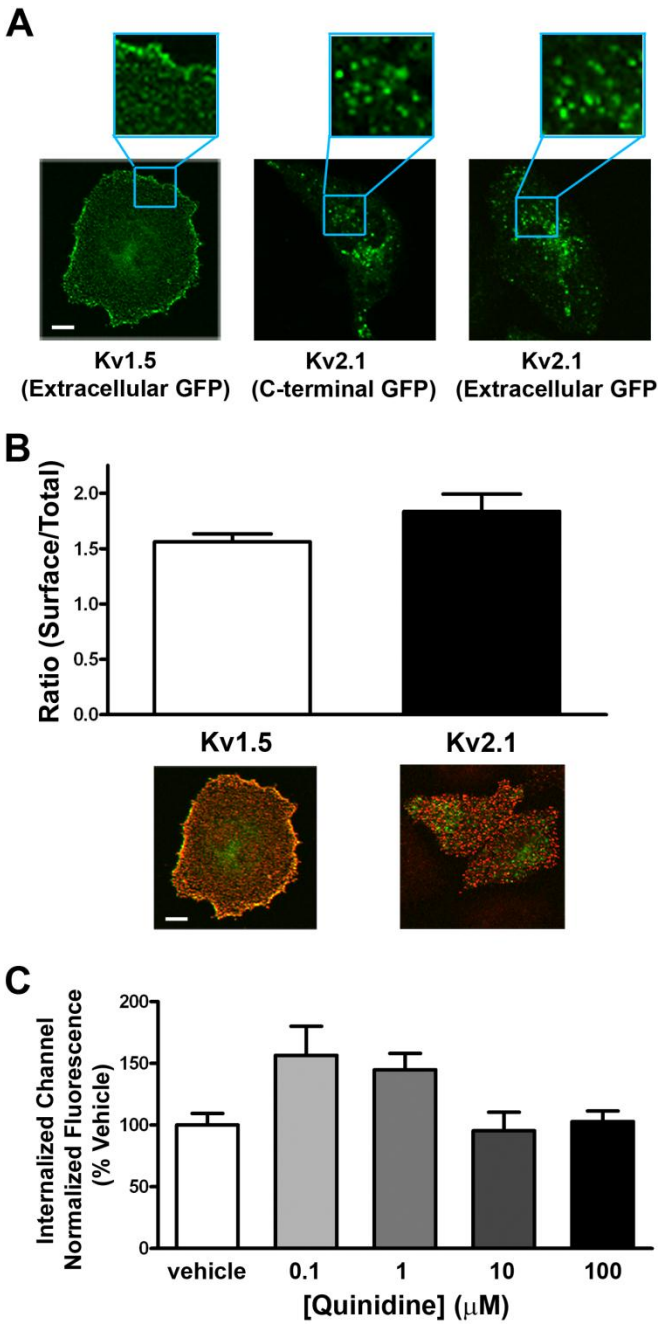

Figure 2.7 Kv2.1 differs from Kv1.5 in expression pattern; however, surface to total protein ratios are similar.

(A) Representative images showing total-GFP fluorescence patterns for Kv1.5 with an extracellular GFP tag, Kv2.1 with a C-terminal GFP tag, and Kv2.1 with an extracellular GFP tag. **(B)** HL-1 cells overexpressing Kv1.5-GFP or Kv2.1-GFP were surface-labeled and the ratio of surface (red) to total protein (green) was quantified. Representative images are shown for both channel subunits. **(C)** Quantification of internalized Kv2.1 following treatment with increasing concentrations of quinidine for 10min at 37°C. Scale bar = 10μm.

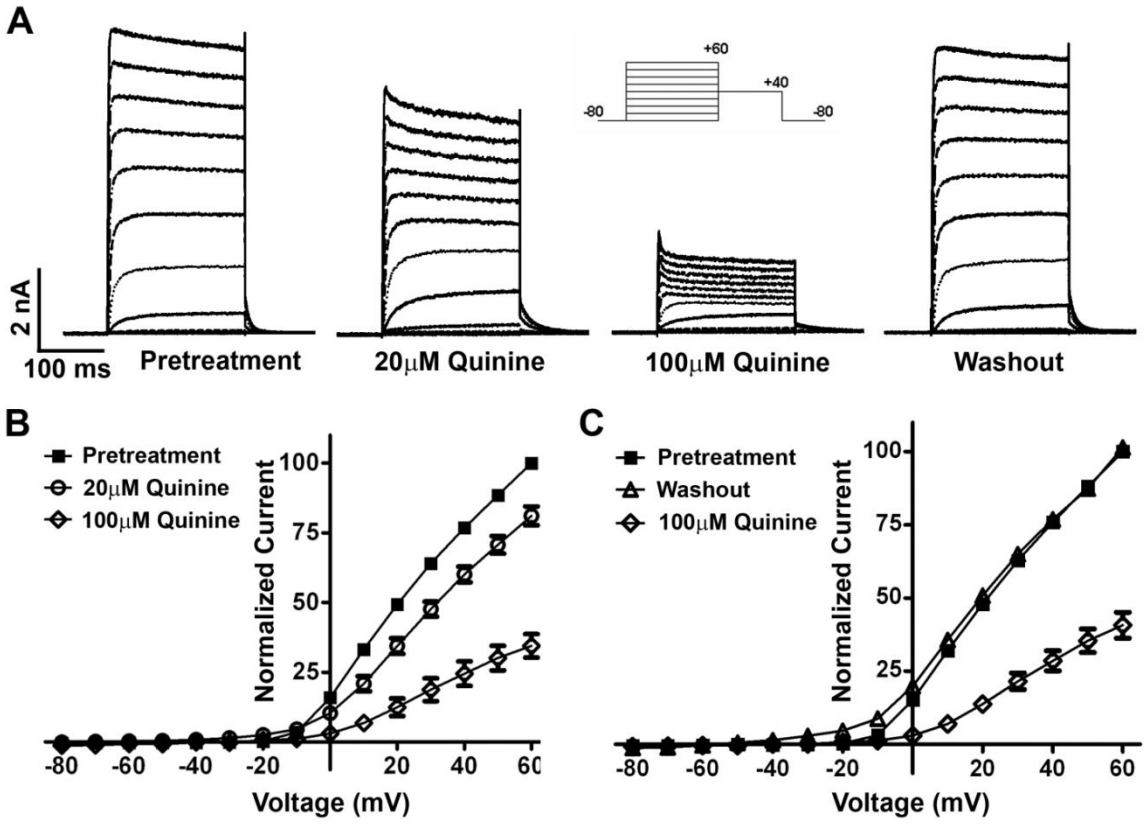

Figure 2.8 Quinine treatment causes a reversible, dose-dependent block of Kv1.5.

(A) Whole-cell voltage clamp experiments were performed on HL-1 cells stably expressing Kv1.5-pHluorin. Recordings were taken before and after 10 min perfusion with 20 or 100μmol/L quinine, and following 20 min of drug washout. Representative traces for sequential dosing of a single cell are shown. **(B)** Cells were treated as described above and I-V curves are shown for cells prior to treatment and following 10 min perfusion with 20 and 100μmol/L quinine. **(C)** I-V curves are shown for cells prior to treatment, and following 10 min perfusion with 100μmol/L quinine and 20 min washout of quinine.

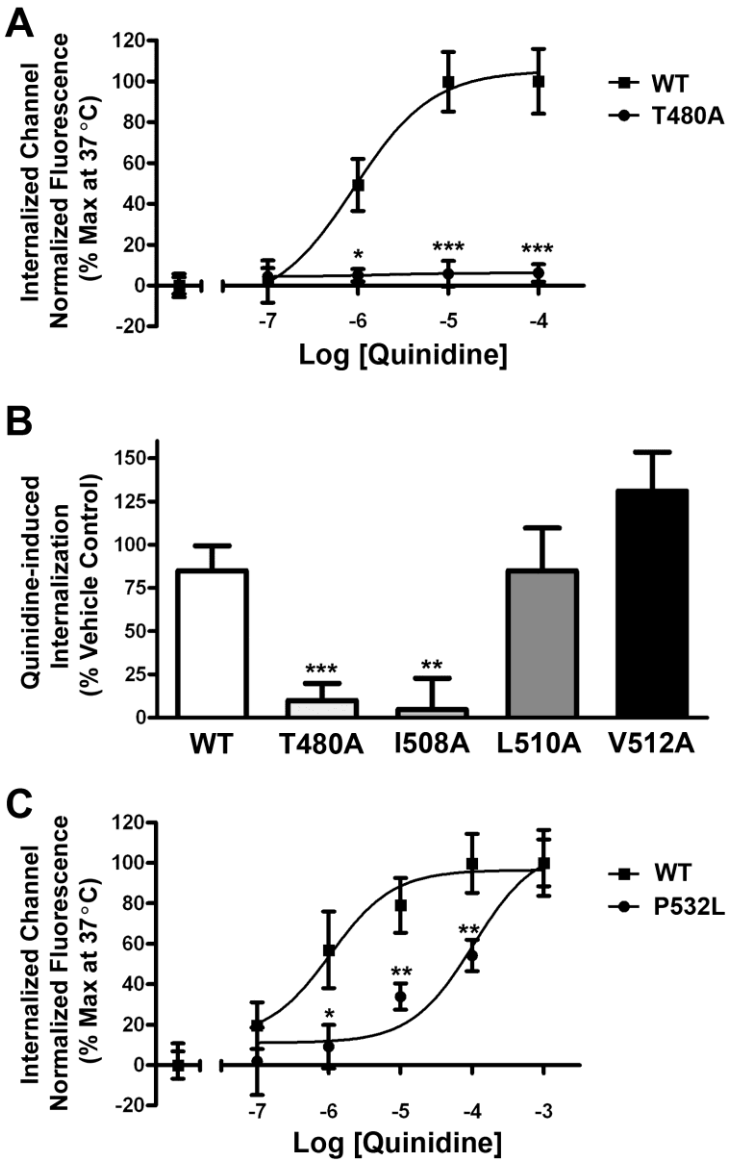

Figure 2.9 Structural requirements for quinidine binding are partially conserved for pore block and channel internalization.

(A) Dose-response for HL-1 cells expressing Kv1.5-GFP or the quinidine-insensitive Kv1.5-T480A mutant treated with increasing concentrations of quinidine for 10min at 37°C. **(B)** Quinidine-induced internalization for HL-1 cells expressing Kv1.5-GFP containing the T480A, I508A, L510A, or V512A mutation treated with 100 μmol/L quinidine for 10min at 37°C. **(C)** Dose-Response for HL-1 cells expressing Kv1.5-GFP or the Kv1.5-P532L mutant treated as described in (A). * indicates $p < 0.05$; ** indicates $p < 0.01$; *** indicates $p < 0.001$ as determined by one-way ANOVA.

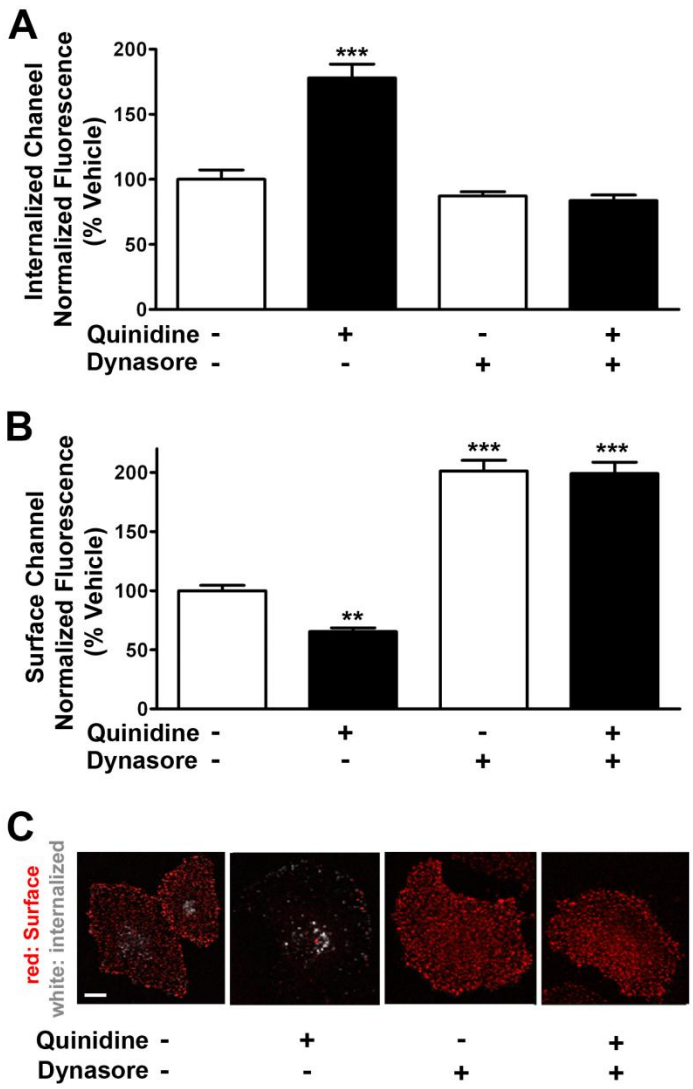

Figure 2.10 Channel internalization is prevented by pharmacologic disruption of the endocytic machinery.

(A) HL-1 cells expressing Kv1.5-GFP were treated for 1 hour with 80 µmol/L Dynasore at 37˚C prior to surface-labeling with anti-GFP antibody. Quantification of internalized Kv1.5 following treatment with 100 µmol/L quinidine for 10min at 37°C in the continued presence of Dynasore. **(B)** Quantification of surface Kv1.5 for cells treated as described in (A). **(C)** Representative images of surface (red) and internalized (white) Kv1.5 in cells treated as described in (A). Scale bars = 10 µm. ** indicates $p < 0.01$; *** indicates $p < 0.001$ as determined by one-way ANOVA with Tukey post-test.

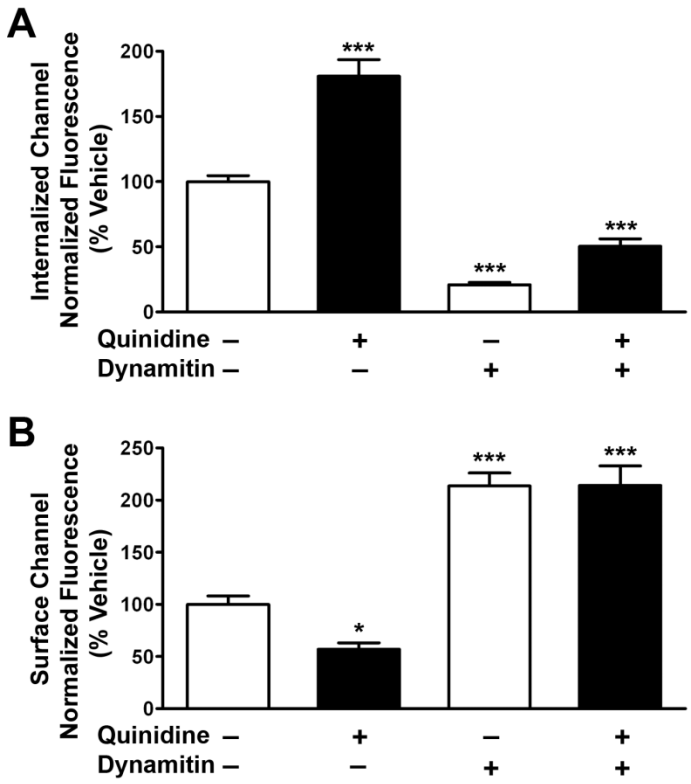

Figure 2.11 Channel internalization is prevented by dominant-negative disruption of the endocytic machinery.

(A) HL-1 cells co-expressing Kv1.5-mCherry and dynamitin-GFP were live-cell labeled with anti-DsRed followed by treatment with increasing concentrations of quinidine for 10min at 37°C, and internalized Kv1.5 was quantified. **(B)** Quantification of surface Kv1.5 for cells treated as described in (A). * indicates $p < 0.05$; *** indicates $p < 0.001$ as determined by one-way ANOVA with Tukey post-test.

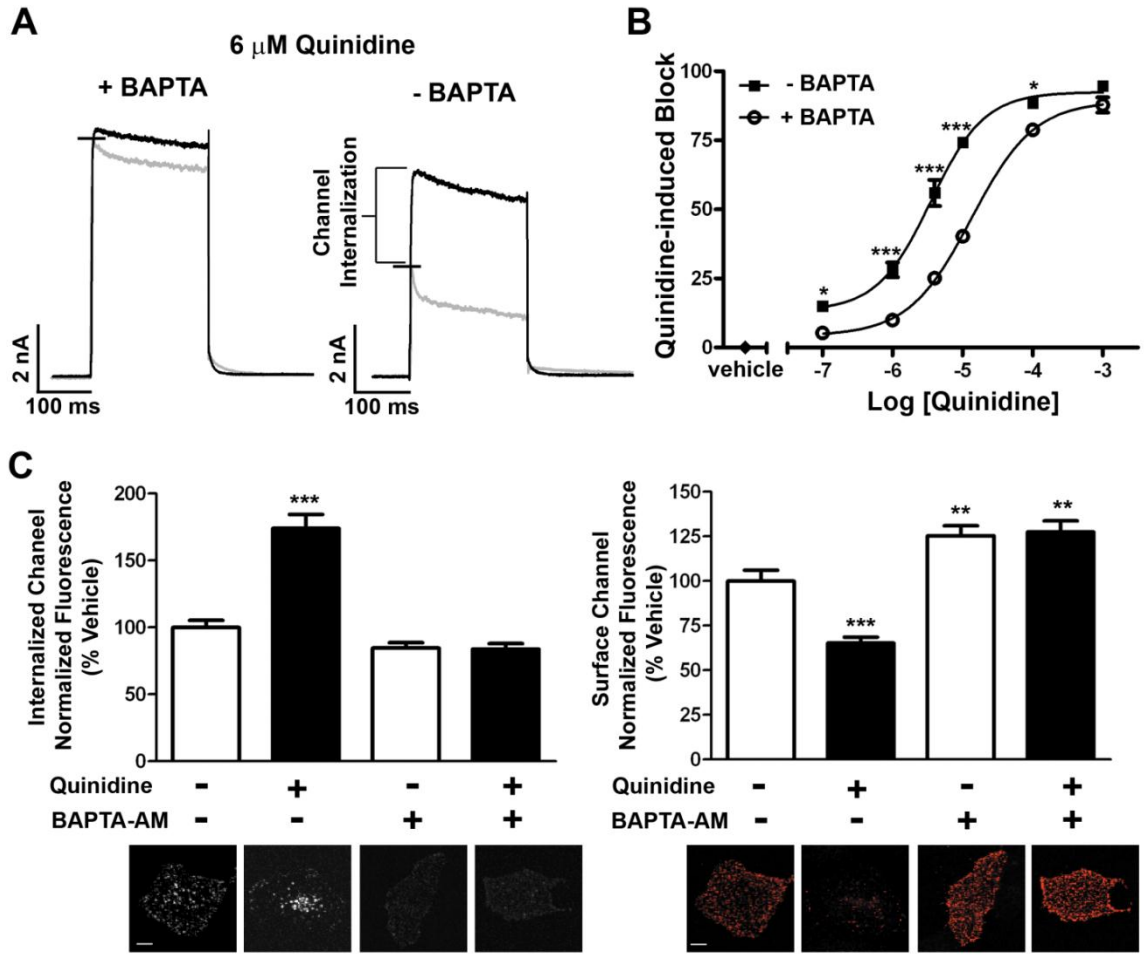

Figure 2.12 Quinidine-induced internalization occurs via a calcium-dependent mechanism.

Whole-cell voltage clamp experiments were performed on HL-1 cells stably expressing Kv1.5-pHluorin. A single depolarizing pulse to +60mV was applied as described in methods. **(A)** Current traces are shown for a single cell prior to (black) and following (gray) 10min exposure to 6 μmol/L quinidine in the presence (left) or absence (right) of BAPTA in the pipette solution (n=10 cells). **(B)** Dose-response curve upon treatment with increasing concentrations of quinidine for 10min at room temperature in the presence or absence of BAPTA in the pipette solution (IC_{50} = 13 μmol/L + BAPTA and 3.5 μmol/L - BAPTA; n=5 cells; Hill slope = 1.042 + BAPTA and 1.135 - BAPTA). **(C)** HL-1 cells expressing Kv1.5-GFP were pretreated for 1 hour with 10 μmol/L BAPTA-AM before surface-labeling with anti-GFP antibody. Quantification of internalized (left) and surface (right) Kv1.5 following treatment with 100 μmol/L quinidine for 10min at 37°C in the continued presence of BAPTA-AM. Below each bar graph is a representative image for that condition. Scale bars = 10 μm. * indicates $p < 0.05$; ** indicates $p < 0.01$; *** indicates $p < 0.001$ as determined by one-way ANOVA with Tukey post-test.

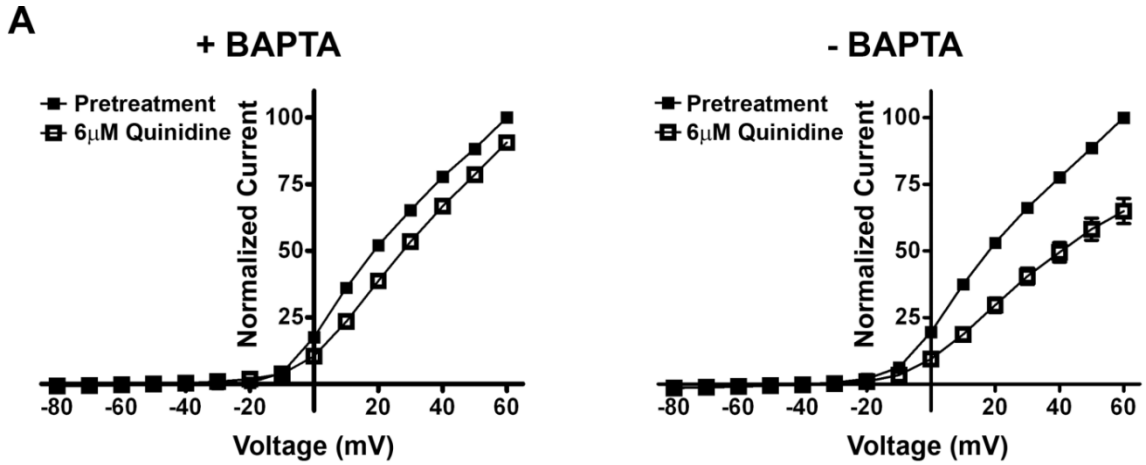

Figure 2.13 Quinidine-induced internalization occurs via a calcium-dependent mechanism.

Whole-cell voltage clamp experiments were performed on HL-1 cells stably expressing Kv1.5-pHluorin. I-V curves are shown for recordings taken in the presence (left) or absence (right) of BAPTA before and after 10 min perfusion with 6μmol/L quinidine.

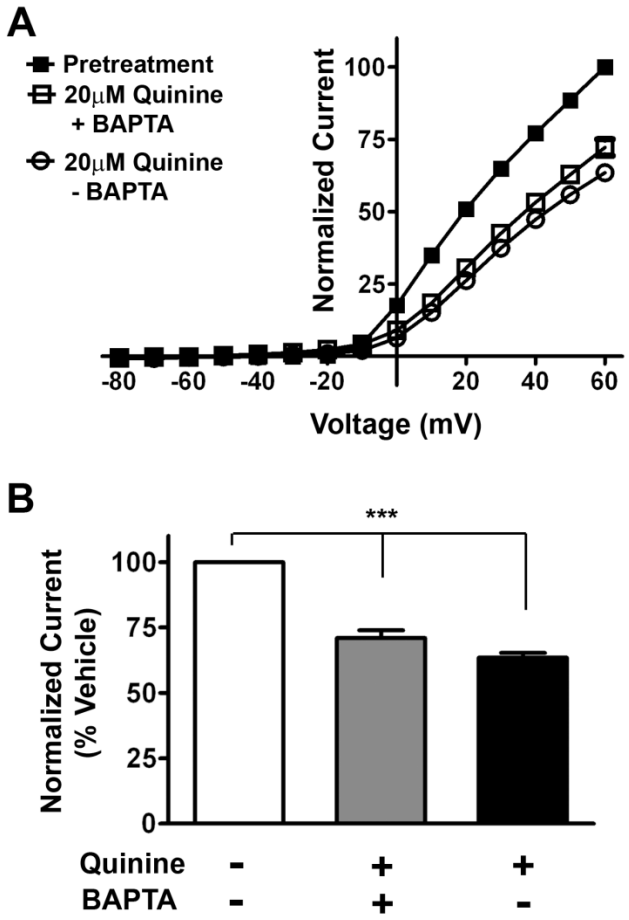

Figure 2.14 Quinine-mediated block of Kv1.5 current is calcium-independent.

Whole-cell voltage clamp experiments were performed on HL-1 cells stably expressing Kv1.5-pHluorin. **(A)** I-V curves for recordings taken prior to treatment and following 10 min perfusion with 20μmol/L quinine in the presence or absence of BAPTA. **(B)** Quantification of Kv1.5 current following quinine treatment in the presence or absence of BAPTA. *** indicates $p < 0.001$ as determined by one-way ANOVA with Tukey post-test.

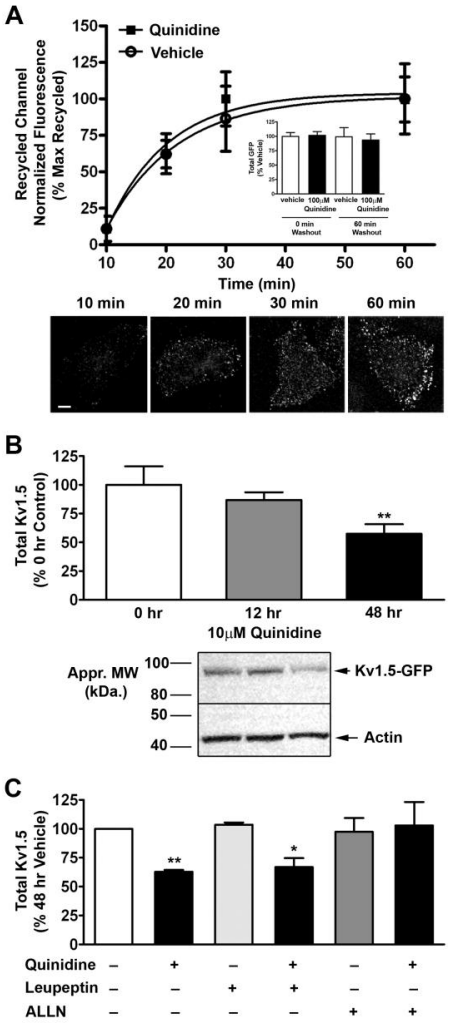

Figure 2.15 Acute quinidine-induced internalization is reversible, whereas chronic treatment results in channel degradation.

(A) Quantification of recycled Kv1.5 at 0, 10, 20, 30, and 60 min at 37˚C post treatment with 100 μmol/L quinidine for 10 min at 37˚C. Vehicle and quinidine treated data sets were each normalized to their own baseline (no washout) and maximum. Corresponding total GFP levels are provided for 0 and 60 min of recycling (inset). Below are representative images showing the increase in recycled Kv1.5-GFP with time, post quinidine treatment. Scale bar = 10 μm. **(B)** HL-1 cells stably expressing Kv1.5-pHluorin were treated with 10 μmol/L quinidine for 0, 12, or 48 hours at 37°C. Quantification of total Kv1.5 protein levels normalized to actin and control (48 hour DMSO) levels. Below is a representative image of a Western blot for 0, 12, and 48 hours of quinidine treatment. **(C)** HL-1 cells stably expressing Kv1.5-pHluorin were treated with vehicle, 10 μmol/L quinidine, 10 μmol/L leupeptin, 500 nmol/L ALLN, quinidine and leupeptin, or quinidine and ALLN for 48 hours at 37°C (63% or 67% decrease with 48 hr quinidine or quinidine and leupeptin (n = 8); no statistical decrease for quinidine and ALLN (n = 4)). Quantification was performed as in B. * indicates $p < 0.05$; ** indicates $p < 0.01$ as determined by one-way ANOVA with Tukey post-test.

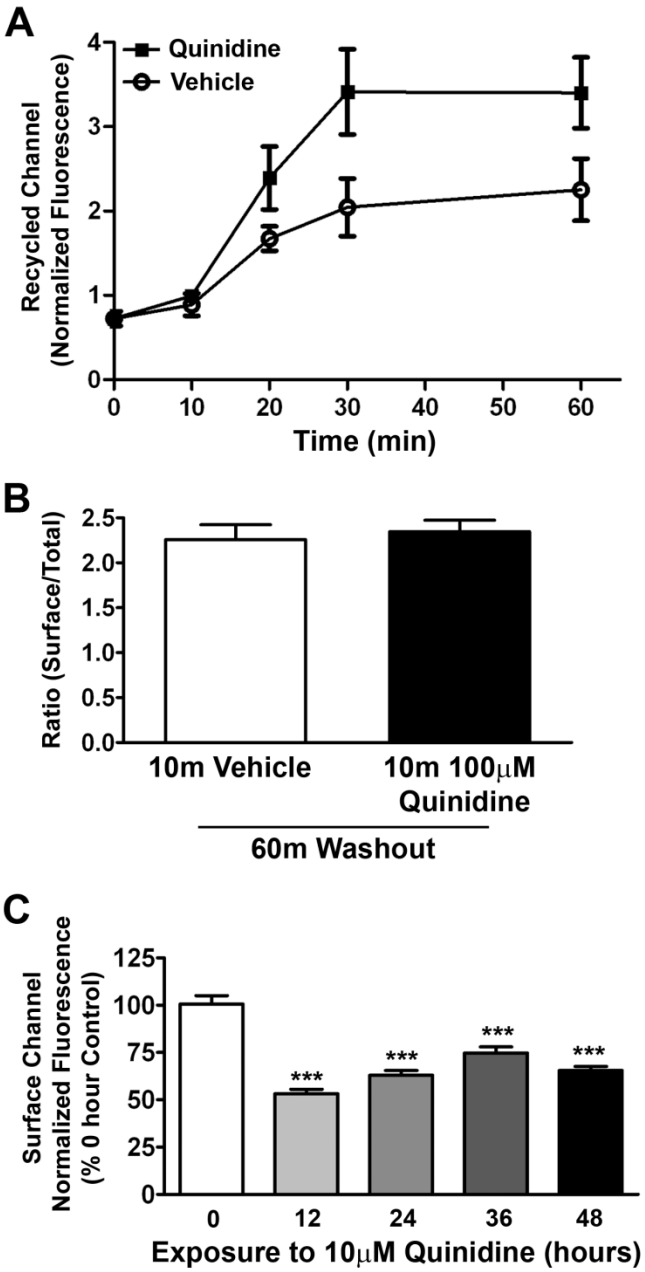

Figure 2.16 Recovery of surface Kv1.5 following acute, but not chronic, quinidine treatment.

(A) Quantification of recycled Kv1.5 at 0, 10, 20, 30, and 60 min at 37˚C post treatment with 100 μmol/L quinidine for 10 min at 37˚C. **(B)** HL-1 cells expressing Kv1.5-GFP were surface labeled with anti-GFP antibody, incubated 10 min in 100μmol/L quinidine at 37°C, and incubated 60 min in drug-free medium at 37°C, and surface Kv1.5 was quantified. **(C)** Quantification of surface Kv1.5, in HL-1 cells stably expressing Kv1.5, following treatment for 0, 12, 24, 36, or 48 hours at 37°C with 10μmol/L quinidine. *** indicates $p < 0.001$ as determined by one-way ANOVA with Tukey post-test.

CHAPTER 3

A ROLE FOR MYOSIN V MOTOR PROTEINS IN THE SELECTIVE DELIVERY OF KV CHANNEL ISOFORMS TO THE MEMBRANE SURFACE OF CARDIAC MYOCYTES

ABSTRACT

Rationale: Kv1.5 (KCNA5) mediates the I_{Kur} current that controls atrial action potential duration. Given its atrial-specific expression and alterations in human atrial fibrillation (AF), Kv1.5 has emerged as a promising target for treatment of AF. Contribution of drug-induced internalization to pore block of Kv1.5, highlights the importance of channel trafficking in drug development. A necessary step in the development of novel agents that selectively modulate trafficking pathways is identification of the cellular machinery controlling surface density, of which little is yet known.

Objective: To investigate the role of the unconventional myosin V motors in determining the cell surface density of Kv1.5.

Methods and Results: Western Blot analysis confirmed myosin Va and Vb expression in the heart, while disruption of endogenous motors selectively reduced I_{Kur} current in adult rat cardiomyocytes. Dominant negative (DN) myosin V constructs and shRNA silencing demonstrated a role for Va and Vb in the surface trafficking of Kv1.5, but not hERG (KCNH2). Live-cell imaging of Kv1.5-GFP and retrospective labeling of actin tracts demonstrated motility of Kv1.5 vesicles. Myosin Va participated in anterograde trafficking, while myosin Vb regulated post-endocytic recycling. Over-expression of

mutant motors revealed a selective role for Rab 11 in coupling myosin Vb to Kv1.5 recycling.

Conclusions: Myosin Va and Vb control functionally distinct steps in the surface trafficking of Kv1.5. These isoform-specific trafficking pathways determine the Kv1.5-encoded I_{Kur} in adult myocytes to regulate repolarizing current and consequently cardiac excitability. Therapeutic strategies that manipulate specific trafficking pathways may prove useful in treatment of cardiovascular arrhythmias.

INTRODUCTION

The diversity and cell surface density of cardiovascular ion channels determines electrical profiles in the heart. In the human atria, the voltage-gated potassium channel Kv1.5 underlies a major repolarizing current I_{Kur}. The role of I_{Kur} in the control of action potential duration and atrial refractory period highlights its importance in atrial excitability and recognition as a major target for the treatment of AF. Despite the emergence of multiple compounds, some with promising atrial selectivity, effective cardioversion by I_{Kur} blockers as well as clinical efficacy and safety has yet to be achieved. Our recent demonstration of selective antiarrhythmic drug-induced internalization of Kv1.5 in atrial myocytes suggests a novel therapeutic avenue for acute termination of AF through alterations in ion channel trafficking. One complication to this strategy is that during paroxysmal and persistent atrial fibrillation (AF), there is a marked reduction in I_{Kur} that is accompanied by a decrease in Kv1.5 protein expression.[144] This contribution to electrical remodeling and evidence of decreased Kv1.5 sensitivity to

antiarrhythmic compounds during chronic AF[145] highlights the need for understanding the molecular mechanisms regulating Kv1.5 surface density.

Chronic AF is characterized by both electrical and structural remodeling that includes cytoskeletal rearrangement during the progression of this disease.[25, 146-148] Given that protein trafficking is thought to occur through a cooperation of long-range trafficking along microtubules and short-range movement along actin filaments in the periphery, such a disruption could significantly abrogate cell surface levels and localization of cardiovascular ion channels. There is evidence for elements of the microtubule and actin cytoskeleton in the regulation of Kv1.5 current.[94, 101, 103, 107, 109-112, 142, 149, 150] In general, however, the molecular machinery including the precise identities of the molecular motors and adaptors regulating ion channel trafficking in the cardiovascular system remain unknown.

Cell surface density of ion channels is controlled by a balance of anterograde and retrograde trafficking. Previously, our lab has shown that Kv1.5 undergoes constitutive internalization and recycling at the atrial myocyte membrane.[111] Internalization occurs through a dynamin-dependent, dynein-mediated microtubule pathway.[50, 111, 112] Internalized channel is then sorted into rab-dependent endocytic compartments, where association with Rab4- or Rab11-containing vesicles targets the channel for recycling back to the myocyte membrane, while association with Rab7-containing vesicles denotes degradation.[111-113] An understanding of the mechanistic intricacies and how they differ for individual ion channels may reveal novel therapeutic targets for the regulation of channel densities and treatment of cardiovascular disease. Here we report, for the first time, the role of unconventional myosin motors Va and Vb in determining the cell

surface level of Kv1.5 in cardiomyocytes, with myosin Vb coupling to Rab 11 for channel recycling.

RESULTS

Unconventional Myosin Motors Va and Vb Play a Functional Role in Determining I_{Kur} Current in Adult Rat Myocytes.

Kv1.5 trafficking and cell surface density depends upon interaction with the actin cytoskeleton. Disruption of the actin cytoskeleton with cytochalasin D has been shown to alter surface levels and current density of Kv1.5.[94, 103] Moreover, Kv1.5 has been shown to directly interact via an N-terminal/core (T1) region with PDZ domains of PSD-95, SAP97, and alpha-actinin-2 in a manner critical for determining functional cell surface channel.[99, 101, 103, 107, 109] While these data provide a link to the actin cytoskeleton, they do not address the potential trafficking of Kv1.5 along actin filaments for plasma membrane delivery. Two candidate unconventional myosin motors, myosin Va and myosin Vb, transport cargo along actin filaments and have been shown to play a critical role in normal function and excitability in a number of cell types.[151] While much has been discovered about the function of these motor proteins in the brain, little is known regarding their role in the excitability and function of cardiomyocytes. Previous reports indicate that myosin Va and Vb mRNA is detected in the heart.[152, 153] In order to demonstrate whether these myosin motor proteins were endogenously expressed in the cardiovascular system, we performed western blot analysis on lysates of rat heart, as well as HL-1 immortalized mouse atrial myocytes. Compared to brain lysate controls,

labeling with isoform-specific antibodies demonstrated endogenous myosin Va and myosin Vb expression in both rat heart and HL-1 atrial myocytes (Figure 1A).

To address the importance of myosin Va and myosin Vb in determining Kv1.5 current levels in native myocytes, we developed adenoviral vectors coding for the cargo-binding domain of myosin Va or Vb, which function as dominant-negative constructs by sequestering cargo in the presence of the endogenous motor.[154] Infection of acutely dissociated adult rat ventricular myocytes with adenovirus was confirmed by visualization of fluorescence from RFP fused to both myosin V DN isoforms (Figure 1B). Isolation of the I_{Kur} current from adult myocytes was achieved by sequential whole cell voltage clamp traces using a -40 mV prepulse to inactivate I_{to} and a 10 min treatment with 50 μmol/L 4-Aminopyridine (4-AP) to selectively inhibit I_{Kur} (Figure 1C). The remaining I_{ss} was then subtracted from the previous trace ($I_{Kur} + I_{ss}$) to achieve a measure of I_{Kur}. Infection with myosin Va DN or myosin Vb DN adenovirus resulted in a significant decrease in I_{Kur} current in acutely dissociated adult rat ventricular myocytes 24 post infection, with a 53 ± 8% and 58 ± 6% decrease in I_{Kur}, respectively ($n \geq 7$ myocytes; $p < 0.01$ and 0.001, respectively) (Figure 1D). Interestingly, myosin V DN infection did not alter corresponding I_{ss} current in adult myocytes, demonstrating a lack of generalized toxicity due to adenoviral infection. Myosin Va and Vb are endogenously expressed in the heart, and interference with myosin V-dependent trafficking results in a decrease in the Kv1.5-encoded I_{Kur} current in cardiomyocytes.

Myosin Va and Vb Control Steady-state Cell Surface Levels of Kv1.5.

The selective decrease in I_{Kur} could be the result of alterations in channel conductance or in the cell surface density of Kv1.5 channel protein. In order to investigate the underlying mechanism for the reduction in I_{Kur}, studies were initiated in HL-1 immortalized mouse atrial myocytes expressing an extracellular GFP epitope-tagged Kv1.5 construct that mimics wild-type channel function.[50, 111] In agreement with our native myocyte data, under whole cell voltage clamp, co-expression with myosin Va DN or myosin Vb DN resulted in a significant decrease in Kv1.5 current density (64 ± 29% and 34 ± 28% decrease in current density, respectively; $n \geq 5$) (Figure 2A). This decrease in current density was greater in the presence of both myosin V DN isoforms, resulting in a 92 ± 4% decrease in Kv1.5 current. To determine whether the decrease in current density was the result of a decrease in cell surface trafficking, we measured the effect of co-expression of myosin Va DN or myosin Vb DN on steady-state cell surface levels of Kv1.5. We found that co-expression of myosin Va DN or myosin Vb DN with Kv1.5 resulted in a 47 ± 2% and 32 ± 3% decrease in surface channel, respectively ($n \geq 73$, $p < 0.001$) (Figure 2B, Supplemental Figure 1A). Co-expression with both myosin V DN constructs further reduced cell surface Kv1.5 by 63 ± 2%. In contrast, co-expression with either or both myosin V DN constructs did not alter the cell surface levels of extracellular tagged hERG-GFP ($n \geq 27$) (Figure 2C, Supplemental Figure 1B). This is consistent with the myocyte data demonstrating no effect of the myosin V DNs on I_{ss} current, encoded by hERG and Kv2.1. The decrease in Kv1.5, not hERG, surface channel density indicates that myosin V motors may act selectively to traffic Kv channel isoforms.

As an alternative, but complimentary approach for testing the role for myosin V motor proteins in the control of Kv1.5 surface density, we used a gene silencing

approach. We generated short hairpin RNA (shRNA) constructs targeted specifically against endogenous myosin Va and myosin Vb, which can avoid potential off-target effects with dominant-negative strategies. To control for transfection efficiency the shRNA constructs were expressed using lentiviral vector infection. The shRNA was shown to effectively downregulate the expression of recombinant myosin Va and Vb in transfected HL-1 myocytes (Supplemental Figure 2B, C). shRNA knockdown resulted in a 53 ± 3% and 36 ± 9% decrease in myosin Va in response to shRNA Va 1 and Va 2, respectively ($n = 3$; $p < 0.001$ and 0.01, respectively) and a 54 ± 10% and 56 ± 9% decrease in myosin Vb in response to shRNA Vb 1 and Vb 2, respectively ($n = 3$, $p < 0.001$) with no effect of scrambled shRNA virus. As an additional control for shRNA specificity, HL-1 cells were transfected with myosin Va or myosin Vb carrying silent mutations (myosin V resistant) that create a partial mismatch with the shRNA sequence. Under these conditions, no decrease in corresponding myosin V motor protein expression was observed upon infection with myosin Va or Vb shRNA.

With the effectiveness and specificity of the myosin gene silencing established, we measured the effects on Kv1.5 surface density. Importantly, infection of cells expressing only Kv1.5-GFP resulted in a significant decrease in cell surface levels of channel in response to the myosin Va or Vb shRNA, but not the scrambled shRNA (Figure 2D, Supplemental Figure 2A). This led to a 59 ± 2% and 51 ± 2% decrease after infection with myosin Va and Vb shRNA, respectively, with a significant difference between the two ($n \geq 93$; $p < 0.001$). Therefore, myosin Va- and myosin Vb-mediated trafficking plays a role in determining the steady-state cell surface levels and current density of Kv1.5.

Myosin Va and Vb Regulate the Intracellular Trafficking of Kv1.5 along Actin Filaments at the Periphery of the Myocyte.

To investigate whether the decrease in Kv1.5 surface levels was due to a loss in channel trafficking on actin filaments, we first confirmed a role for the intact actin cytoskeleton in modulating surface density of the channel. Acute treatment with cytochalasin D to inhibit actin polymerization resulted in a time-dependent decrease in surface Kv1.5 that was significant after one hour and culminated in a $56 \pm 6\%$ decrease after 6hr ($n \geq 85$; $p < 0.001$) (Figure 3A, Supplemental Figure 3). To directly demonstrate the motility of Kv1.5 vesicles on actin filaments within myocytes, we performed live-cell, time-lapse imaging of Kv1.5-containing vesicles followed by retrospective immunofluorescence labeling and static imaging of the actin cytoskeleton (Figure 3B, Supplemental Movie 1). Kv1.5-GFP labeled vesicles were clearly visualized moving on phalloidin-labeled actin tracts at the myocytes periphery. Retrospective labeling of both phalloidin and tubulin showed Kv1.5-GFP vesicles moving in the anterograde direction on microtubules and transitioning to actin filaments at the myocyte edge (Supplemental Movie 2). To measure the ensemble characteristics of Kv1.5-GFP motility events, we used a standard deviation (SD) map to sum all motility events of a time series into one image.[149] An overlay of the SD map of Kv1.5-GFP with a retrospectively labeled image of the actin cytoskeleton clearly demonstrates movement of Kv1.5-containing vesicles on linear tracts marked by phalloidin (Figure 3C). This processivity of Kv1.5-containing vesicles on actin is lost in the presence of myosin Va DN or myosin Vb DN co-expression. Quantification of trafficking events revealed that co-expression with either myosin V DN construct

significantly reduced both the average distance traveled and average net velocity of Kv1.5-contatining vesicles along actin filaments (Figure 3D).

Kv1.5 alone exhibited an average travel distance of 0.8 μm and velocity of approximately 0.4 μm/s (400 nm/s) consistent with previous literature,[155-159] whereas co-expression with myosin Va DN and myosin Vb DN resulted in a 30 ± 1% and 33 ± 2% decrease in distance and velocity, respectively ($n = 20$ tracks from 16 cells, 17 tracks from 4 cells, and 9 tracks from 2 cells for Kv1.5 alone, Kv1.5 + myosin Va DN, and Kv1.5 + myosin Vb DN, respectively; $p < 0.001$). Myosin Va and Vb contribute to the actin-based transport of Kv1.5 vesicles in HL-1 myocytes.

Myosin V Isoforms Act at Distinct Steps in the Kv1.5 Trafficking Pathway.

The additive nature of the myosin Va- and Vb-mediated decrease in current density and surface levels suggested that these two myosin V isoforms may function in different steps in the trafficking pathway of Kv1.5 (Figure 2B). Myosin Va contributes to anterograde trafficking in a number of cell types,[160-162] while myosin Vb is implicated in the post-endocytic recycling of a number of proteins.[163-167] Therefore, we next tested if this functional distinction of myosin Va and Vb in intracellular trafficking may be conserved in the cardiovascular system with Kv1.5. Previously, we demonstrated acute inhibition of constitutive endocytosis of Kv1.5 with Dynasore, a small molecule inhibitor of dynamin.[50] Disruption of dynamin-mediated endocytosis thereby permits investigation of the role of myosin Va and myosin Vb in the pre- and post-endocytic trafficking of Kv1.5. Introduction of a single point mutation S61D into the GTPase domain of dynamin significantly reduces the GTP hydrolysis efficiency resulting in a DN form of dynamin

for chronic inhibition of constitutive endocytosis.[168] As with Dynasore, expression of dynamin S61D significantly increased steady-state cell surface Kv1.5 by 27 ± 5.3%, whereas overexpression of wild-type (WT) dynamin resulted in a 25 ± 2.6% decrease in surface Kv1.5 ($n \geq 110$; $p < 0.001$) (Supplemental Figure 4A, B). More importantly, while co-expression with WT dynamin led to a significant increase, channel internalization was attenuated in the presence of dynamin S61D (Supplemental Figure 4C, D). Co-expression with WT dynamin resulted in a 30 ± 8.6% increase in internalized Kv1.5 versus a 39 ± 7.1% decrease in internalization in the presence of dynamin S61D ($n \geq 69$; $p < 0.05$, 0.001, and 0.01, respectively). Based on these data we utilized co-expression with the DN dynamin to elucidate whether myosin Va and Vb are acting upstream or downstream of channel endocytosis. Dynamin S61D was able to block the myosin Vb DN-mediated decrease in steady-state cell surface Kv1.5 (Figure 4A, Supplemental Figure 5A, B). In contrast, dynamin S61D was not able to alter the decrease in surface Kv1.5 mediated by myosin Va DN ($n \geq 59$; $p < 0.001$). These data suggest that myosin Va acts in the pre- and Vb in the post-endocytic trafficking of Kv1.5. The inability of dynamin S61D to induce an increase in steady-state surface Kv1.5 (Supplemental Figure 4A) in the presence of myosin Vb DN may be the result of the incomplete block of constitutive endocytosis demonstrated in Supplemental Figure 4B. Myosin Vb DN may then inhibit the recycling of residual endocytosed channel. To investigate the potential role of myosin Va in anterograde delivery of Kv1.5 to the plasma membrane we measured the effect of the myosin V DNs at 6hr of channel expression, a time point at which the majority of surface Kv1.5 is derived from anterograde delivery of newly synthesized channel. At 6 hr of expression myosin Va DN, but not myosin Vb

DN, significantly reduced cell surface levels of Kv1.5 (41 ± 4.7%, n ≥ 25) (Figure 4B, Supplemental Figure 6A, B). Myosin Va and Vb act in two distinct steps in the cell surface trafficking of Kv1.5, where myosin Va likely participates in anterograde trafficking to the plasma membrane, while myosin Vb acts in the post-endocytic trafficking of Kv1.5, likely through recycling of channel protein back to the plasma membrane.

Myosin Vb-mediated Channel Recycling is Dependent Upon Coupling to Rab 11.

Interaction of myosin Vb with recycling endosomes has been shown in the literature to occur through the adaptor protein Rab 11.[163-167, 169] Previously, we have demonstrated a role of Rab 11, but not Rab 8, in the post-endocytic recycling of Kv1.5 in atrial myocytes.[111] To test if myosin Vb is associating with Kv1.5-containing vesicles during channel recycling through the adaptor protein Rab 11, we utilized recently characterized mutations in myosin Vb that uncouple association with Rab-GTPases.[170] Co-expression of Kv1.5 with the Rab 11 binding-deficient myosin Vb mutant Y1684E/Q1718R resulted in a 52 ± 1.5% decrease in channel surface density (n ≥ 74, $p < 0.001$) (Figure 5A, Supplemental Figure 7A). In contrast, co-expression with the Rab 8 binding-deficient myosin Vb mutant Q1296L/Y1303C did not significantly alter the steady-state cell surface levels of Kv1.5. We then utilized a live-cell recycling assay to observe the effect of the myosin V DN and Rab binding-deficient mutants on Kv1.5 channel recycling. Using this method, myosin Va DN and Rab 8 binding-deficient myosin Vb QL/YC did not significantly alter Kv1.5 channel recycling (Figure 5B, Supplemental Figure 7B). In contrast, myosin Vb DN and Rab 11 binding-deficient myosin Vb YE/QR significantly

decreased channel recycling, resulting in a 72.5 ± 2.8% and 76 ± 2.2% decrease in recycled channel, respectively ($n \geq 60$, $p < 0.001$). To further demonstrate the necessity of Rab 11 coupling for myosin Vb-mediated recycling of Kv1.5, we co-expressed Kv1.5 together with both the constitutively active (CA) Rab 11 construct and myosin Vb YE/QR. As previously demonstrated, Rab 11 CA co-expression resulted in a significant increase in the steady-state cell surface levels of Kv1.5 (29 ± 3.5%, $n \geq 74$, $p < 0.001$) (Figure 5C, Supplemental Figure 7C). Interestingly, this increase in cell surface Kv1.5 was abrogated by co-expression with myosin Vb YE/QR. Furthermore, this loss of channel recycling through myosin Vb led to an accumulation of Kv1.5 in Rab 11 positive perinuclear endosomes in the presence of myosin Vb DN and Vb YE/QR, but not myosin Va or control (Figure 5D, Supplemental Figure 8). Therefore, Kv1.5 channel recycling via myosin Vb occurs through selective Rab 11-mediated coupling to Kv1.5-contaning endosomes. These coordinate trafficking events contribute to the steady-state cell surface levels of Kv1.5 channel protein and thereby likely play a role in determining the electrical excitability of native cardiac myocytes (Figure 6).

DISCUSSION

Here, we report a previously uncharacterized role of the myosin V motor family in the selective membrane trafficking of Kv1.5 in cardiac myocytes. We elucidated the mechanism by which myosin Va and Vb act in functionally distinct steps in the cell surface trafficking of Kv1.5 to selectively determine I_{Kur} current density in adult myocytes. The subunit specificity and functional specialization demonstrated in this study denotes a potential therapeutic avenue for modulation of I_{Kur} in the treatment AF.

In considering channel trafficking pathways as valid therapeutic targets, it is important to consider that cell surface delivery of cardiovascular ion channels may occur through selective molecular trafficking mechanisms. Unlike Kv1.5, myosin Va and Vb do not play a role in determining cell surface levels of hERG or I_{ss} current. This is somewhat surprising given that Loewen *et al.* demonstrated a common mechanism for K^+ channel retrograde microtubule-dependent trafficking by the dynein motor complex, including Kv2.1, Kv3.1, Kv4.3, hERG, and Kir2.1.[171] In addition, we and others have demonstrated a role for the dynein motor complex in retrograde trafficking of Kv1.5.[111, 112] Potassium channel subunits also demonstrate a conserved mechanism for ER retention of misfolded protein through RXR motifs that are masked during proper protein folding.[76] In contrast, there are distinct differences in the forward trafficking signals of channel subunits, implying a complex system for differential regulation of ER to Golgi trafficking. In addition, different members of the MAGUK family have been shown to interact with specific K^+ channel subunits to direct localization and regulate surface density. In particular, overexpression of SAP97 has been shown to increase surface levels of Kv1.5[99, 107, 109] and down-regulate other Kv channels[108], while CASK participates in the targeting of Kir2 channels[172]. Kv channel subunits also show a significant degree of specialization in their association with actin-binding proteins that effecting their stabilization or trafficking. While alpha-actinin-2 directly interacts with Kv1.5,[94, 103, 110] filamin interacts with Kv4.2[173] and cortactin with Kv1.2[174] to alter the cell surface levels of channel protein. Therefore, while some mechanisms of K^+ channel subunit trafficking may be conserved, there are also specialized steps along the trafficking pathway regulated by selective molecular motors, adaptors, and anchoring

proteins. While additional channels would need to be investigated to determine the extent of selectivity of myosin Va and Vb for Kv1.5 channel trafficking, the data presented here further emphasize the potential for selectivity in ion channel trafficking pathways.

Anterograde trafficking of Kv1.5 likely requires coordination of microtubule-based trafficking with myosin Va-mediated transport. Recent evidence suggests that Kif5b mediates anterograde microtubule-based trafficking of Kv1.5.[150] In addition, our laboratory has recently discovered a role for Kif17 in the post-Golgi transport and cell surface density of Kv1.5.[149] It remains to be determined whether Kif5b and Kif17 represent general or selective mechanisms for Kv channel trafficking. Our live cell imaging data clearly shows the transfer from a microtubule to actin tracts at the cell periphery (Supplemental Movie 2). Evidence of coordinated microtubule- and actin-based trafficking components has sparked significant interest regarding the mechanism by which vesicles are transferred from one cytoskeletal network to the other. One potential mechanism is that kinesin and myosin motors both reside on a single endosomal compartment,[175-177] providing the opportunity to bind to and propagate along either cytoskeletal network in the vicinity of the endosome. Another potential mechanism is the association of Rab GTPases with multiple motor proteins or subunits to link intracellular transport pathways.[169, 178] For instance, Rab 4 interacts both with KIF3B and the light intermediate chain of dynein, while Rab 27a interacts with myosin Va and VIIa.[169] In fact, the Rab GTPase-mediated coupling of distinct endosomal compartments to targeted transport processes has been well characterized.[169] The importance of Rab 11 in myosin Vb-mediated membrane protein recycling has been demonstrated in diverse, non-

cardiovascular systems.[163-167] Rab 11 has also been implicated in non-anterograde delivery of Kv1.5 to the plasma membrane of rat atrial myocytes upon depletion of cholesterol, by an unknown molecular mechanism.[113] Here, we demonstrate a direct coupling of myosin Vb to Rab 11 positive endosomes for the recycling of Kv1.5 in atrial myocytes. None-the-less, the potential involvement of microtubule-based transport in channel recycling and possible role of Rab 11 in both trafficking components remains to be determined. Recent large-scale profiling of Rab GTPase interactions highlights the unknown diversity of their binding partners for directing complex intracellular transport.[178] Future studies are required to fully elucidate whether molecular motors, vesicular adaptors, or both exhibit selectivity for ion channel trafficking.

While the modulation of trafficking pathways may have promise for acute cardioversion of arrhythmias, its role in the treatment of paroxysmal or persistent AF is less clear. AF is a progressive disorder marked by electrical and structural remodeling that becomes more established with prolonged arrhythmia. Electrical remodeling is characterized by a significant decrease in atrial effective refractory period due to alterations in ion channel densities in the membrane.[25] In addition, electrical remodeling of the atria has been demonstrated to alter sensitivity of ion channels to antiarrhythmic drug-mediated block.[145] This may be due in part to the marked decrease in Kv channel surface density during AF,[25] in particular Kv1.5 channel protein and I_{Kur} current,[144] that would decrease the functional channel available for pore block by antiarrhythmic drugs. Therefore, the dependence of Kv1.5 trafficking on actin filaments demonstrated here may provide insight to explain the correlation between electrical and structural remodeling during AF. These two pathophysiologies may be mechanistically linked through the rate-

induced induction of calcium-activated neutral proteases called calpains.[30, 31, 179] Calpains, activated by calcium overload during AF, mainly cleave cytoskeletal and membrane-associated proteins and may underlie the significant decrease in actin protein levels[180] and disorganization of the cytoskeletal networks observed in AF. Calpain has also been implicated in the degradation of alpha-actinin-2 during ischemia reperfusion injury.[181-184] Kv1.5 directly interacts with alpha-actinin-2 through an N-terminal T1/core region and disruption of the actin cytoskeleton with cytochalasin or antisense oligonucleotide knockdown of alpha-actinin-2 alters channel current density.[94, 103, 110] Therefore, given the importance of the intact cytoskeleton and direct interaction with alpha-actinin-2 in determining the cell surface levels of Kv1.5 in myocytes, calpain activation may be a contributing mechanism that links cytoskeletal disruption to the decrease in I_{Kur} during AF. In addition, our results predict that deterioration of the actin cytoskeleton would disrupt myosin-mediated delivery of Kv1.5 to the plasma membrane. Therefore, the ~ 50% decrease in I_{Kur} and Kv1.5 protein levels in AF may reflect a combination of decreased cell surface trafficking and enhanced endocytosis of Kv1.5 leading to channel degradation.

In summary, this report reveals the importance of the myosin V motors Va and Vb in regulating the plasma membrane targeting and cell surface density of Kv1.5 in the myocardium. This is the first report of a role for these motor proteins in the trafficking and regulation of a cardiovascular ion channel with a functional consequence of their disruption. As evidenced by these data, continued elucidation of the molecular machinery involved in cardiovascular ion channel trafficking may reveal novel

therapeutic targets for the regulation of channel densities and treatment of cardiovascular disease.

EXPERIMENTAL PROCEDURES

Materials

Kv1.5-GFP was generated from human Kv1.5 as previously described.[111] HL-1 cells were a generous gift from Dr. William Claycomb (Louisiana State University Health Sciences Center, New Orleans, LA). Polyclonal anti-GFP and Alexa Fluor secondary antibodies were from Invitrogen (Carlsbad, CA). Horseradish peroxidase-conjugated secondary antibodies were from Zymed (San Francisco, CA). Full-length mouse brain isoform myosin Va and rabbit polyclonal anti-myosin Va antibodies DiL2 123 and HAM-5, and full-length mouse myosin Vb and rabbit polyclonal anti-myosin Vb antibodies were from Dr. John Hammer (NIH, Bethesda, MD) and Dr. Michael Ehlers (Duke University, Durham, NC), respectively. Full-length myosin Va and Vb were tagged with 3x-mCherry. Myosin Va dominant-negative (DN)-RFP, myosin Vb DN-RFP, and Rab 11 wild-type (WT) and constitutively active (CA) were provided by Dr. José Esteban (Universidad Autónoma de Madrid, Madrid, Spain). Rab 11 WT was tagged with a c-myc epitope tag. Dynamin WT and S61D were a gift from Dr. Sandra Schmid (The Scripps Research Institute, La Jolla, CA). Dynamin constructs were tagged with an HA epitope tag. Full-length myosin Va and myosin Vb were tagged with 3x-mCherry and myosin Vb Y1684E/Q1718R and Q1296L/Y1303C were generated from full-length myosin Vb 3x-mCherry using the QuikChange® site-directed mutagenesis kit from

Stratagene (Santa Clara, CA). Mouse anti-HA was purchased from Covance (Princeton, New Jersey). Mouse anti-myc 9E10 was provided by Dr. Kristen Verhey. Biotin-conjugated goat anti-rabbit secondary antibody was purchased from Jackson ImmunoResearch Laboratories (West Grove, PA). Cy5-Streptavidin secondary antibody was purchased from GE Healthcare (Piscataway, NJ). Cytochalasin D from Sigma (St. Louis, MO) was dissolved in DMSO and diluted 1:1000 in culture medium. All vehicle treatments were DMSO diluted 1:1000 in culture medium equivalent to drug addition. DNA transfection of HL-1 cells was carried out using Lipofectamine 2000 reagent (Invitrogen), according to the manufacturer's specifications. Lipofectamine 2000 was used at a ratio of 3:1 (3 μL Lipofectamine 2000 per 1 μg of DNA) in Opti-MEM I (Invitrogen). 0.5 μg of DNA was used for each construct transfected. DsRed, more specifically pDsRed2-C1 from Clontech (Mountain View, CA), was used as a transfection control.

Western Blot Analysis

HL-1 cells were harvested by resuspension in lysis buffer (50 mmol/L tris/HCl, 150 mmol/L NaCl, 5 mmol/L EDTA, 1% Triton) containing Complete® protease inhibitors (Roche Applied Science, Indianapolis, IN). 40 μg of cell lysis sample was run on a NuPAGE, Novex 4-12% Bis-Tris acrylamide gel (Invitrogen). After electrophoretic transfer to nitrocellulose, membranes were incubated with primary anti-myosin Va, anti-myosin Vb, or anti-tubulin (Sigma) antibodies (1:1000, 1:1000 or 1:2000 dilution respectively) for 1 hour at room temperature. Bound primary polyclonal antibody was detected with a 1:5000 dilution of HRP-conjugated goat anti-rabbit IgG (Invitrogen) for anti-myosin Va and anti-myosin Vb antibodies, or HRP-conjugated goat anti-mouse IgG

(Invitrogen) for anti-tubulin antibody and visualized using the Western Lightning enhanced chemiluminescent reagent according to the manufacturer's protocol (Perkin-Elmer Life Sciences, Wellesley, MA). Images were captured using the EpiChemi3 Darkroom (UVP, Inc., Upland, CA).

Adenovirus Preparation

Myosin Va DN-RFP and myosin Vb DN-RFP were first cloned into the vector pENTR. Adenoviral constructs were generated using the vector pAD/V5/-dest (Invitrogen). Adenoviral constructs were digested with PacI and transfected into HEK293 cells. Crude viral lysates were produced from 10cm dishes and adenovirus was amplified by infection of HEK293 cells in 60 mm dishes. Virus was purified using the Virapur Adenovirus mini purification Virakit (Virapur, San Diego, CA) according to the manufacturer's recommendations.

Adult Rat Ventricular Myocyte Isolation

The procedures used in this study were in accordance with the guidelines of the University of Michigan Committee on the Use and Care of Animals. Veterinary care was provided by the University of Michigan Unit for Laboratory Animal Medicine. The animal care and use program conformed to the standards in the *Guide for the Care and Use of Laboratory Animals* (NIH Publication No. 85-23, Revised 1996). Adult rat ventricular myocytes were isolated using previously established protocols.[185] Briefly, Sprague-Dawley rats (~200g) were injected with 1500 U/Kg heparin. Following

dissection, each heart was mounted on a modified Langendorff apparatus and perfused for 2 min with oxygenated KHB-A (pH=7.4; in mmol/L: NaCl 118; KCl 4.8; Hepes 25; K2HPO4 1.25; MgSO4 1.25; Glucose 11; CaCl2 1), followed by 5 min perfusion of oxygenated KHB-B (pH=7.4; in mmol/L: NaCl 118; KCl 4.8; Hepes 25; K2HPO4 1.25; MgSO4 1.25; Glucose 11). A recirculating enzyme solution (KHB-B perfusate containing ~0.5 mg/mL of collagenase type II and 0.017% blebbistatin), was applied for 13 min. Isolated hearts were finely minced, gently run through a pipette, and cells were collected in sequential fractions. Cells were resuspended in KHB-A containing 2% BSA and 0.1% (v/v) blebbistatin, followed by resuspension in supplemented growth media 199 containing 26 mmol/L NaHCO3,10 mmol/L L-glutathione, 0.2 g/L BSA, 5% FBS and 1% P/S. Coverslips were precoated with Laminin and cells were plated at $2x10^4$ cells/coverslip for 2 hours at 37°C. After the initial 1 hour, serum-free supplemented growth media was added to the cells with 20 µL of myosin Va DN or myosin Vb DN adenovirus (~$0.7\text{-}1x10^{12}$ particles/mL) per 200 µL medium. After 1 hour an additional 2 mL of serum-free supplemented growth media was added. Media was replaced 24 hr post-infection and electrophysiological recordings were taken.

Electrophysiology

For electrophysiological studies of HL-1 cells, recordings were performed on cells transiently expressing Kv1.5-GFP alone or co-expressing myosin Va DN-RFP, myosin Vb DN-RFP, or both DN isoforms. Whole-cell voltage clamp experiments were performed as described previously.[142] The intracellular pipette solution contained (in

mmol/L): Potassium aspartate 110, KCl 20, NaCl 8, HEPES 10, K_2ATP 4, CaCl2 1, $MgCl_2$ 1, and K_2BAPTA 10; and was adjusted to pH 7.2 with KOH. The bath solution contained (in mmol/L): NaCl 110, KCl 4, $MgCl_2$ 1, $CaCl_2$ 1.8, HEPES 10, and glucose 1.8; and was adjusted to pH 7.35 with NaOH. All currents were normalized to the peak current measured at +60 mV for each cell tested. For electrophysiological studies of adult rat ventricular myocytes, current mediated by Kv1.5 (I_{Kur}) was determined using a series of 2 voltage protocols in conjunction with pharmacological inhibition of Kv1.5. Ca^{2+} current was inhibited by the addition of 200 µM CdCl to the bath solution. Total current was obtained using a single 500 ms depolarizing pulse from -80 mV to +30 mV. The I_{Kslow} (I_{Kur} + I_{ss}) current component was then isolated by the addition of a 100 ms pre-pulse to -40 mV to inhibit Na^+ current and current mediated by Kv4.x channels (I_{to}), prior to depolarization to +30 mV. The I_{ss} (current mediated by Kv2.1 and hERG) current component was then isolated by perfusion with 50 µmol/L 4-AP prior to running the second voltage protocol. I_{Kur} was obtained by electronic subtraction as the difference between I_{Kslow} and I_{ss}.

Immunocytochemistry

Immunocytochemistry was performed and analyzed as previously described.[111]

To measure steady-state surface Kv1.5 and hERG in the presence of myosin Va and Vb DN, HL-1 cells were transfected with either Kv1.5-GFP or hERG-GFP co-transfected with DsRed, myosin Va DN-RFP, myosin Vb DN-RFP or both myosin Va and Vb DN-RFP. 48 hr post transfection, HL-1 cells were live cell stained with a polyclonal anti-GFP antibody (1:500) in 2% goat serum for 40 min on ice to minimize

internalization of membrane proteins. For surface labeling, cells were then incubated with goat anti-rabbit Alexa Fluor 405 secondary antibody (1:500) in 2% goat serum for 45 min on ice, fixed with 4% paraformaldehyde for 10 min on ice, and mounted with ProLong Gold anti-fade reagent (Invitrogen).

To measure steady-state surface Kv1.5 in the presence of myosin Va and Vb shRNA, HL-1 cells were transfected with Kv1.5-GFP either alone, or co-infected with either scrambled, myosin Va, or myosin Vb shRNA lentivirus. 48 hr post transfection, HL-1 cells were live cell stained with a polyclonal anti-GFP antibody (1:500) in 2% goat serum for 40 min on ice to minimize internalization of membrane proteins. For surface labeling, cells were then incubated with goat anti-rabbit Alexa Fluor 405 secondary antibody (1:500) in 2% goat serum for 45 min on ice, fixed with 4% paraformaldehyde for 10 min on ice, and mounted with ProLong Gold.

To measure steady-state surface Kv1.5 in the presence of cytochalasin D, HL-1 cells were transfected with Kv1.5-GFP. 48 hr post transfection, HL-1 cells were treated with DMSO for 30 min and 6 hr and with cytochalasin D for 30 min, 1 hr, 2 hr, 4 hr, or 6 hr at 37°C. HL-1 cells were then live cell stained with a polyclonal anti-GFP antibody (1:500) in 2% goat serum for 40 min on ice to minimize internalization of membrane proteins. For surface labeling, cells were then incubated with goat anti-rabbit Alexa Fluor 405 secondary antibody (1:500) in 2% goat serum for 45 min on ice, fixed with 4% paraformaldehyde for 10 min on ice, and mounted with ProLong Gold.

To measure steady-state surface Kv1.5 in the presence of dynamin WT or S61D, HL-1 cells were transfected with Kv1.5-GFP and co-transfected with DsRed, dynamin WT-HA, or dynamin S61D-HA. 48 hr post transfection, HL-1 cells were live cell stained

with a polyclonal anti-GFP antibody (1:500) in 2% goat serum for 40 min on ice to minimize internalization of membrane proteins. For surface labeling, cells were then incubated with goat anti-rabbit Alexa Fluor 405 secondary antibody (1:500) in 2% goat serum for 45 min on ice. Cells were then fixed with 4% paraformaldehyde for 10 min on ice, permeabilized with 0.1% Triton X-100 in 2% goat serum for 10 min on ice, and labeled for dynamin expression by incubation with mouse anti-HA (1:500) in 2% goat serum for 40 min on ice, followed by incubation with goat anti-mouse Alexa Fluor 594 antibody (1:500) in 2% goat serum for 40 min on ice and mounted with ProLong Gold.

To measure internalized Kv1.5 in the presence of dynamin WT or S61D, HL-1 cells were transfected with Kv1.5-GFP and co-transfected with DsRed, dynamin WT-HA, or dynamin S61D-HA. 48 hr post transfection, HL-1 cells were live cell stained with a polyclonal anti-GFP antibody (1:500) in 2% goat serum for 40 min on ice to minimize internalization of membrane proteins. Cells were then incubated at 37°C for 0 or 30 min to allow for internalization of channel with primary antibody prior to incubation with goat anti-rabbit Alexa Fluor 405 antibody (1:200) in 2% goat serum for 45 min on ice to saturate remaining surface channel populations. Cells were then fixed with 4% paraformaldehyde for 10 min on ice, permeabilized with 0.1% Triton X-100 in 2% goat serum for 10 min on ice, and internalized channel was labeled by incubation with goat anti-rabbit Alexa Fluor 647 antibody (1:500) in 2% goat serum for 35 min on ice. Dynamin expression was then labeled by incubation with mouse anti-HA (1:500) in 2% goat serum for 40 min on ice, followed by incubation with goat anti-mouse Alexa Fluor 594 antibody (1:500) in 2% goat serum for 40 min on ice and mounted with ProLong Gold.

To measure steady-state surface Kv1.5 in the presence of myosin Va or Vb DN and dynamin S61D, HL-1 cells were transfected with Kv1.5-GFP and co-transfected with DsRed, myosin Va DN-RFP, myosin Va DN-RFP + dynamin S61D-HA, myosin Vb DN-RFP, or myosin Vb DN-RFP + dynamin S61D-HA. 48 hr post transfection, HL-1 cells were live cell stained with a polyclonal anti-GFP antibody (1:500) in 2% goat serum for 40 min on ice to minimize internalization of membrane proteins. For surface labeling, cells were then incubated with goat anti-rabbit Alexa Fluor 405 secondary antibody (1:500) in 2% goat serum for 45 min on ice. Cells were then fixed with 4% paraformaldehyde for 10 min on ice, permeabilized with 0.1% Triton X-100 in 2% goat serum for 10 min on ice, and labeled for dynamin expression by incubation with mouse anti-HA (1:500) in 2% goat serum for 40 min on ice, followed by incubation with goat anti-mouse Alexa Fluor 647 antibody (1:500) in 2% goat serum for 40 min on ice and mounted with ProLong Gold.

To measure newly-synthesized surface Kv1.5 in the presence of myosin Va or Vb DN, HL-1 cells were transfected with Kv1.5-GFP and co-transfected with DsRed, myosin Va DN-RFP or myosin Vb DN-RFP. At 6 hr of expression (post the 4 hr incubation in serum-free medium for transfection) HL-1 cells were live cell stained with a polyclonal anti-GFP antibody (1:500) in 2% goat serum for 40 min on ice to minimize internalization of membrane proteins. For surface labeling, cells were then incubated with goat anti-rabbit Alexa Fluor 405 secondary antibody (1:500) in 2% goat serum for 45 min on ice, fixed with 4% paraformaldehyde for 10 min on ice, and mounted with ProLong Gold.

To measure steady-state surface Kv1.5 in the presence of the myosin Vb mutants, HL-1 cells were transfected with Kv1.5-GFP and co-transfected with DsRed, myosin Vb mutant Y1684E/Q1718R-mCherry (Rab 11 binding-deficient), or myosin Vb mutant Q1296L/Y1303C-mCherry (Rab 8 binding-deficient). 48 hr post transfection, HL-1 cells were live cell stained with a polyclonal anti-GFP antibody (1:500) in 2% goat serum for 40 min on ice to minimize internalization of membrane proteins. For surface labeling, cells were then incubated with goat anti-rabbit Alexa Fluor 405 secondary antibody (1:500) in 2% goat serum for 45 min on ice, fixed with 4% paraformaldehyde for 10 min on ice, and mounted with ProLong Gold.

To measure recycled Kv1.5 in the presence of the myosin DNs and myosin Vb mutants, HL-1 cells were transfected with Kv1.5-GFP and co-transfected with DsRed, myosin Va DN-RFP, myosin Vb DN-RFP, myosin Vb mutant Y1684E/Q1718R-mCherry (Rab 11 binding-deficient), or myosin Vb mutant Q1296L/Y1303C-mCherry (Rab 8 binding-deficient). 48 hr post transfection, HL-1 cells were live cell stained with a polyclonal anti-GFP antibody (1:500) in 2% goat serum for 40 min on ice to minimize internalization of membrane proteins. Cells were then incubated at 37°C for 30 min to allow for internalization of channel with primary antibody. Cells were then incubated with goat anti-rabbit Alexa Fluor 405 antibody (1:200) in 2% goat serum for 45 min on ice to saturate remaining surface channel populations. Cells were then returned to 37°C for 60 min, removed, and incubated with goat anti-rabbit biotinylated antibody (1:500) in 2% goat serum for 40 min on ice. Cells were then incubated with streptavidin-Cy5 (1:500) in 2% goat serum for 40 min on ice, and mounted with ProLong Gold.

To measure steady-state surface Kv1.5 in the presence of Rab 11 CA and Rab 11 binding-deficient myosin Vb, HL-1 cells were transfected with Kv1.5-GFP and co-transfected with DsRed, Rab 11 CA-RFP, myosin Vb mutant Y1684E/Q1718R-mCherry (Rab 11 binding-deficient), or Rab 11 CA-RFP and myosin Vb mutant Y1684E/Q1718R-mCherry. 48 hr post transfection, HL-1 cells were live cell stained with a polyclonal anti-GFP antibody (1:500) in 2% goat serum for 40 min on ice to minimize internalization of membrane proteins. For surface labeling, cells were then incubated with goat anti-rabbit Alexa Fluor 405 secondary antibody (1:500) in 2% goat serum for 45 min on ice, fixed with 4% paraformaldehyde for 10 min on ice, and mounted with ProLong Gold.

To observe co-localization of Kv1.5 with Rab 11 positive endosomes, HL-1 cells were transfected with Kv1.5-GFP and co-transfected with Rab 11-myc and with DsRed, myosin Va DN-RFP, myosin Vb DN-RFP, or myosin Vb mutant Y1684E/Q1718R-mCherry (Rab 11 binding-deficient). 48 hr post transfection, HL-1 cells were live cell stained with a polyclonal anti-GFP antibody (1:500) in 2% goat serum for 40 min on ice to minimize internalization of membrane proteins. Cells were then incubated at 37°C for 30 min to allow for internalization of channel with primary antibody. Cells were then incubated with goat anti-rabbit Alexa Fluor 405 antibody (1:200) in 2% goat serum for 45 min on ice to saturate remaining surface channel populations. Cells were then returned to 37°C for 60 min, removed, fixed with 4% paraformaldehyde for 10 min on ice, permeabilized with 0.1% Triton X-100 in 2% goat serum for 10 min on ice, and labeled for Rab 11 expression by incubation with mouse anti-myc (1:500) in 2% goat serum for

40 min on ice, followed by incubation with goat anti-mouse Alexa Fluor 647 antibody (1:500) in 2% goat serum for 40 min on ice and mounted with ProLong Gold.

Images of transfected cells displaying fluorescent signals were acquired on an Olympus Flouview 500 confocal microscope with a 60 by 1.35 N.A. oil objective or a Nikon TI81 A1R confocal microscope with a 60 by 1.40 N.A. oil objective. Signal intensities were adjusted so that the maximal pixel intensities were at least half saturation. Images were obtained by taking a series of images every 0.5 μm through the cell (generally 3–4 μm) and combining the images into a composite Z-stack. To minimize effects of overexpression on Kv1.5-GFP localization, we analyzed only cells with low to mid levels of expressed protein. Each immunocytochemical experiment was performed a minimum of three times. While the microscope settings were optimized for each experimental group, they were kept consistent for every repetition of a given experiment. For every repetition of a given experiment, 10-20 images were acquired for each condition. Overall, approximately 30-100 cells were analyzed for each condition of an experimental group. Fluorescent signals of Z-stacks were quantified with ImageJ software (NIH, Bethesda, MD) by drawing a region of interest around each analyzable cell and a neighboring untransfected cell in the image and measuring the average fluorescence intensity for each fluorescent signal for every region of interest. To determine specific fluorescence, the average fluorescence intensity measured for each fluorescent signal from a neighboring untransfected cell was subtracted from the corresponding fluorescent signal measured for each transfected cell. The ratio of surface, internalized, or recycled Kv1.5 fluorescent signals to total Kv1.5-GFP fluorescence was then calculated for each cell. Normalized surface, internalized, and recycled Kv1.5

values were then expressed as percent change from the control condition. Statistical analysis was performed using Prism 5 software from GraphPad Prism Software (San Diego, CA). The resolution obtained in these imaging experiments was 512 by 512 pixels with a z resolution of 0.5μm for each filter set.

Design of shRNA and shRNA Resistant Constructs of Myosin Va and Vb

Four shRNA sequences targeting myosin Va and Vb were designed using shRNA sequence designer (Invitrogen). Sequences used to target myosin Va were as follows: 5'-GCAAAGCACATCTATGCAAAG (nucleotides 1210-2130 – Va 1) and 5'-GATCATTGCTGAC ATCAAC (nucleotides 4632-4650 – Va 2). Sequences used to target myosin Vb were as follows: 5'-GGACCTACCTGACTTCTTCA (nucleotides 2096-2116 – Vb 1) and 5'-GCTGAAGGC CCTCAAGATTGA (nucleotides 2709-2729 – Vb 2). The scrambled shRNA sequence had the same nucleotide composition as shRNA targeting myosin Vb (nucleotides 2709-2729) but with randomized order creating mismatch with any mRNA sequence in the mouse nucleotide database: 5-GCAAGCGATACGGCGACTTTA (siRNA Wizard). For shRNA resistant myosin constructs, the QuikChange® site-directed mutagenesis kit (Stratagene) was used to make silent mutations in wild-type myosin Va (C1218T, C1221T and T1224C) and wild-type myosin Vb (C2718A, C2719T, C2721A and G2724A) to create partial mismatch between the shRNA sequence and targeted mRNA.

Lentiviral Vector Construction, Virus Production, and Infection

Plasmids containing myosin Va, myosin Vb or scrambled shRNA were constructed by Lenlox3.7 in order to obtain lentivirus. Five pairs of complementary DNA oligo nucleotides containing shRNA sequences were synthesized by IDT (Integrated DNA technologies) and hybridized to generate dsDNA. Each dsDNA was cloned into a lenlox 3.7 vector and the recombinant lentiviral vectors were produced by transfection into human HEK293T cells. 48 hours post transfection, viral supernatants were collected and filtered through a 0.45 um filter. To find a minimum effective multiplicity of infection (MOI), several MOI doses (1, 5, 10, 20 µl) of lentiviral preparations were used to infect HL-1 cells. The minimum effective dose was estimated by qRTPCR after 48 hours of infection (data not shown). Following transfection, growth media was added to the HL-1 cells with 20 µL of scrambled, myosin Va, or myosin Vb shRNA lentivirus per 2 mL medium.

Live-cell Imaging

HL-1 cells in glass-bottom dishes (MatTek) were imaged live on a Nikon TE2000 microscope with a Plan-APO 100X/NA1.4 objective and Photometrics CS ES2 camera. 16-20 hours post transfection HL-1 cells transiently expressing Kv1.5-GFP alone or in the presence of myosin Va or myosin Vb DN were imaged every 3 seconds for 30 minutes. Both the objective and perfusion solutions were maintained at 37°C throughout the experiment. Cells were maintained in phenol free DMEM for the duration of imaging. Immediately after imaging cells were fixed for 7 min with 4%

paraformaldehyde, quenched for 10 min with 50 mmol/L NH_4Cl, permeabilized for 10 min in 0.1% Triton X-100 in 2% goat serum in PBS, and washed 2 times for 5 min with PBS and once for 10 min in PBS with rhodamine conjugated phalloidin (1:1000) to label actin filaments. Images were prepared with ImageJ (NIH) and Photoshop CS2 (Adobe). Generation of the SD maps and speed and run length of vesicles using home-made plug-ins for ImageJ were performed as described previously.[149] For colocalization of Kv1.5-GFP with actin filaments, the SD map of vesicle motility was overlaid with a static image of the rhodamine-phalloidin fluorescence.

Statistical Analysis

Statistics were performed using GraphPad Prism 5 Software (San Diego, CA). All data are expressed as the mean ± SEM of n cells. Comparisons between groups were made using One-way ANOVA as indicated. Values of $p<0.05$ were considered significant.

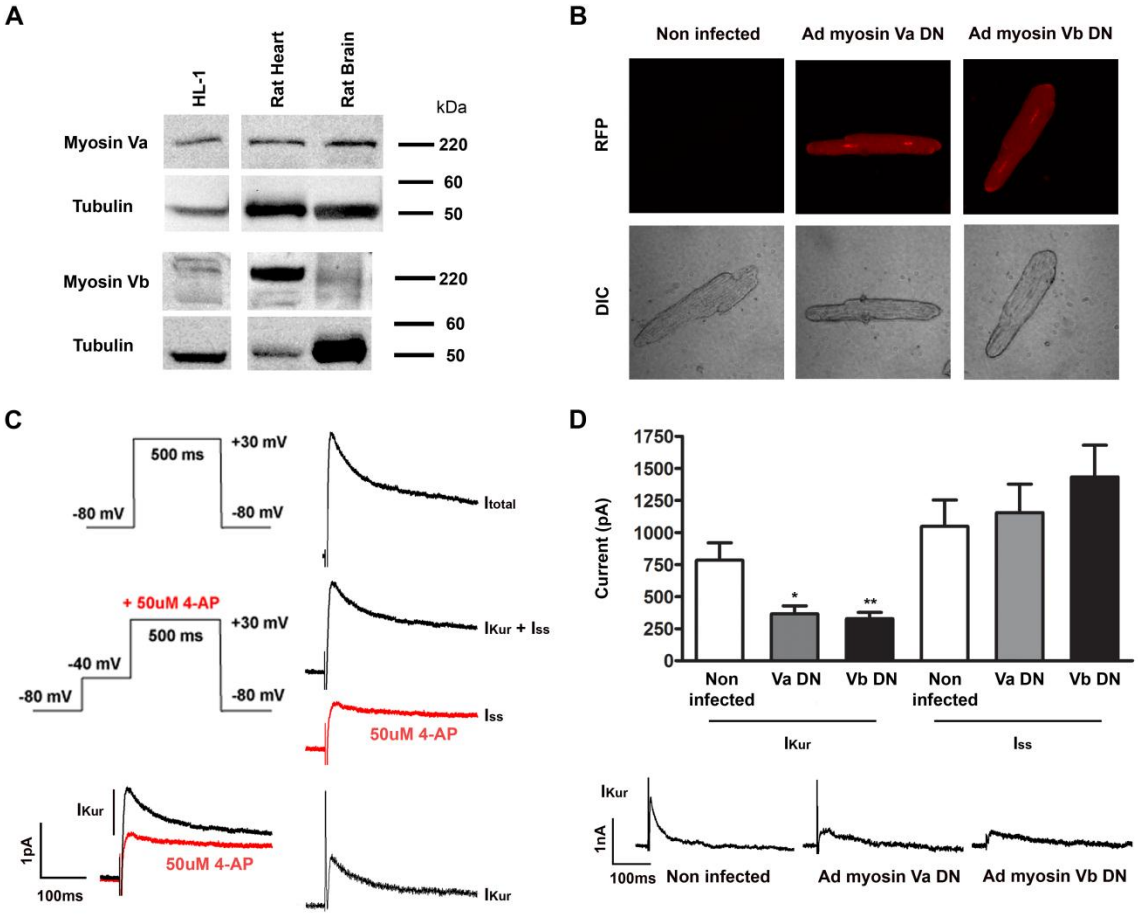

Figure 3.1 Endogenous myosin Va and myosin Vb regulate I_{Kur}.

(A) Representative western blot image of endogenous myosin Va and Vb and tubulin from non-transfected HL1 cells and rat heart and brain. **(B)** Representative images of adult rat ventricular myocytes demonstrating RFP fluorescence and differential interference contrast (DIC) for a non-infected myocyte and myocytes 24 hr post infection with myosin Va or Vb DN adenovirus. **(C)** Representative traces depicting the voltage protocol, pharmacological steps, and electronic subtraction for isolation of I_{Kur} current in acutely dissociated rat ventricular myocytes. **(D)** Quantification of I_{Kur} and I_{ss} current, and representative traces of I_{Kur} current, in acutely dissociated adult rat ventricular myocytes 24 hr post infection with myosin Va DN or myosin Vb DN adenovirus ($n \geq 7$ myocytes). * indicates $p < 0.05$; ** indicates $p < 0.01$ as determined by one-way ANOVA with Tukey post-test.

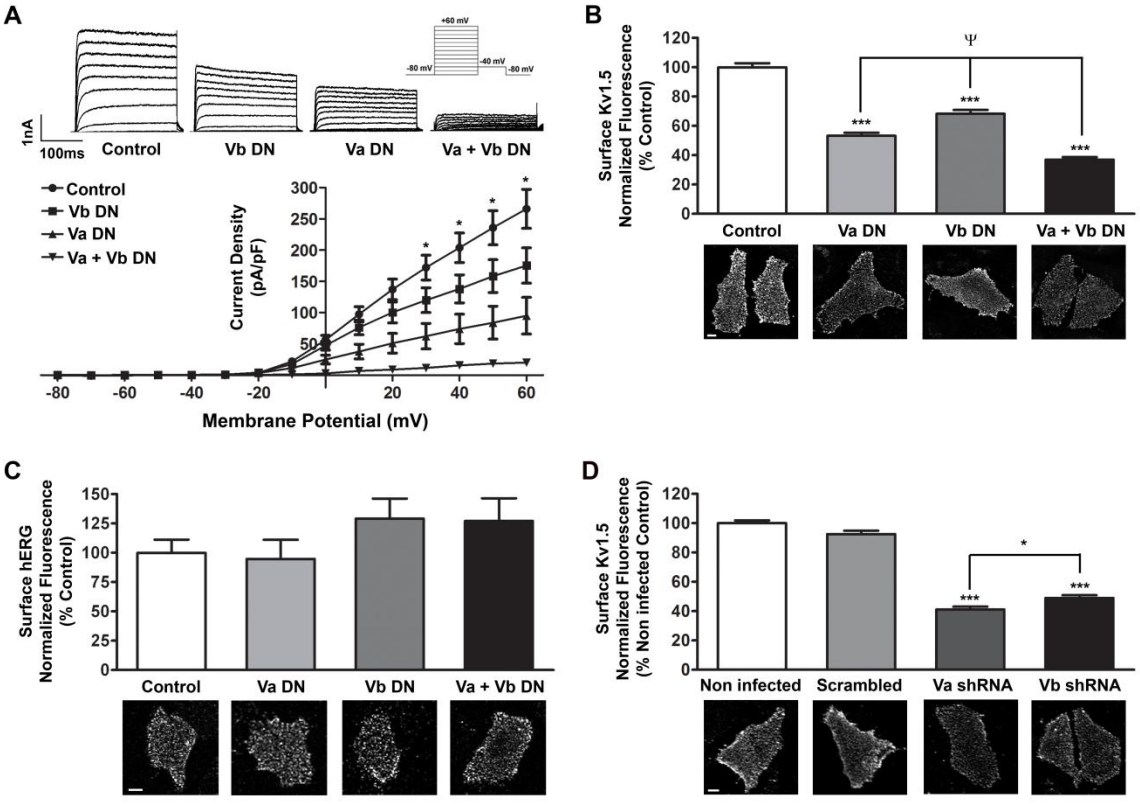

Figure 3.2 Disruption of myosin Va and Vb function decreases current density and cell surface levels of Kv1.5.

HL-1 cells transiently expressing Kv1.5-GFP or hERG-GFP co-expressing DsRed vector control, or myosin Va DN or myosin Vb DN alone or in combination 48 hr post transfection. **(A)** Representative whole cell voltage clamp current traces and the corresponding IV curve for Kv1.5 current density ($n \geq 5$ cells). **(B)** Quantification of surface Kv1.5 with representative images for each condition ($n \geq 73$ cells). **(C)** Quantification of surface hERG with representative images for each condition ($n \geq 27$ cells). **(D)** Quantification of surface Kv1.5 in HL-1 cells transiently expressing Kv1.5-GFP following 48 hr of lentiviral infection with scrambled, myosin Va, or myosin Vb shRNA ($n \geq 93$ cells). Below are representative images for each condition. Scale bars = 10μm. * indicates $p < 0.05$; *** indicates $p < 0.001$ as determined by one-way ANOVA with Tukey post-test.

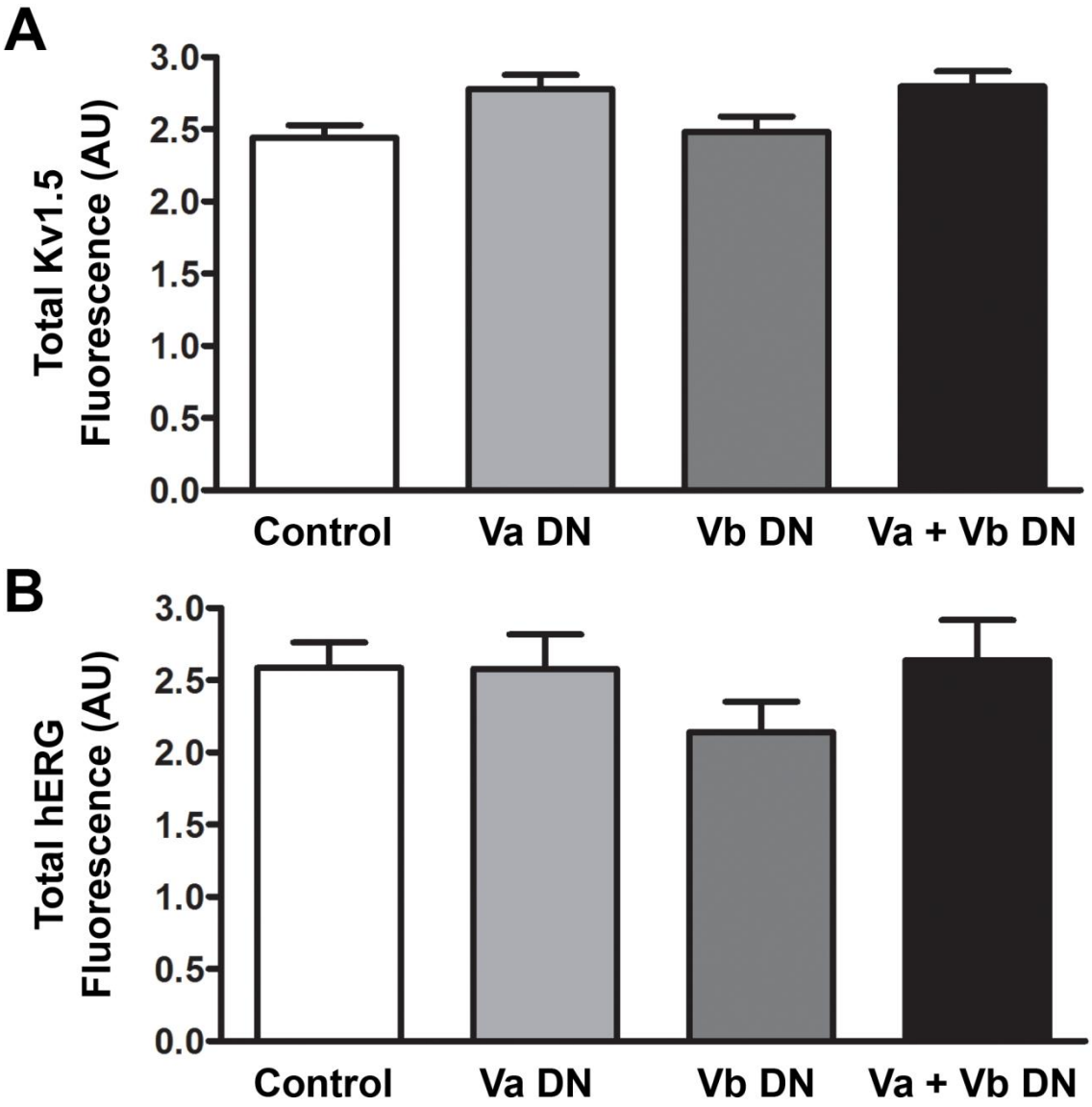

Figure 3.3 Co-expression with myosin Va or Vb DN does not alter total channel.

Quantification of total GFP in HL-1 cells transiently expressing either **(A)** Kv1.5-GFP or **(B)** hERG-GFP and co-expressing DsRed vector control or myosin Va DN or myosin Vb DN alone or in combination 48 hr post transfection ($n \geq 73$ and $n \geq 27$ cells, respectively).

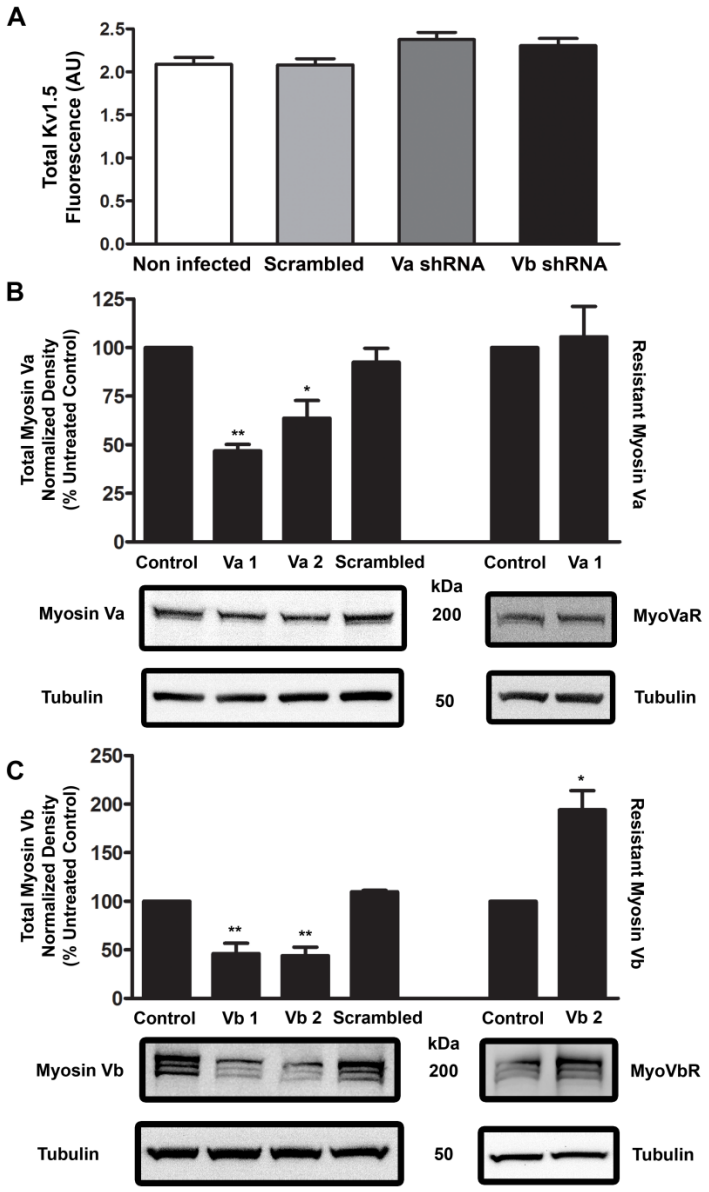

Figure 3.4 Lentiviral shRNA targeting myosin Va and Vb does not alter total Kv1.5-GFP and specifically knocks down the respective myosin isoform.

(A) Quantification of total GFP in HL-1 cells transiently expressing Kv1.5-GFP 48 hr post transfection and lentiviral infection with scrambled, myosin Va, or myosin Vb shRNA ($n \geq 93$ cells). HL-1 cells transiently expressing full-length wild-type (left) and shRNA resistant (right) myosin Va **(B)** or myosin Vb **(C)** 48 hr post transfection and infection with lentiviral shRNA. Quantification of total myosin Va and myosin Vb normalized to tubulin loading control in response to two targeted lentiviral constructs compared to non-infected, scrambled shRNA, and shRNA resistant controls ($n = 3$ blots). Below are representative images of corresponding western blots. * indicates $p < 0.05$; ** indicates $p < 0.01$; *** indicates $p < 0.001$ as determined by one-way ANOVA with Tukey post-test.

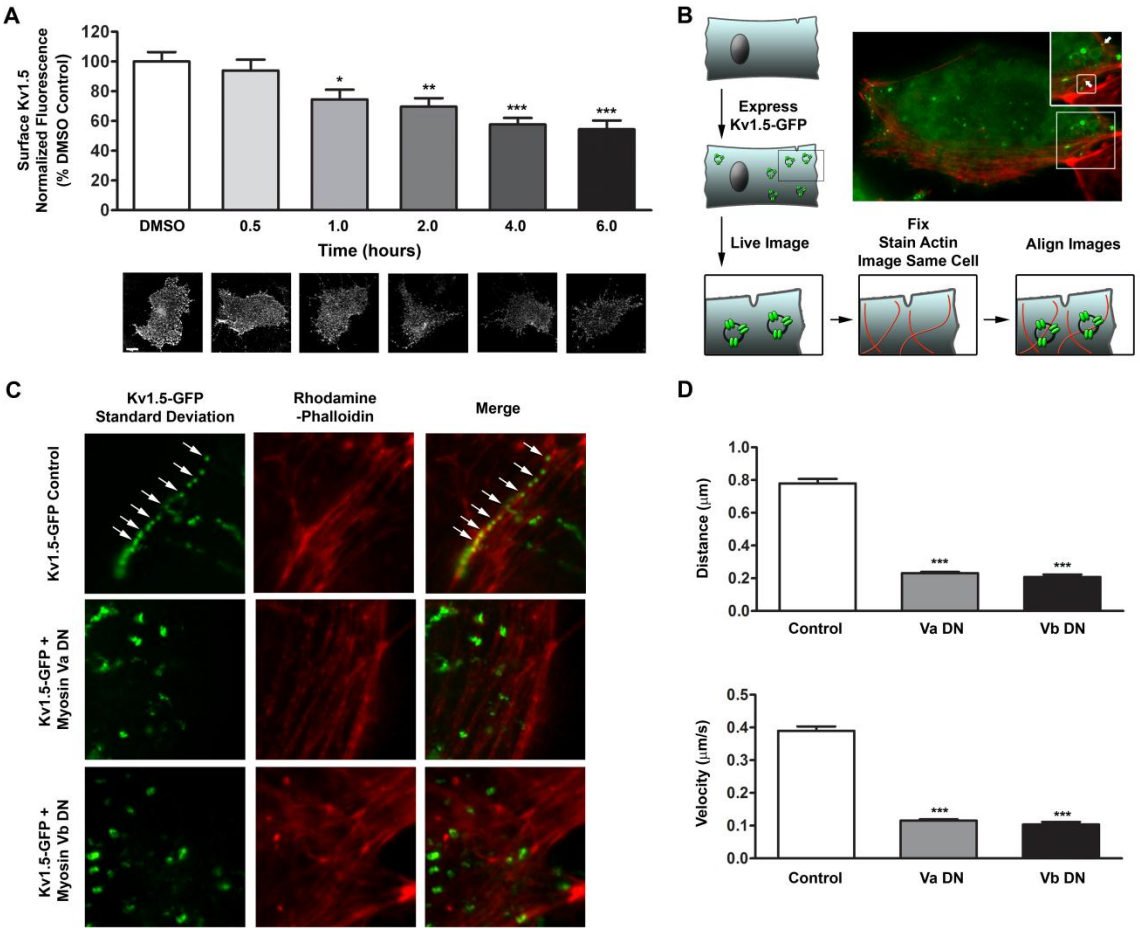

Figure 3.5 Processivity of Kv1.5-containing vesicles is lost upon inhibition of myosin Va and Vb function.

(A) Quantification of surface channel and representative images for HL-1 cells 48 hr post transfection with Kv1.5-GFP. Cells were treated with 0.1% DMSO vehicle control or 5 μmol/L cytochalasin D for 0.5, 1, 2, 4, and 6 hr ($n \geq 85$ cells). Live cell imaging of HL-1 cells transiently expressing Kv1.5-GFP alone or co-expressing myosin Va DN or myosin Vb DN 16-20 hr post transfection, followed by retrospective labeling for actin filaments with rhodamine-phalloidin. **(B)** A cartoon representation and representative image of the protocol for live cell imaging of Kv1.5-contatining vesicle trafficking and retrospective actin filament labeling. **(C)** Representative images showing the SD map for Kv1.5-containing vesicle motility, rhodamine phalloidin fluorescence, and the merged image. **(D)** Quantification of the distance traveled and velocity of Kv1.5-containing vesicles trafficking along actin filaments in the periphery of the cell (n = 20 tracks from 16 cells, 17 tracks from 4 cells, and 9 tracks from 2 cells for Kv1.5 alone, Kv1.5 + myosin Va DN, and Kv1.5 + myosin Vb DN, respectively). Scale bars = 10μm. * indicates $p < 0.05$; ** indicates $p < 0.01$; *** indicates $p < 0.001$ as determined by one-way ANOVA with Tukey post-test.

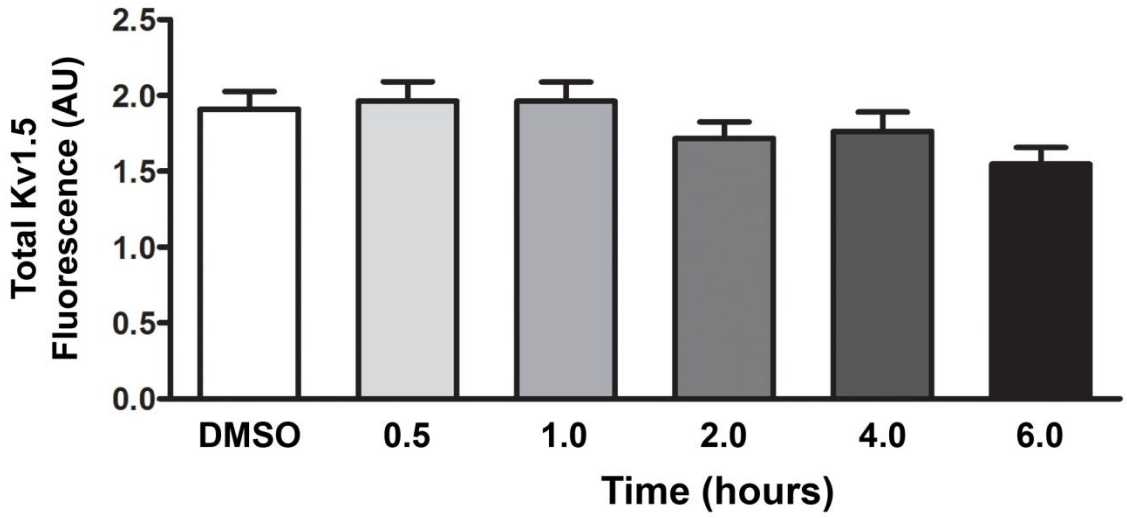

Figure 3.6 Treatment with cytochalasin D does not alter total Kv1.5-GFP.

Quantification of total GFP in HL-1 cells 48 hr post transfection with Kv1.5-GFP. Cells were treated with 0.1% DMSO vehicle control or 5 µmol/L cytochalasin D for 0.5, 1, 2, 4, and 6 hr ($n \geq 85$ cells).

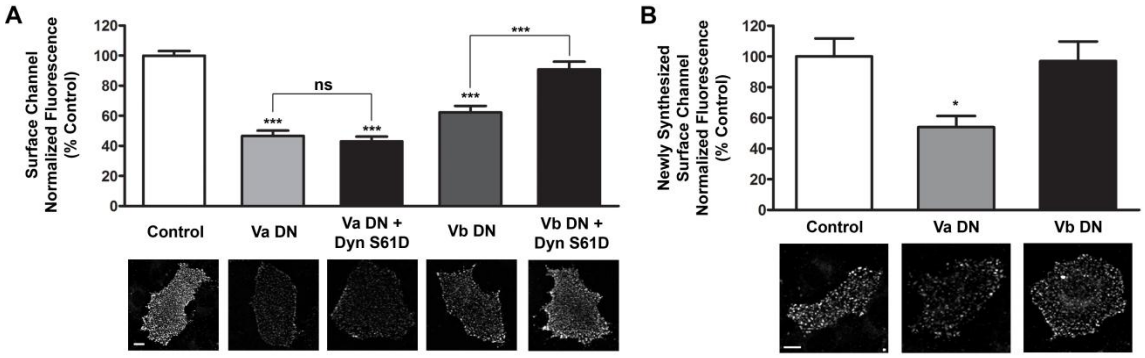

Figure 3.7 Myosin Va acts in the anterograde and myosin Vb in the post-endocytic trafficking of Kv1.5.

HL-1 cells transiently expressing Kv1.5-GFP 48 hr post transfection. **(A)** Quantification and representative images of steady-state surface Kv1.5 upon co-expression with DsRed, myosin Va DN, myosin Va DN + dynamin S61D, myosin Vb DN, or myosin Vb DN + dynamin S61D ($n \geq 59$ cells). **(B)** Quantification and representative images of newly synthesized surface Kv1.5 6 hr post expression of Kv1.5-GFP co-transfected with DsRed, myosin Va DN or myosin Vb DN ($n \geq 25$ cells). Scale bars = 10μm. * indicates $p < 0.05$; *** indicates $p < 0.001$ as determined by one-way ANOVA with Tukey post-test.

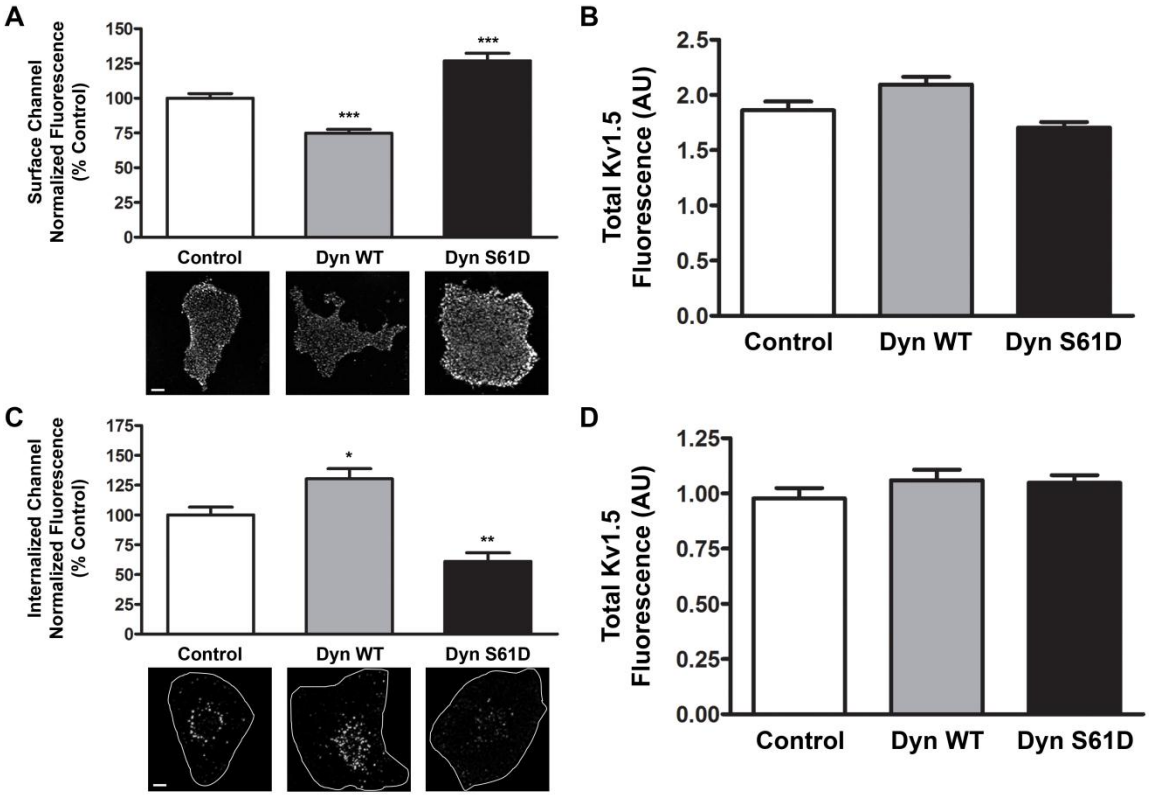

Figure 3.8 Co-expression with dynamin WT or S61D does not alter total Kv1.5-GFP.

HL-1 cells transiently expressing Kv1.5-GFP and co-expressing DsRed, WT dynamin, or dynamin S61D 48 hr post transfection. **(A)** Quantification and representative images of steady-state surface Kv1.5 ($n \geq 110$ cells). **(B)** Quantification of total GFP when measuring steady-state surface Kv1.5. **(C)** Quantification and representative images of internalized Kv1.5 ($n \geq 69$ cells). **(D)** Quantification of total GFP when measuring internalized Kv1.5. Scale bars = 10µm. * indicates $p < 0.05$; ** indicates $p < 0.01$; *** indicates $p < 0.001$ as determined by one-way ANOVA with Tukey post-test.

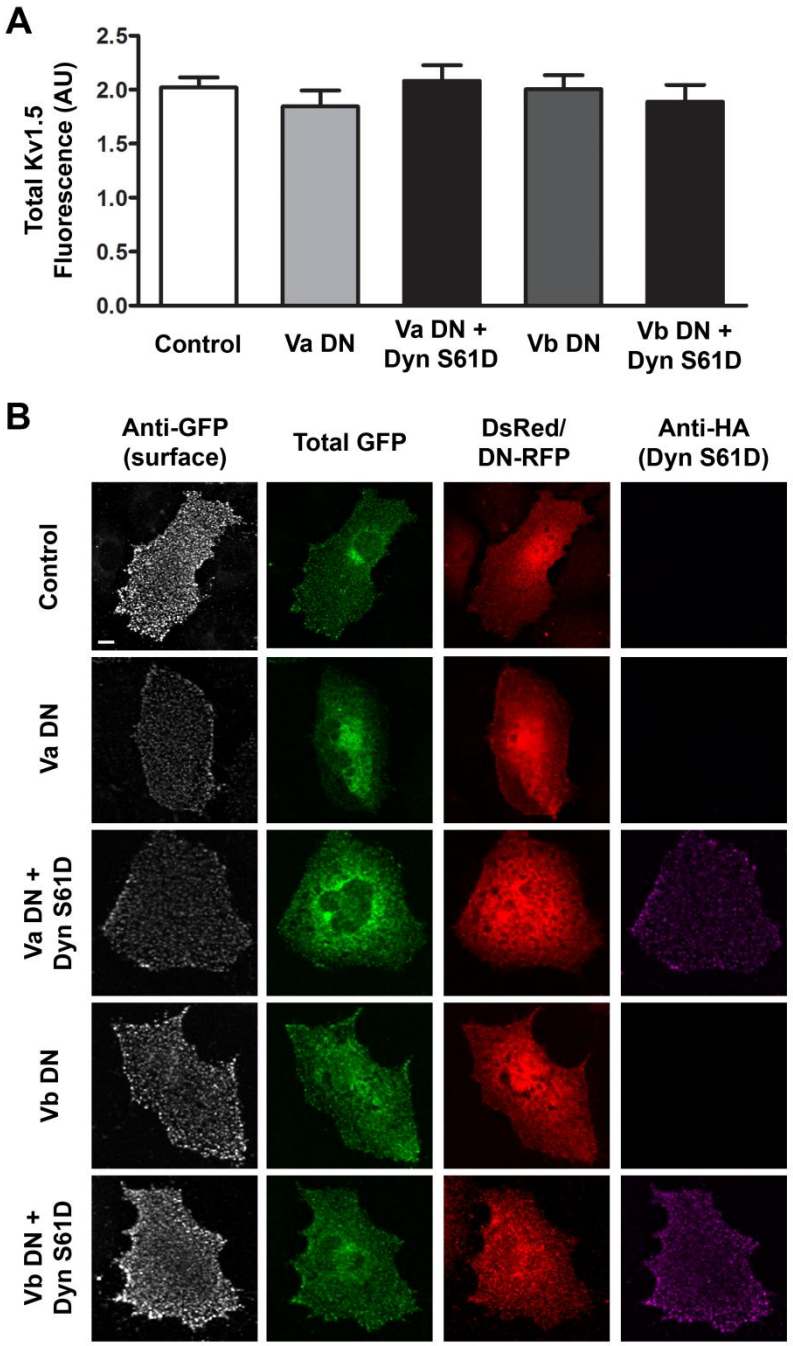

Figure 3.9 Co-expression with myosin Va or Vb DN and dynamin S61D does not alter total Kv1.5-GFP.

HL-1 cells transiently expressing Kv1.5-GFP and co-expressing DsRed, myosin Va DN, myosin Va DN + dynamin S61D, myosin Vb DN, or myosin Vb DN + dynamin S61D. **(A)** Quantification of total GFP ($n \geq 59$ cells). **(B)** Representative images of anti-GFP labeling for surface channel (left, white), total Kv1.5-GFP (left middle, green), DsRed or myosin V DN-RFP fluorescence (right middle, red), and anti-HA labeling for dynamin S61D (right, magenta).

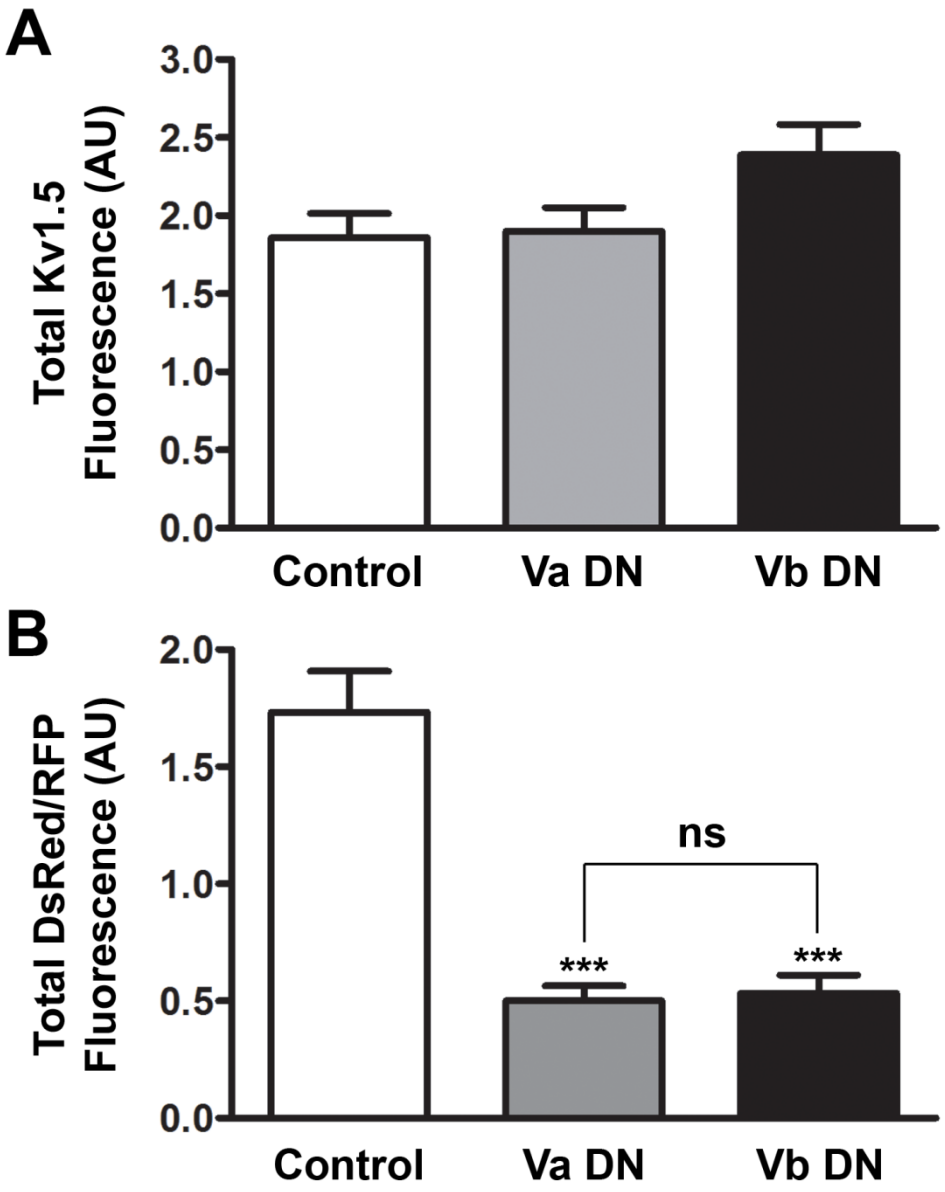

Figure 3.10 Co-expression with myosin Va or Vb DN at an early time point does not alter total Kv1.5-GFP.

Quantification of **(A)** total GFP and **(B)** total DsRed/RFP in HL-1 cells 6 hr post expression of Kv1.5-GFP co-expressing DsRed, myosin Va DN or myosin Vb DN ($n \geq 25$ cells).

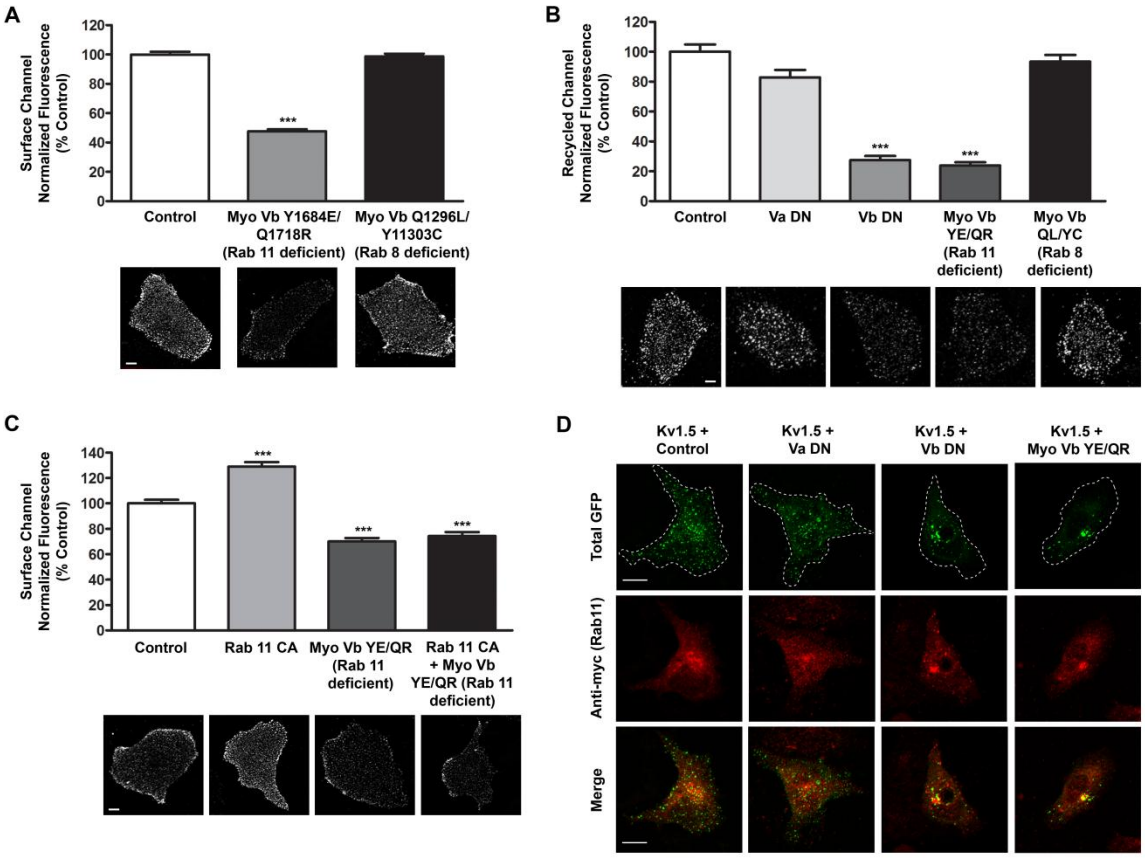

Figure 3.11 Recycling of Kv1.5 requires selective interaction of myosin Vb with Rab 11.

Quantification and representative images of HL-1 cells transiently expressing Kv1.5-GFP 48 hr post transfection. **(A)** Steady-state surface Kv1.5 upon co-expression with DsRed, myosin Vb YE/QR, or myosin Vb QL/YC ($n \geq 74$ cells). **(B)** Recycled Kv1.5 upon co-expression with DsRed, myosin Va DN, myosin Vb DN, myosin Vb YE/QR, or myosin Vb QL/YC ($n \geq 60$ cells). **(C)** Steady-state surface Kv1.5 upon co-expression with Rab 11 CA, myosin Vb YE/QR, or Rab 11 CA and myosin Vb YE/QR ($n \geq 74$ cells). **(D)** Co-localization for Kv1.5-GFP, Rab 11, and myosin Va DN, myosin Vb DN, or myosin Vb YE/QR in perinuclear endosomes. Scale bars = 10μm. *** indicates $p < 0.001$ as determined by one-way ANOVA with Tukey post-test.

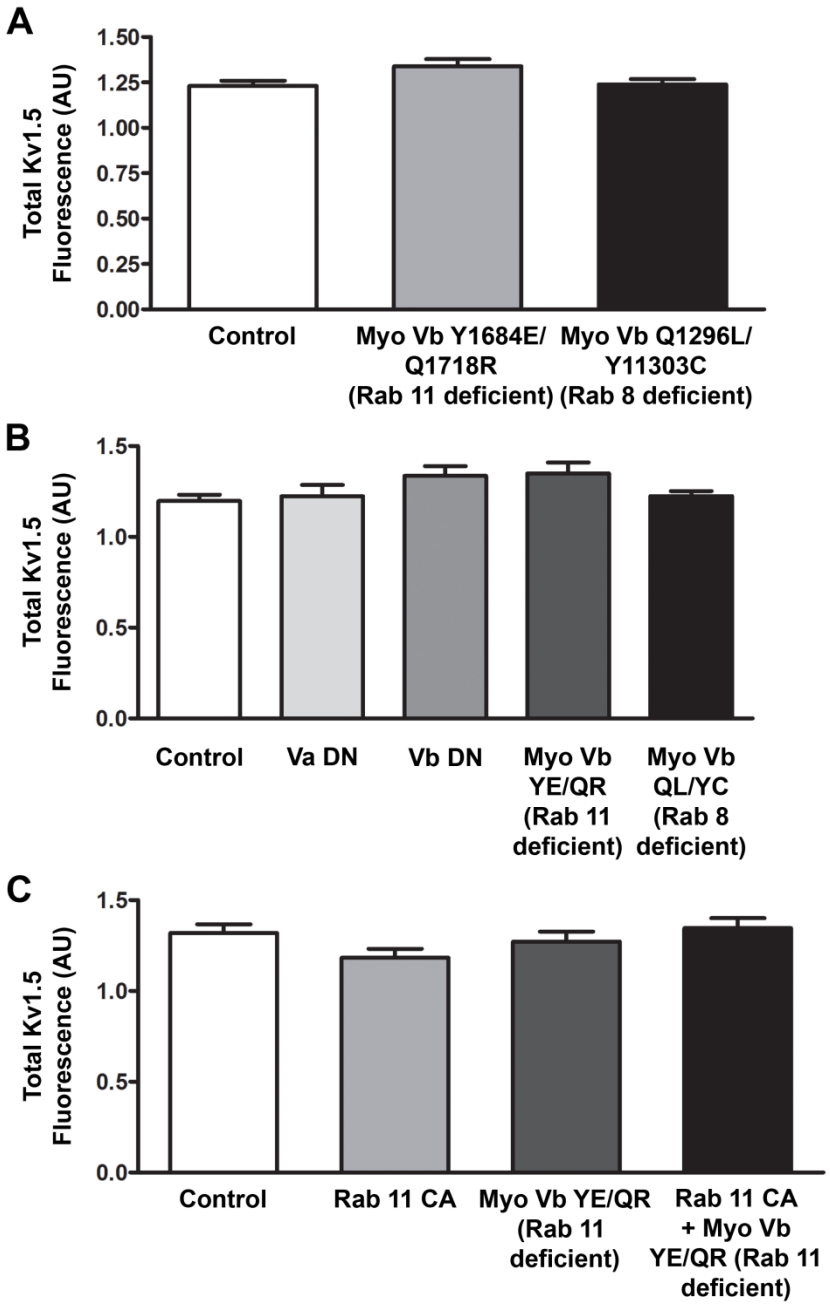

Figure 3.12 Co-expression with myosin Vb mutants or myosin V DNs does not alter total Kv1.5-GFP.

(A) Quantification of total GFP in HL-1 cells transiently expressing Kv1.5-GFP and co-expressing DsRed, myosin Vb YE/QR, or myosin Vb QL/YC 48 hr post transfection ($n \geq 74$ cells). **(B)** Quantification of total GFP in HL-1 cells transiently expressing Kv1.5-GFP and co-expressing DsRed, myosin Va DN, myosin Vb DN, myosin Vb YE/QR, or myosin Vb QL/YC 48 hr post transfection ($n \geq 60$ cells). **(C)** Quantification of total GFP in HL-1 cells transiently expressing Kv1.5-GFP and co-expressing Rab 11 CA, myosin Vb YE/QR, or Rab 11 CA and myosin Vb YE/QR 48 hr post transfection ($n \geq 74$ cells).

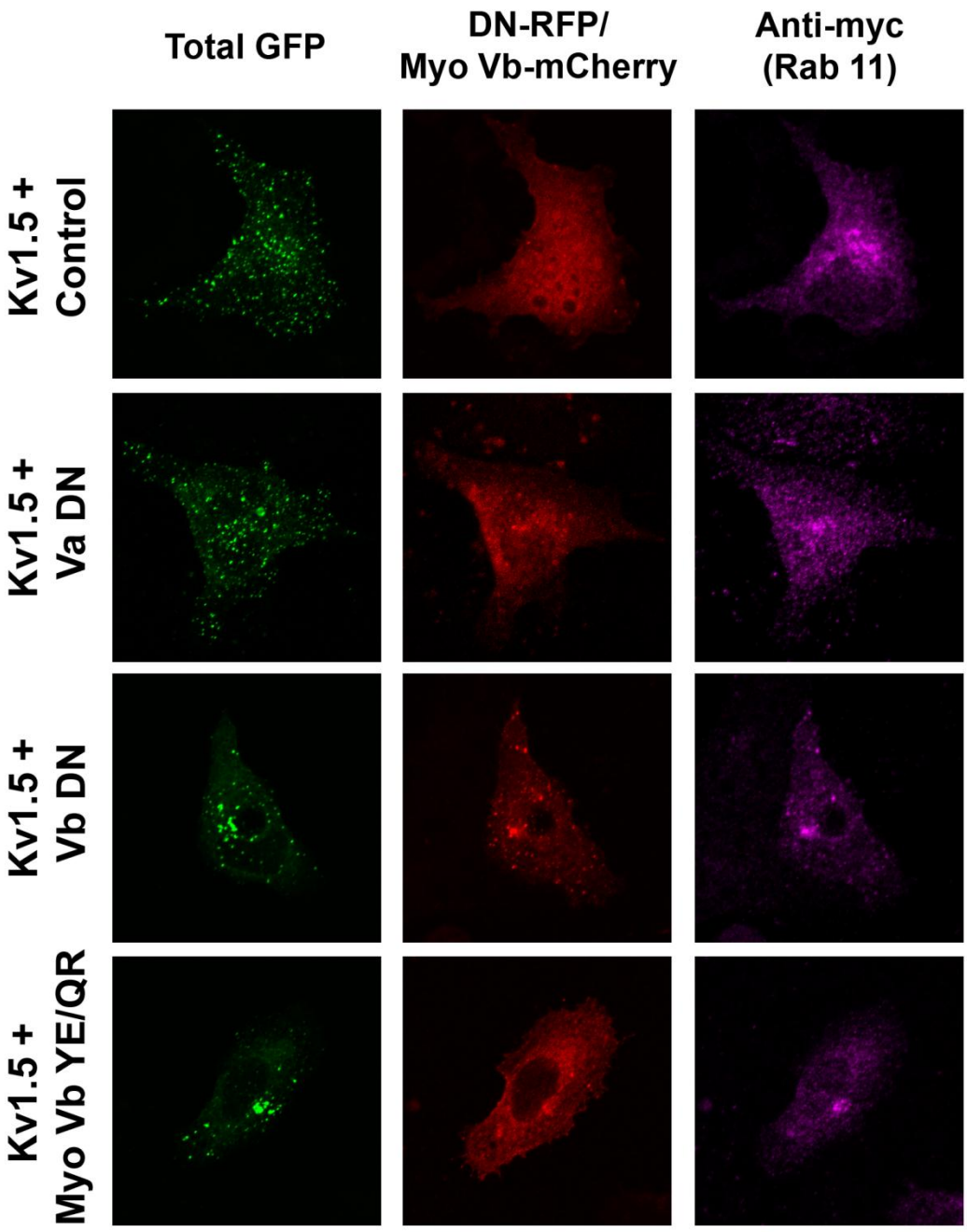

Figure 3.13 Loss of channel recycling leads to accumulation of Kv1.5 in Rab 11 positive endosomes.

HL-1 cells transiently expressing Kv1.5-GFP and Rab 11 WT, and co-expressing myosin Va DN, myosin Vb DN, or myosin Vb YE/QR 48 hr post transfection. Representative images of total Kv1.5-GFP (left, green), DsRed or myosin V DN-RFP or myosin Vb YE/QR-mCherry fluorescence (middle, red), and anti-myc labeling for Rab 11 (right, magenta).

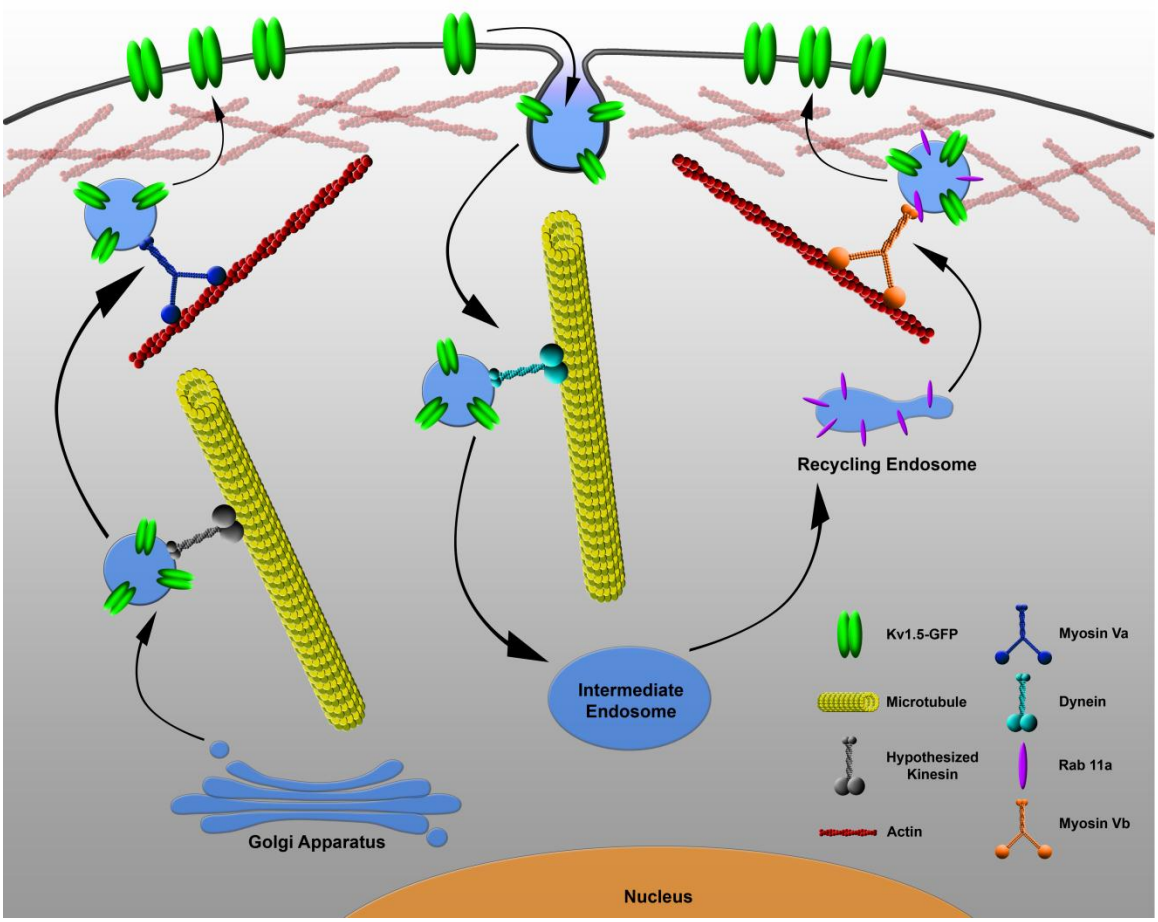

Figure 3.14 Cartoon representation of the current running model for Kv1.5 trafficking in atrial myocytes.

CHAPTER 4

DISCUSSION

STRUCTURAL REQUIREMENTS FOR DRUG-INDUCED INTERNALIZATION

As described in chapter 2, we have reported a previously unrecognized mechanism of antiarrhythmic drug action in the acute modulation of Kv1.5 channel trafficking.[50] Using quinidine, an antiarrhythmic agent which has both class Ia actions[140, 141] and class III actions in mammalian atrium and ventricle, we demonstrated that channel blockers can both inhibit ion conductance and regulate the stability of the channel protein within the membrane. In this study, quinidine resulted in a dose- and time-dependent internalization of Kv1.5, concomitant with channel block. Interestingly, this quinidine-induced internalization of Kv1.5 was found to be subunit-dependent and stereospecific[50] which highlights the possibility for the development of atrial selective agents that specifically modulate surface density.

Drug-induced internalization may occur for channel subunits selectively expressed in the atria.[50] Quinidine exhibits promiscuous block of cardiovascular ion channels, including several members of the Kv channel family. This lack of specificity

---

Part of Chapter 4 is published as **Schumacher SM**, **Martens JR**. (2010). Ion channel trafficking: a new therapeutic horizon for atrial fibrillation. Heart Rhythm. Sep;7(9):1309-15. For copyright release, please see Appendix I.

raised the question as to whether the drug-induced internalization was specific to Kv1.5 or a general mechanism contributing to the block of current through multiple ion channels. To address this specificity, we examined the effect of quinidine on two other prominent cardiovascular potassium channel subunits expressed endogenously in the human atrium and ventricle, Kv4.2 and Kv2.1. Although ion permeability of both channels is blocked by quinidine (IC_{50} of 10 μmol/L and 20 μmol/L quinidine, respectively),[123, 124] neither Kv4.2 nor Kv2.1 internalized in response to any drug concentration tested over the time course studied. These studies have been expanded to include the Kv1.x family channel Kv1.4. Although ion permeability of Kv1.4 is blocked by quinidine (IC_{50} of approximately 186 μmol/L),[186, 187] Kv1.4 did not exhibit quinidine-induced internalization, further supporting the subunit dependence of this drug action (Figure 4.1). This subunit specificity may permit the development of drugs that avoid or reduce undesired proarrhythmic ventricular side effects.

The potential to separate drug-induced channel internalization from pore block stimulates further interest in the design of drugs to modulate trafficking pathways. As discussed in chapter 2, within the Kv1.5 channel protein there is incomplete overlap in the binding sites required for quinidine-induced internalization and pore block.[50] This was revealed through alanine-scanning mutagenesis of amino acid residues within the highly conserved drug binding site of Kv channels.[42, 129] Previous studies had used alanine-scanning mutagenesis of the amino acids lining the ion conducting pore of Kv1.5 to observe alterations in pore block by various antiarrhythmic compounds.[42, 46, 129, 188] We chose to study the four single alanine mutant channels that exhibited the greatest reduction of pore block and showed that quinidine-induced internalization was abolished

with the T480A and I508A mutations. In contrast, L510A and V512A underwent quinidine-induced internalization indistinguishable from wild-type.[42, 50, 129] Expansion of these studies include four additional amino acids that demonstrated varying degrees of reduction of pore block. These data revealed that I502A completely inhibited internalization, similar to T480A and I508A (Figure 4.2). V505A exhibited partial inhibition of internalization, while similar to L510A and V512A, quinidine-induced internalization was not altered by the L506A or V516A mutations. Interestingly P532L, a naturally occurring mutation (outside of the conserved drug binding site) in atrial fibrillation patients that results in a rightward shift in the dose response curve for quinidine block of channel current[130] caused an equivalent (~10-fold shift in the EC_{50} value) decrease in the sensitivity to quinidine-induced channel internalization.[50] Together, the fact that these mutations alter channel block and/or internalization of Kv1.5 demonstrate that quinidine is inducing its effects through direct binding to the channel and not through off-target mediators of channel trafficking.

The subunit dependence and incomplete overlap in amino acid requirements indicate that individual components of the Kv1.5 channel structure are critical for the quinidine-induced internalization. However, additional studies of alanine-scanning mutants within the putative conserved drug-binding site are necessary to compare effects on surface density to those reported for pore block. Nevertheless, these data highlight the possibility for development of new agents that specifically enhance Kv1.5 channel internalization as an alternative and potentially beneficial new therapeutic strategy. A future goal of this study would be to elucidate the effect of these alanine mutations on pore block of Kv1.5 by quinidine compared to the other antiarrhythmic compounds

studied previously. Correlative electrophysiological analysis and immunocytochemical studies would be performed to determine alterations in pore block and channel internalization in response to quinidine for each single alanine mutant of Kv1.5, quantifying any shift in the dose-response for quinidine or the extent of pore block and internalization. This study would include an observation of any alterations in channel current kinetics or current density as a result of the alanine mutation. Information obtained through these experiments would elucidate the amino acid components of the Kv1.5 channel that are necessary and/or sufficient for quinidine-induced internalization. Furthermore, these results would shed light on the potential separability of pharmacophores within the Kv1.5 pore region for pore block versus channel internalization, providing insight for future drug discovery or design.

In order to develop new compounds that selectively modulate Kv1.5 surface density, the pharmacophore(s) responsible for pore block and internalization must be isolated (Figure 4.3). The observation that quinine, a diastereomer of quinidine, blocks Kv1.5 current in a dose-dependent fashion without enhancing internalization, suggests that a highly stereospecific binding event is required to induce channel internalization, rather than some non-stereospecific interaction with the cell membrane. Therefore, quinidine embodies structural features that enable it to induce endocytosis of Kv1.5. The individual components of the quinidine structure critical for this stereospecific internalization/effect remain to be identified. To initiate these studies we analyzed chloroquine, which maintains only the quinoline ring and tertiary amine of the quinidine structure. While less potent and efficacious, this compound was able to enhance internalization of Kv1.5 above constitutive levels (EC_{50} = 8 μM) (Figure 4.4). These data

support the hypothesis of structural elements within quinidine that are both necessary and sufficient for the drug-mediated internalization. Future studies would include correlative electrophysiological and immunofluorescence analysis of both pore block and channel internalization of Kv1.5 in response to a number of quinidine related and unrelated compounds to determine preliminary structure-activity relationships (SAR). Studies would begin with the commercially available analogs of quinidine, including chloroquine and hydroquinidine for which studies are underway. In addition, these studies would be expanded to modern, more clinically relevant antiarrhythmic drugs. Structural features will be identified through the determination of SAR and then exploited in the design of novel chemical compounds with greater potency and selectivity for inducing endocytosis versus direct block of the channel.

Initial SAR to identify individual components of the quinidine structure that are critical for inducing internalization through stereospecific binding will begin with potential binding components. The divergent positioning of the bicyclic aromatic and the bicyclic amine of quinidine and quinine suggest that both of these moieties may contain elements essential for channel internalization. Binding components include the following: three hydrogen bond acceptors (aryl methoxy and two basic nitrogens), one hydrogen bond donor (OH), pi-stacking of the quinoline ring, and charge-charge interactions of the basic nitrogens with negatively charged residues. The relative importance of these binding components for pore block and channel internalization will be evaluated through: removal of the aryl methoxy, replacement of the aryl methoxy with hydroxyl, replacement of the aliphatic hydroxyl with ketone, saturation of the vinyl group, acylation of the aliphatic and aromatic hydroxyl groups with various carboxylic

acids, and appending a hydroxyl group alpha to vinyl group. Candidate compounds, including 16 commercially available analogs of quinidine that vary in the potential binding moieties noted, will be used to establish preliminary SAR. Subsequent analogs will focus on further modification of those areas of the quinidine template that prove critical for inducing channel internalization to improve potency and selectivity. This may include the generation of synthetic analogs to incorporate additional esters of the aryl and aliphatic alcohols. The dose-dependence of internalization for each candidate analogs will be tested for Kv1.5 and other related Kv channels. These experiments would be done in collaboration with Dr. Scott D. Larsen, Research Professor of Medicinal Chemistry and Co-Director of the Medicinal Chemistry Core Synthesis Laboratory (MCCSL) at the University of Michigan.

Quinidine analogs examined must have sufficient membrane permeability to access the channel pore/active site and induce internalization. As insufficient permeability would lead to the misinterpretation of negative data as a lack of intrinsic activity of the analog, the MCCSL has developed an in vitro assay for membrane permeability (PAMPA).[189] This assay would be able to detect the membrane permeability of all quinidine analogs and synthetic compounds relative to the parent drug quinidine. In the case that initial SAR does not provide guidance towards chemical components necessary for channel internalization as opposed to pore block, the scope of commercially available analogs could be broadened to include simpler compounds that contain only the quinoline or bicyclic amine components. Evidence that such compounds may retain selective channel internalization was demonstrated through preliminary studies with chloroquine. In addition, in collaboration with the Center for Chemical

Genomics (CCG) at the University of Michigan, we could develop and execute a high throughput assay based on Kv1.5-pHluorin that would interrogate a library of over 150,000 compounds for the ability to induce endocytosis. This strategy would provide the opportunity to identify leads divergent from quinidine-related compounds. In chapter 2, we observed that Kv1.5-pHluorin permits the real-time monitoring of cell surface channel protein. This was achieved through generation of a Kv1.5 channel construct in which the pH-sensitive GFP (pHluorin) was inserted into the extracellular S1-S2 loop. This GFP mutant displays variable fluorescence dependent upon the pH of the immediate environment. Cell surface Kv1.5-pHluorin fluoresces strongly at pH 7.4, however internalization of channel into acidified intracellular vesicles at pH 5.0-5.5 quenches fluorescence providing a live read-out of channel endocytosis in response to specific stimuli and independent of antibody labeling.[190] The generation of HL-1 cells stably expressing Kv1.5-pHluorin allows the application of this technology to high-throughput measurements of quinidine analogs.

To date, there is no crystal structure for Kv1.5; however, the crystal structure for the transmembrane domains of the related Kv1.2 channel has been elucidated. Molecular modeling of the Kv1.5 pore/active site will be undertaken using homology models based on Kv1.2 crystal structure. Data from our alanine-scanning mutagenesis studies of the amino acid requirements within the channel pore, as well as our preliminary SAR of the chemical structure of the drug molecule would be used to further validate or refine the model of the Kv1.5 pore region and drug-binding site. This model would then be used to dock quinidine related and unrelated compounds and guide the study towards compounds that would promote Kv1.5 internalization without pore block, focusing on analogs from

commercially available compound collections containing the minimized structural components of quinidine. In addition to guiding additional SAR targets, creation of a valid binding model will permit the incorporation of structure based drug design (SBDD) for compounds that would display selectivity and efficacy for Kv1.5 channel internalization. Testing will be facilitated by high-throughput assays using HL-1 cells stably expressing Kv1.5-pHluorin. Again, these studies will be done in collaboration with Dr. Larsen who has extensive experience with SBDD, and the MCCSL has the resources to dock and score candidate targets prior to ordering of compounds. Promising compounds identified would be tested in native myocytes by recording I_{Kur} function in the presence and absence of calcium-chelators. The end goal of these studies would be to discover a compound that could selectively induce internalization of Kv1.5 without inducing pore block in order to exhibit ventricular sparing clinical efficacy and safety in the treatment of atrial fibrillation in clinical trials.

Another important therapeutic aspect of quinidine-induced internalization of Kv1.5 is that it is acute and reversible, further suggesting that it may be effective for acute cardioversion. In our study we found that the quinidine-induced internalization was rapid, reaching a plateau within 10 minutes. Combined with the fact that this drug-mediated trafficking effect occurred at resting membrane potential in our immunocytochemical assays, these data indicate that the rate-limiting factor for this effect is likely equilibration of drug across the membrane. Importantly, upon drug washout the quinidine-induced internalized Kv1.5 recycled back to the plasma membrane at a rate indistinguishable from constitutive channel recycling. Thus, the quinidine-mediated trafficking effect results in an acute increase in channel endocytosis,

specifically, without altering the endogenous recycling of Kv1.5. If a drug were designed to specifically modulate Kv1.5 channel trafficking it could, in theory, be used to cause a rapid internalization of channel with recovery after drug withdrawal. Therefore, acute modulation of ion channel surface levels may offer the selective advantage for a rapid, reversible decrease in I_{Kur} with a subsequent increase in action potential duration that may terminate acute onset of AF without altering the overall pool of Kv1.5 channel. In contrast, we found that chronic treatment with quinidine diverted Kv1.5 channel to the proteasomal degradation pathway. It is unclear if this chronic decrease in surface expression is advantageous or an unwanted side-effect of the long-term drug treatment. For instance, the time course of recovery from this repression may precipitate drug-withdrawal side effects. Furthermore, long-term suppression of channel expression may contribute to remodeling of heart tissue in which a decrease in Kv1.5 channel protein levels has already been documented. The alternative is that this chronic suppression of Kv1.5 channel protein levels may overcome the current limitations of acute cardioversion which fails to terminate breakthrough AF or adequately subdue the arrhythmogenic substrate and may result in the benefit of maintained rhythm control.

An important finding that goes beyond the therapeutic potential of this approach is that the drug-induced trafficking effect is calcium-dependent and raises significant issues for drug safety screening.[50] The calcium-dependent trafficking component was responsible for a 3-fold shift in the dose response for quinidine and is therefore critically important when considering the *in vivo* effects of this drug and likely many others. It has been well established that non-antiarrhythmic drugs can have proarrhythmic effects through off target inhibition of cardiovascular ion channel currents. This has been

reported for psychiatric drugs, antihistamines, antimicrobials and other compounds, many of which can induce QT prolongation with subsequent risk of torsade de pointes.[191] As a result, pharmaceutical companies and regulatory agencies mandate that cardiac ion channel testing be part of the drug safety profiling of all new compounds. Current drug safety profiling is almost entirely focused on a drug's capacity to block ion conduction. This is commonly tested through electrophysiological measurement of current in the presence or absence of drug, using a calcium chelating agent to isolate the drug-channel interaction. Therefore antiarrhythmic, and non-antiarrhythmic, compounds that alter ion channel trafficking may show greater efficacy and potency *in vivo* than can be predicted by current drug safety profiling. This may result in a dramatic underestimation of the desired clinical effect and/or undesired side effects of a drug.

The results discussed here highlight the potential for development of new agents that selectively modulate ion conduction and/or the stability of channel protein in the membrane. In addition, manipulation of the trafficking of functional membrane channel may provide an avenue for developing new therapies with atrial selectivity and clinical efficacy and safety for the treatment of AF and potentially other cardiovascular arrhythmias.

ACCESSORY SUBUNITS

In the human heart Kv channels are composed of four alpha subunits arranged as homo or heterotetramers that may associate with one or more auxiliary beta subunits to form the functional ion channel in the plasma membrane. Association with Kv beta subunits has been shown to alter both the cell surface expression and kinetics of Kv

current.[88, 92, 93, 192-202] It is the combination of alpha and beta subunits in the membrane that ultimately defines the biological and pharmacological activity of channels in vivo. In particular, specific alteration of Kv1.5 upon association with hKvBeta1.3 and hKvBeta2.1 has been shown.[88, 92, 203] We therefore extended our study to include an investigation of the effects of these auxiliary beta subunits on the mechanism and regulation of endogenous and quinidine-induced internalization of Kv1.5. In our system hKvBeta1.3 alters Kv1.5 current kinetics as shown in the previous literature (Figure 4.5). Electrophysiological analysis of Kv1.5 current kinetics upon functional association of Kv1.5 with hKvBeta2.1 will also be performed. Unlike hKvBeta2.1, co-expression with hKvBeta1.3 significantly decreased cell surface levels of Kv1.5 (Figure 4.6). As this may occur through a decrease in anterograde delivery of newly synthesized channel, increase in endocytosis, or decrease in channel recycling, future studies will investigate the underlying mechanism of this decrease. Preliminary data show that while hKvBeta1.3 does not alter the rate of constitutive internalization of Kv1.5, both hKvBeta1.3 and hKvBeta2.1 alter the rate of channel recycling (Figure 4.7). Future studies will determine the amount of total recycled channel as well and further elucidate the mechanisms by which hKvBeta1.3 and hKvBeta2.1 are altering Kv1.5 surface density and trafficking. Importantly, quinidine-induced internalization of Kv1.5 was completely blocked by co-expression with either hKvBeta1.3 or hKvBeta2.1 (Figure 4.8).

It has been previously shown that hKvBeta1.3 contains and N-terminal “ball and chain” motif which rapidly inactivates Kv1.5 current by blocking the cytosolic pore of the channel.[93] More importantly, it has been shown that this interaction of hKvBeta1.3 can alter drug binding to Kv1.5 due to a competition for the conserved drug binding site

in the channel pore.[89, 93, 204, 205] Therefore we hypothesized that the mechanism by which hKvBeta1.3 inhibited quinidine-induced internalization of Kv1.5 was through a loss quinidine binding to the channel pore. This hypothesis was supported by the shift in the IC_{50} of quinidine for Kv1.5 from 6.2 μM to 49.9 μM as demonstrated by Gonzalez *et al*.[89] To confirm this hypothesis, we chose to study the Kv1.5-V512A mutant discussed above, which we have shown does not alter the quinidine-induced internalization of Kv1.5. Decher *et al.* demonstrated that KvBeta1.3 was not able to induce rapid inactivation of Kv1.5-V512A, suggesting a disruption in association of the N-terminal inactivation domain of hKvBeta1.3 with the cytosolic pore of Kv1.5.[204] We found that this single point mutation completely restored the quinidine-induced internalization of Kv1.5 in the presence of hKvBeta1.3 (Figure 4.9). Unlike hKvBeta1.3, hKvBeta2.1 does not contain the N-terminal inactivation domain and does not confer rapid inactivation to non-inactivating Kv alpha subunits. Therefore, a future goal of this study will be to investigate the mechanisms by which hKvBeta2.1 inhibits the quinidine-induced internalization of Kv1.5, which may occur through specific protein-protein interactions or post-translational modification of the beta subunit. In addition, hKvBeta1.2 expression has been demonstrated in human atria and ventricles,[195, 199] and hKvBeta1.2 co-expression has been shown to alter Kv1.5 current kinetics. Future studies will also include an investigation of the effect of hKvBeta1.2 co-expression on quinidine-induced internalization in cardiomyocytes.

Kv channels are expressed as homo and heterotetramers. The majority of investigations into the existence and subunit stoichiometry of these heteroterameric populations have focused on neuronal tissues in the central nervous system.

Electrophysiological studies have revealed that native K^+ currents in the cardiovascular system cannot be fully reconstituted by expression of single cloned Kv alpha subunits in heterologous systems.[206] While several effectors may contribute to this disparity, heterotetrameric channel assembly cannot be ruled out. Our lab has recently developed a bimolecular fluorescence complementation (BiFC) technique to visualize heterotetrameric channel populations and their regulation.[207] This technique employs the insertion of either half of a split fluorescent molecule into the extracellular loop of a Kv channel alpha subunit. Co-translational association of the alpha subunits allows formation of the complete fluorophore and restores fluorescence, demonstrating expressing of the heterotetramer. Live-cell labeling with antibodies against the fluorescent molecules and electrophysiological analysis then reveal the cell surface expression of functional heterotetrameric channels. Future studies will utilize this technique to study the formation of heterotetrameric channels within cardiovascular Kv channel subunits. Specifically they will investigate the effects of subunit assembly on the current kinetics, constitutive trafficking, and sensitivity of Kv1.5 to quinidine-mediated pore block and channel internalization.

The composition of Kv channels in the membrane determines their activity *in vivo*. Therefore, knowledge of the interaction of alpha and beta subunits, and the effect of these associations on channel function and pharmacological activity, is important for our understanding not only of normal physiology, but pathophysiology and therapeutics. Shown here, association of Kv1.5 with the accessory subunits hKvBeta1.3 and hKvBeta2.1 blocked quinidine-induced internalization of Kv1.5. Given the distribution of hKvBeta1.3, which is more highly expressed in the ventricles than atria,[195] and the co-

localization of Kv1.5 with hKvBeta2.1 in the vasculature,[208-211] this association with Kv1.5 may provide additional tissue specificity for the quinidine-induced internalization of Kv1.5. For instance, hKvBeta subunit association may block non-specific, off-target effects of drug-mediated internalization of Kv1.5, while allowing for the desired effect in reducing Kv1.5 encoded I_{Kur} in the atria. This tissue specificity may provide additional clinical efficacy and safety in the development of compounds for Kv1.5 internalization as a therapeutic avenue for the treatment of atrial fibrillation.

MOLECULAR MOTORS AND ADAPTORS

Previously, our lab has demonstrated a role for the dynein retrograde motor complex in the constitutive internalization of Kv1.5.[111] In addition, we demonstrated a role for the Rab GTPases Rab 4 and Rab 11, but not Rab 5 or Rab 8, in the post-endocytic recycling of Kv1.5. In agreement with our studies, work from the lab of Dr. Fedida has independently described a role for the dynein motor complex and Rabs 4 and 11 in the trafficking of Kv1.5; however, in contrast, their work did indicate a role for Rab 5.[112, 212] This may represent a difference in the cell lines used (HL-1 mouse atrial myocytes versus HEK293 cells and H9c2 rat cardiac myoblasts) or the experimental design used to observe alterations in cell surface Kv1.5. In chapter 3 we describe involvement of the unconventional myosin V motor isoforms in the cell surface trafficking of Kv1.5. Myosin Va facilitates anterograde delivery of Kv1.5 to the plasma membrane, whereas myosin Vb mediates the post-endocytic recycling of Kv1.5 through coupling to Rab 11, providing a mechanistic link to our previous data demonstrating a role for Rab 11. This direct coupling of myosin Vb to Rab 11 for channel recycling was

revealed through the use of a myosin Vb mutant YE/QR that is unable to bind Rab 11. In addition, the decrease in cell surface Kv1.5 by co-expression with myosin Vb YE/QR, was not altered by co-expression with the constitutively active (CA) Rab 11 construct, further supporting this mechanism of Kv1.5 channel recycling. Selectivity was demonstrated through the use of a myosin Vb mutant QL/YC that is unable to bind Rab 8. In agreement with our previous publication in which Rab 8 was not important for Kv1.5 trafficking, we found no alteration in steady-state cell surface levels or recycling of Kv1.5 upon co-expression with myosin Vb QL/YC.

Kv1.5 channel trafficking by myosin Va and myosin Vb occurred along actin filaments in the periphery of the cell. Cell surface trafficking of membrane proteins is believed to be the result of both short-range trafficking along actin filaments in the cell periphery and long-range trafficking along microtubules to the periphery of the cell. As mentioned, constitutive internalization of Kv1.5 occurs via trafficking along microtubules by the dynein retrograde motor complex. It remains to be elucidated, however, whether microtubule based trafficking events participate in the anterograde delivery of newly synthesized Kv1.5 to the plasma membrane or in the recycling of Kv1.5 from perinuclear endosomal populations back to the plasma membrane. It will also be important to identify the molecular motors and adaptors that underlie these trafficking steps. Data from Zadeh *et al.* indicate a role for the kinesin-1 isoform Kif5b in the post-Golgi, pre-endocytic anterograde trafficking of newly synthesized Kv1.5 to the plasma membrane.[150] Published and preliminary data from our lab suggest the involvement of Kif17 and KifC3 in Kv1.5 trafficking events based on a reduction in steady-state cell surface levels of Kv1.5 in response to co-expression with dominant-negative (DN) forms

of these motor proteins.[149] The precise role of these molecular motors in the trafficking of Kv1.5, as well as the mechanism and adaptor proteins underlying this role, remain to be elucidated.

In addition to elucidating the molecular machinery and adaptor proteins involved in the trafficking of Kv1.5, it is important to identify any specificity within these trafficking mechanisms. For instance, in chapter 3 we found that co-expression with myosin Va and myosin Vb DN did not alter the cell surface levels of the hERG potassium channel. In addition, we demonstrate a role for dynamin in the internalization of Kv1.5 that can be enhanced by overexpression of wild-type dynamin 1 and significantly abrogated by the DN form of dynamin 1, dynamin S61D. In contrast to this clear role in the internalization of Kv1.5, we have data demonstrating no effect of dynamin S61D on the steady-state cell surface levels of Kv1.4. Internalization of Kv1.4 is blocked by co-incubation with myristoylated dynamin inhibitory peptide (DIP);[213] however, this compound does not distinguish between dynamin 1, 2, or 3. These data suggest that cell surface trafficking of membrane ion channels may not occur via a conserved mechanism, but may involve varying degrees of specificity in the molecular machinery or pathways utilized. This specificity may provide additional therapeutic targets and avenues for the treatment of various cardiovascular arrhythmias and thereby warrant special attention.

CONCLUSION

Through the work of this thesis, we revealed pleiotropic effects of the antiarrhythmic drug quinidine on Kv1.5, which encodes the major repolarizing current I_{Kur} in the human atria. We characterized quinidine-induced internalization of Kv1.5, in addition to pore block, that was significantly greater than constitutive endocytosis and

exhibited both subunit-dependence and stereospecificity. Furthermore, drug-mediated internalization was conserved in dissociated neonatal mouse cardiomyocytes. In addition, drug-mediated internalization was calcium dependent, and therefore not observed under experimental conditions including a calcium chelating agent, as used in classic electrophysiological analysis. Chronic treatment with a clinically relevant dose of quinidine led to channel degradation, with implications for therapeutic and/or withdrawal effects. While the mechanism for calcium-dependent internalization remains to be determined, these data demonstrate a potential new therapeutic avenue for the selective inhibition of Kv1.5 in order to attain atrial selectivity as well as clinical safety and efficacy for the treatment of atrial fibrillation.

We showed that the unconventional myosin V motor isoforms myosin Va and Vb play an important role in the delivery and cell surface levels of Kv1.5 in cardiomyocytes. The role of myosin Va and Vb in determining surface Kv1.5 effected alterations in I_{Kur} current in adult rat cardiomyocytes. A level of subunit specificity was observed in that myosin Va and Vb did not play a role in determining the cell surface levels of the hERG potassium channel. We demonstrated that myosin Va acts upstream of internalization during delivery of newly synthesized Kv1.5 to the plasma membrane. Myosin Vb is involved in the post-endocytic trafficking of Kv1.5 through recycling endosomes back to the plasma membrane. Coupling of myosin Vb to the Rab GTPase Rab 11 was necessary for this channel recycling. While there are several steps in the trafficking pathway for which the molecular motors and adaptors remain to be elucidated, these data provide some insight into the mechanisms of ion channel trafficking in the cardiovascular system.

Importantly, selective myosin Vb-mediated recycling of Kv1.5 could serve as novel therapeutic target for the treatment of atrial fibrillation.

These findings are significant since they represent new potential therapeutic avenues for the treatment of atrial fibrillation. Selective quinidine-induced internalization of Kv1.5 highlights the potential for the development of new compounds that alter the functional ion channel density in the membrane as a means to alter cardiovascular excitability. These data also raise questions regarding the current methods of drug safety screening as well as the role of internalization in the therapeutic and withdrawal effects of current antiarrhythmic therapy. We also demonstrate selectivity in the molecular machinery underlying cardiovascular ion channel trafficking, with therapeutic potential in the modulation of channel recycling. Continued elucidation of the molecular machinery involved in cardiovascular ion channel trafficking could reveal novel therapeutic targets and strategies for the regulation of surface channel densities in the treatment of cardiovascular arrhythmias.

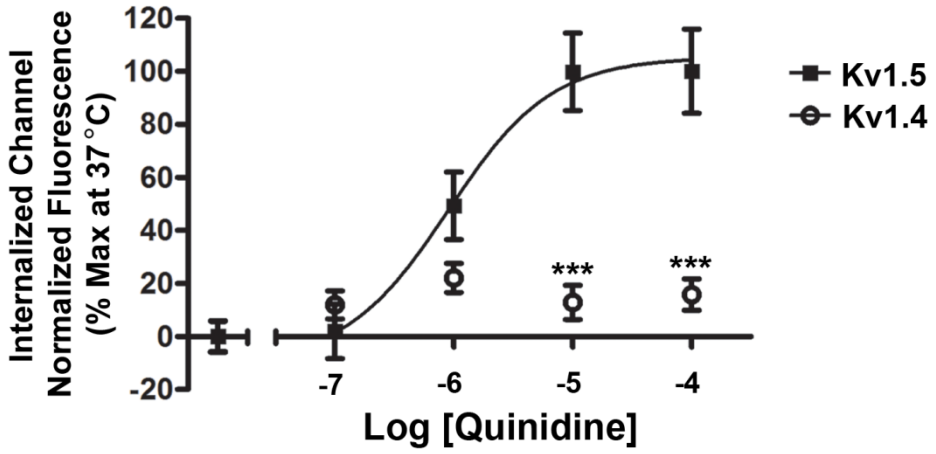

Figure 4.1 Quinidine-induced internalization is subunit-dependent.

Dose–response of internalization for HL-1 cells expressing Kv1.4-GFP treated with increasing concentrations of quinidine for 10 minutes at 37°C. ***$p<0.001$ as determined by 1-way ANOVA with Tukey post test.

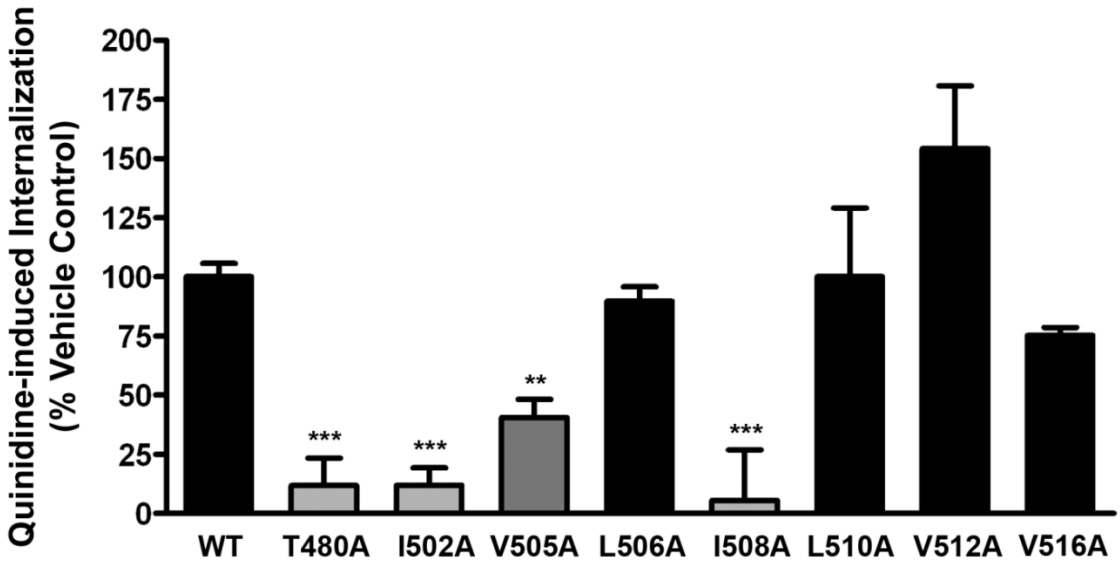

Figure 4.2 Structural requirements for quinidine binding are partially conserved for pore block and channel internalization.

Quinidine-induced internalization for HL-1 cells expressing Kv1.5-GFP containing the T480A, I502A, V505A, L506A, I508A, L510A, V512A, or V516 mutation treated with 100 µmol/L quinidine for 10 minutes at 37°C. $^{**}p<0.01$, $^{***}p<0.001$ as determined by 1-way ANOVA with Tukey post test.

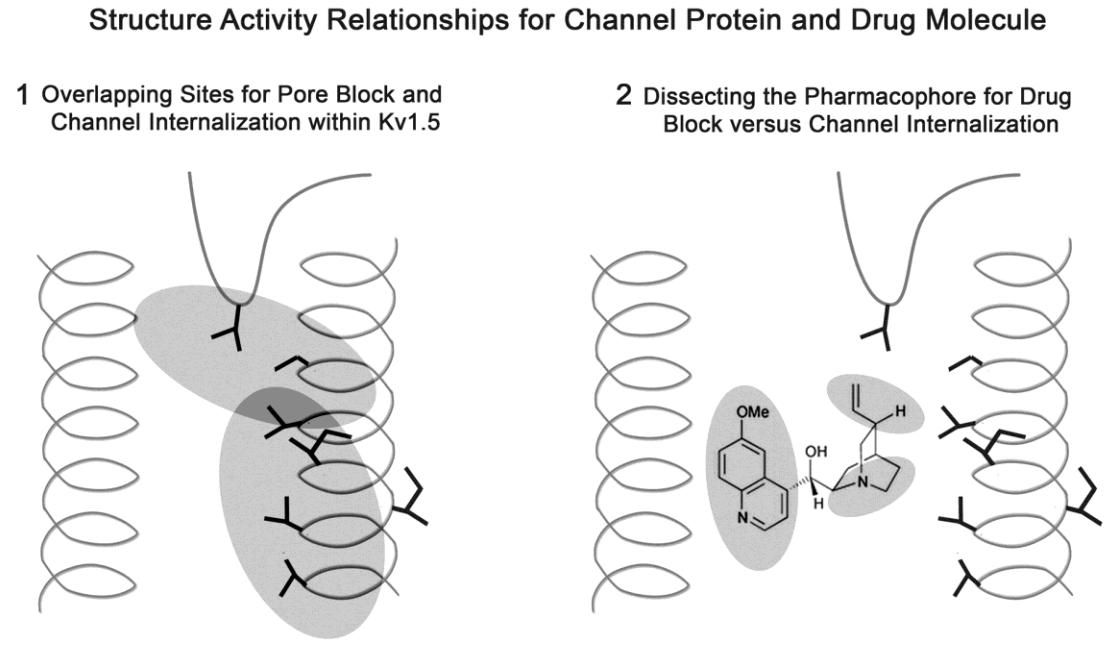

Figure 4.3 Strategies to isolate drug-induced internalization from pore block.

Cartoon representation of the potential drug binding site of the Kv1.5 channel pore. (1) Ion channel mutagenesis can be used to fully characterize the incomplete overlap in the drug binding site for pore block and channel internalization. (2) Multiple moieties within the quinidine molecule can be studied in structure activity analysis to identify the pharmacophore for drug-induced internalization.

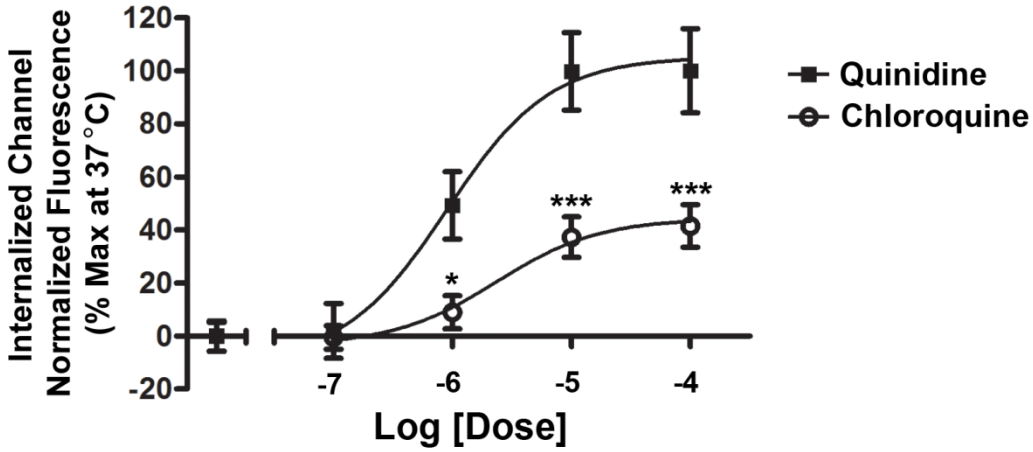

Figure 4.4 Chloroquine stimulates internalization of Kv1.5 in a dose-dependent manner.

Dose–response of internalization for HL-1 cells expressing Kv1.5-GFP treated with increasing concentrations of quinidine or chloroquine for 10 minutes at 37°C. $^{**}p<0.01$, $^{***}p<0.001$ as determined by 1-way ANOVA with Tukey post test.

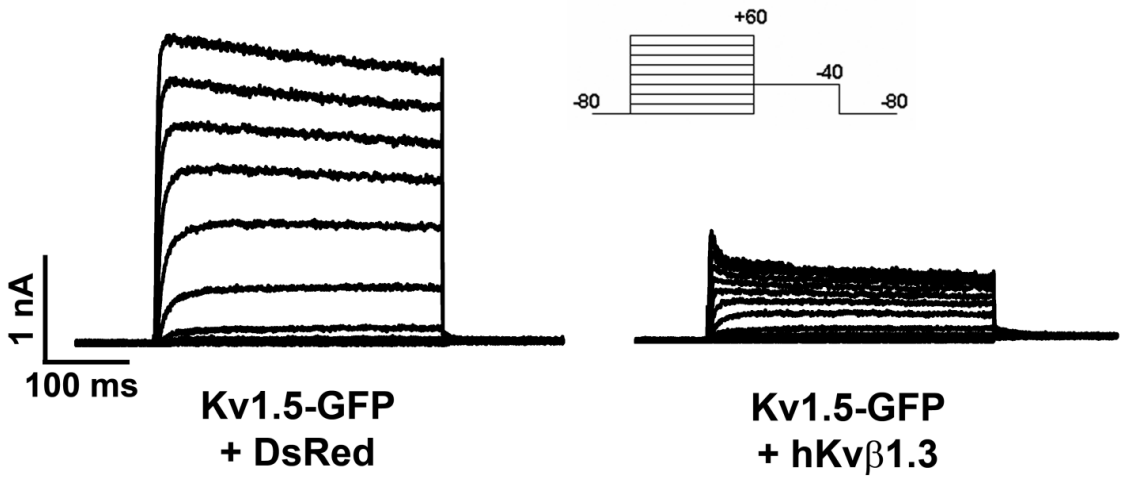

Figure 4.5 hKvβ1.3 induces rapid inactivation of Kv1.5 channel current.

Electrophysiological recordings from HL-1 cells transiently expressing either Kv1.5-GFP and DsRed (left traces) or Kv1.5-GFP and hKvβ1.3 (right traces). Cells were maintained at -80 mV followed by 250 ms pulses applied in 10 mV steps from -80 mV to +60 mV.

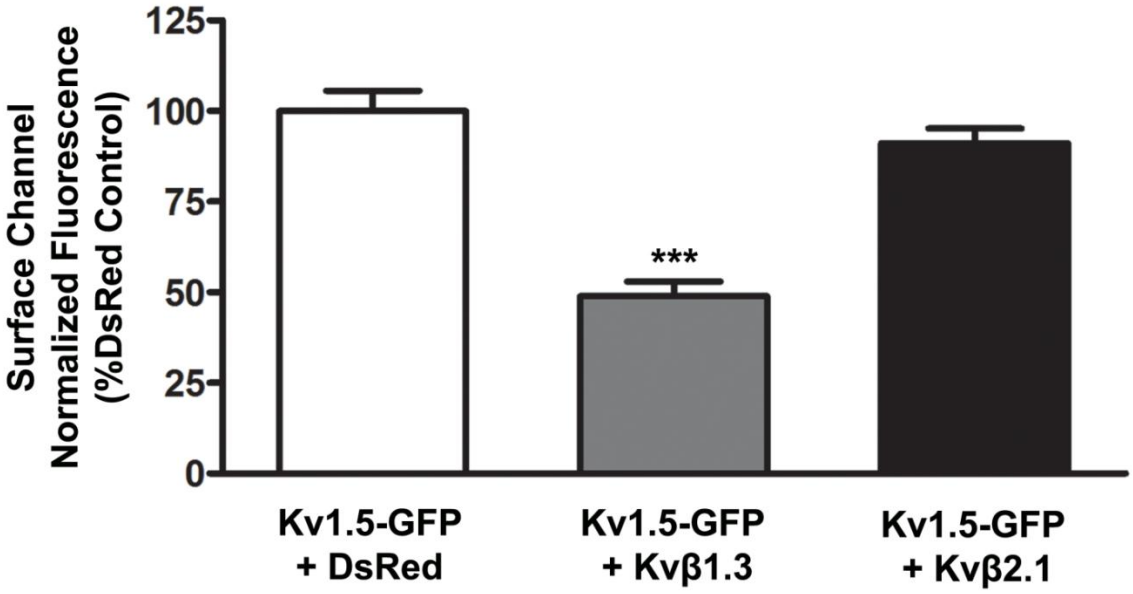

Figure 4.6 hKvβ1.3, but not hKvβ2.1, decreases steady-state cell surface levels of Kv1.5.

Quantification of surface channel in HL-1 cells expressing Kv1.5-GFP and DsRed, hKvβ1.3, or hKvβ2.1. Scale bars, 10 μm. ***$p<0.001$ as determined by 1-way ANOVA with Tukey post test.

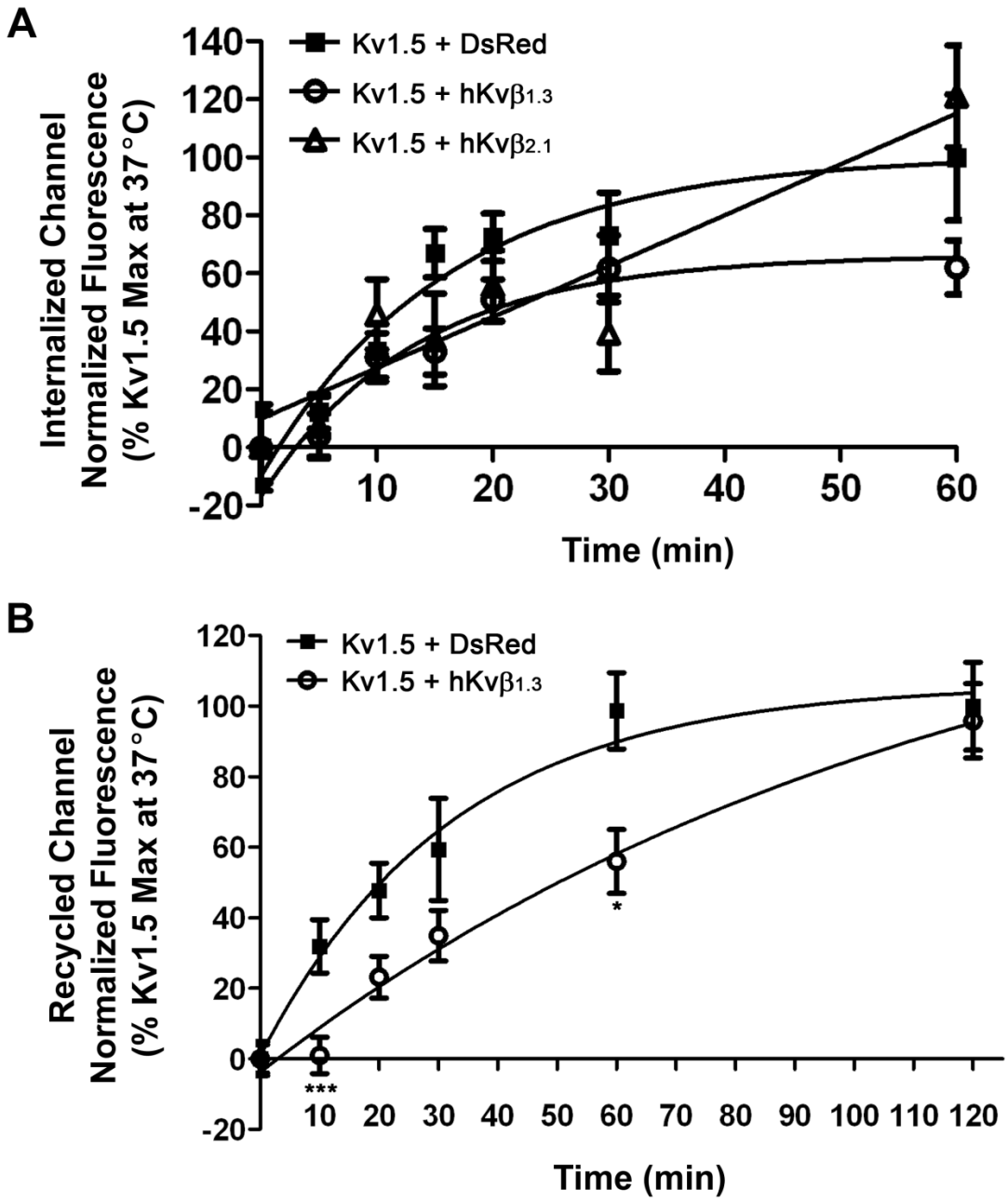

Figure 4.7 hKvβ1.3 alters constitutive internalization, and hKvβ2.1 alters constitutive internalization and recycling of Kv1.5.

(A) Quantification of internalized channel in HL-1 cells expressing Kv1.5-GFP and DsRed, hKvβ1.3, or hKvβ2.1 in response to 0, 5, 10, 15, 20, 30, or 60 min at 37°C. **(B)** Quantification of recycled channel in HL-1 cells expressing Kv1.5-GFP and DsRed, hKvβ1.3, or hKvβ2.1 in response to 0, 10, 20, 30, 60, and 120 min at 37°C. Beta subunit was detected by mouse anti-c-myc followed by goat anti-mouse Alexa Fluor 594. Below each bar graph are representative images for that condition. *** indicates $p < 0.001$ as determined by one way ANOVA with Tukey post-test.

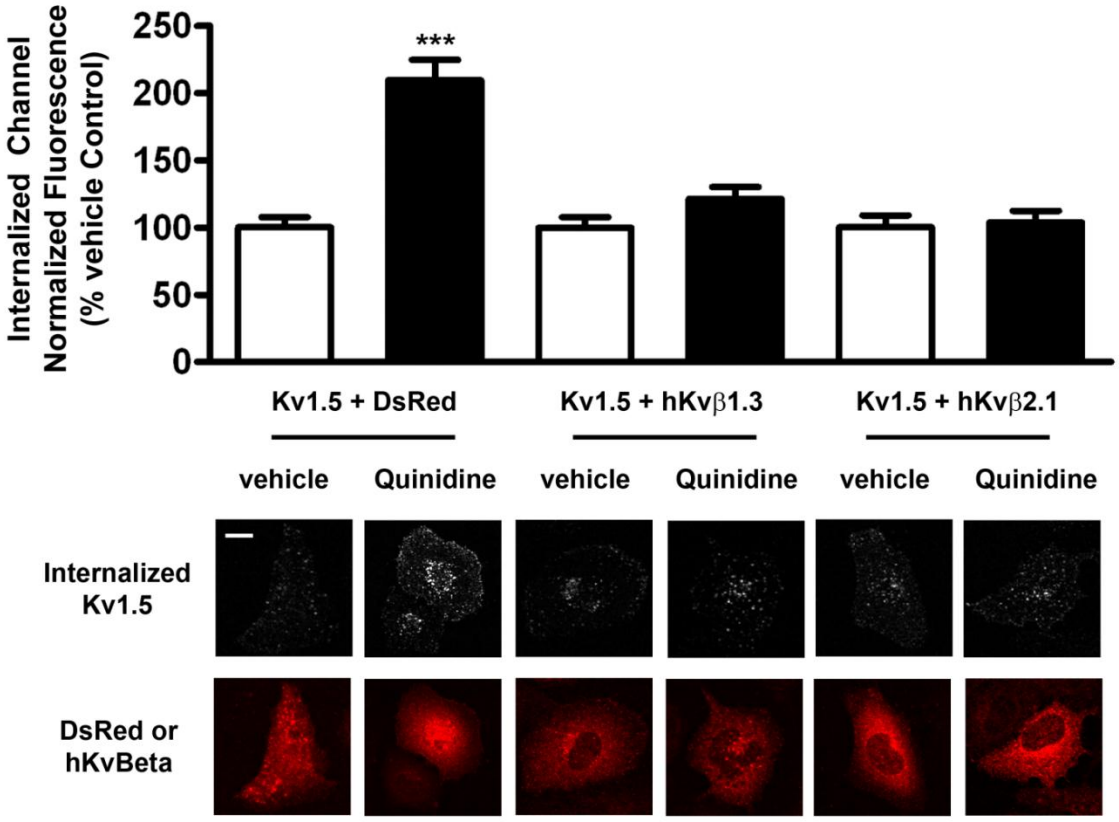

Figure 4.8 Quinidine-induced internalization of Kv1.5 is blocked by co-expression with hKvβ1.3 and hKvβ2.1.

Quantification of internalized channel in HL-1 cells expressing Kv1.5-GFP and DsRed, Kvβ1.3, or Kvβ2.1 following a 10-min incubation at 37 °C with vehicle (0.1% DMSO) or 100 μmol/L quinidine. Beta subunit was detected by mouse anti-c-myc followed by goat anti-mouse Alexa Fluor 594. Below each bar graph are representative images for that condition. Scale bars=10 μm. ***P<0.001 as determined by one-way ANOVA with Tukey post test.

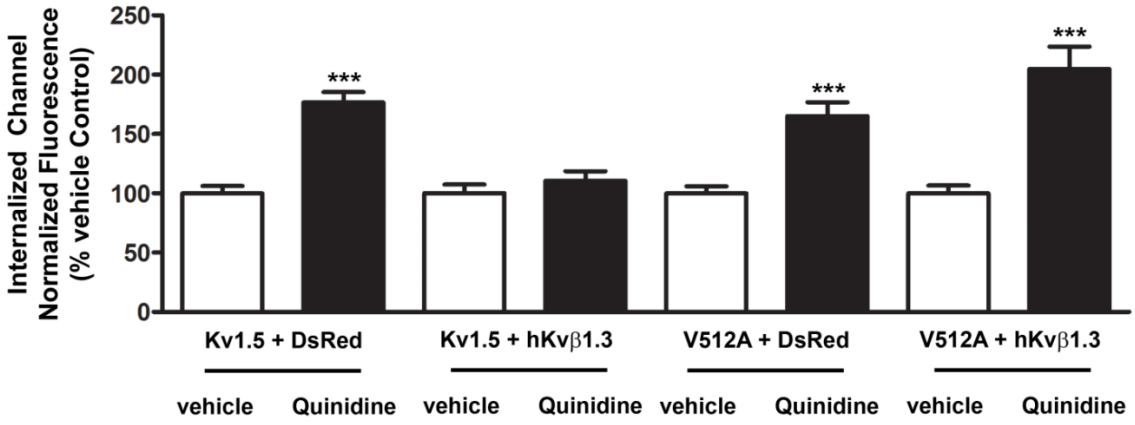

Figure 4.9 The V512A mutation of Kv1.5 restores quinidine-induced internalization in the presence of hKvβ1.3.

Quantification of internalized channel in HL-1 cells expressing Kv1.5-GFP and DsRed or Kvβ1.3, or Kv1.5_V512A_GFP and DsRed or hKvβ1.3 following a 10-min incubation at 37 °C with vehicle (0.1% DMSO) or 100 μmol/L quinidine allowing for internalization. Beta subunit was detected by mouse anti-c-myc followed by goat anti-mouse Alexa Fluor 594. ***P<0.001 as determined by one-way ANOVA with Tukey post test.

APPENDIX I

COPYRIGHT RELEASES

- Schumacher SM, Martens JR. (2010). Ion Channel Trafficking: A New Therapeutic Horizon for Atrial Fibrillation. Heart Rhythm. Sep;7(9):1309-15.

  Pages 1 and 101

- Schumacher SM, McEwen DP, Zhang L, Arendt KL, Van Genderen KM, Martens JR. (2009). Antiarrhythmic Drug-induced Internalization of the Atrial-specific K+ Channel Kv1.5. Circ Res. Jun 19;104(12):1390-8.

  Page 17

ELSEVIER LICENSE
TERMS AND CONDITIONS

Sep 14, 2011

This is a License Agreement between Sarah M Schumacher ("You") and Elsevier ("Elsevier") provided by Copyright Clearance Center ("CCC"). The license consists of your order details, the terms and conditions provided by Elsevier, and the payment terms and conditions.

All payments must be made in full to CCC. For payment instructions, please see information listed at the bottom of this form.

Supplier	Elsevier Limited The Boulevard,Langford Lane Kidlington,Oxford,OX5 1GB,UK
Registered Company Number	1982084
Customer name	Sarah M Schumacher
Customer address	Department of Pharmacology Ann Arbor, MI 48109
License number	2744250856680
License date	Sep 08, 2011
Licensed content publisher	Elsevier
Licensed content publication	Heart Rhythm
Licensed content title	Ion channel trafficking: A new therapeutic horizon for atrial fibrillation
Licensed content author	Sarah M. Schumacher,Jeffrey R. Martens
Licensed content date	September 2010
Licensed content volume number	7
Licensed content issue number	9
Number of pages	7
Start Page	1309
End Page	1315
Type of Use	reuse in a thesis/dissertation
Intended publisher of new work	other
Portion	full article
Format	both print and electronic
Are you the author of this Elsevier article?	Yes
Will you be translating?	No
Order reference number	

Title of your thesis/dissertation	Mechanisms Controlling Kv Channel Surface Density in Cardiac Myocytes
Expected completion date	Sep 2011
Estimated size (number of pages)	140
Elsevier VAT number	GB 494 6272 12
Permissions price	0.00 USD
VAT/Local Sales Tax	0.00 USD / GBP
Total	0.00 USD
Terms and Conditions	

INTRODUCTION

1. The publisher for this copyrighted material is Elsevier. By clicking "accept" in connection with completing this licensing transaction, you agree that the following terms and conditions apply to this transaction (along with the Billing and Payment terms and conditions established by Copyright Clearance Center, Inc. ("CCC"), at the time that you opened your Rightslink account and that are available at any time at http://myaccount.copyright.com).

GENERAL TERMS

2. Elsevier hereby grants you permission to reproduce the aforementioned material subject to the terms and conditions indicated.

3. Acknowledgement: If any part of the material to be used (for example, figures) has appeared in our publication with credit or acknowledgement to another source, permission must also be sought from that source. If such permission is not obtained then that material may not be included in your publication/copies. Suitable acknowledgement to the source must be made, either as a footnote or in a reference list at the end of your publication, as follows:

"Reprinted from Publication title, Vol /edition number, Author(s), Title of article / title of chapter, Pages No., Copyright (Year), with permission from Elsevier [OR APPLICABLE SOCIETY COPYRIGHT OWNER]." Also Lancet special credit - "Reprinted from The Lancet, Vol. number, Author(s), Title of article, Pages No., Copyright (Year), with permission from Elsevier."

4. Reproduction of this material is confined to the purpose and/or media for which permission is hereby given.

5. Altering/Modifying Material: Not Permitted. However figures and illustrations may be altered/adapted minimally to serve your work. Any other abbreviations, additions, deletions and/or any other alterations shall be made only with prior written authorization of Elsevier Ltd. (Please contact Elsevier at permissions@elsevier.com)

6. If the permission fee for the requested use of our material is waived in this instance, please be advised that your future requests for Elsevier materials may attract a fee.

7. Reservation of Rights: Publisher reserves all rights not specifically granted in the combination of (i) the license details provided by you and accepted in the course of this

licensing transaction, (ii) these terms and conditions and (iii) CCC's Billing and Payment terms and conditions.

8. License Contingent Upon Payment: While you may exercise the rights licensed immediately upon issuance of the license at the end of the licensing process for the transaction, provided that you have disclosed complete and accurate details of your proposed use, no license is finally effective unless and until full payment is received from you (either by publisher or by CCC) as provided in CCC's Billing and Payment terms and conditions. If full payment is not received on a timely basis, then any license preliminarily granted shall be deemed automatically revoked and shall be void as if never granted. Further, in the event that you breach any of these terms and conditions or any of CCC's Billing and Payment terms and conditions, the license is automatically revoked and shall be void as if never granted. Use of materials as described in a revoked license, as well as any use of the materials beyond the scope of an unrevoked license, may constitute copyright infringement and publisher reserves the right to take any and all action to protect its copyright in the materials.

9. Warranties: Publisher makes no representations or warranties with respect to the licensed material.

10. Indemnity: You hereby indemnify and agree to hold harmless publisher and CCC, and their respective officers, directors, employees and agents, from and against any and all claims arising out of your use of the licensed material other than as specifically authorized pursuant to this license.

11. No Transfer of License: This license is personal to you and may not be sublicensed, assigned, or transferred by you to any other person without publisher's written permission.

12. No Amendment Except in Writing: This license may not be amended except in a writing signed by both parties (or, in the case of publisher, by CCC on publisher's behalf).

13. Objection to Contrary Terms: Publisher hereby objects to any terms contained in any purchase order, acknowledgment, check endorsement or other writing prepared by you, which terms are inconsistent with these terms and conditions or CCC's Billing and Payment terms and conditions. These terms and conditions, together with CCC's Billing and Payment terms and conditions (which are incorporated herein), comprise the entire agreement between you and publisher (and CCC) concerning this licensing transaction. In the event of any conflict between your obligations established by these terms and conditions and those established by CCC's Billing and Payment terms and conditions, these terms and conditions shall control.

14. Revocation: Elsevier or Copyright Clearance Center may deny the permissions described in this License at their sole discretion, for any reason or no reason, with a full refund payable to you. Notice of such denial will be made using the contact information provided by you. Failure to receive such notice will not alter or invalidate the denial. In no event will Elsevier or Copyright Clearance Center be responsible or liable for any costs, expenses or damage incurred by you as a result of a denial of your permission request, other than a refund of the amount(s) paid by you to Elsevier and/or Copyright Clearance Center for denied permissions.

LIMITED LICENSE

The following terms and conditions apply only to specific license types:

15. **Translation**: This permission is granted for non-exclusive world **English** rights only unless your license was granted for translation rights. If you licensed translation rights you may only translate this content into the languages you requested. A professional translator must perform all translations and reproduce the content word for word preserving the integrity of the article. If this license is to re-use 1 or 2 figures then permission is granted for non-exclusive world rights in all languages.

16. **Website**: The following terms and conditions apply to electronic reserve and author websites:
Electronic reserve: If licensed material is to be posted to website, the web site is to be password-protected and made available only to bona fide students registered on a relevant course if:
This license was made in connection with a course,
This permission is granted for 1 year only. You may obtain a license for future website posting,
All content posted to the web site must maintain the copyright information line on the bottom of each image,
A hyper-text must be included to the Homepage of the journal from which you are licensing at http://www.sciencedirect.com/science/journal/xxxxx or the Elsevier homepage for books at http://www.elsevier.com , and
Central Storage: This license does not include permission for a scanned version of the material to be stored in a central repository such as that provided by Heron/XanEdu.

17. **Author website** for journals with the following additional clauses:

All content posted to the web site must maintain the copyright information line on the bottom of each image, and
he permission granted is limited to the personal version of your paper. You are not allowed to download and post the published electronic version of your article (whether PDF or HTML, proof or final version), nor may you scan the printed edition to create an electronic version,
A hyper-text must be included to the Homepage of the journal from which you are licensing at http://www.sciencedirect.com/science/journal/xxxxx , As part of our normal production process, you will receive an e-mail notice when your article appears on Elsevier's online service ScienceDirect (www.sciencedirect.com). That e-mail will include the article's Digital Object Identifier (DOI). This number provides the electronic link to the published article and should be included in the posting of your personal version. We ask that you wait until you receive this e-mail and have the DOI to do any posting.
Central Storage: This license does not include permission for a scanned version of the material to be stored in a central repository such as that provided by Heron/XanEdu.

18. **Author website** for books with the following additional clauses:
Authors are permitted to place a brief summary of their work online only.
A hyper-text must be included to the Elsevier homepage at http://www.elsevier.com

All content posted to the web site must maintain the copyright information line on the bottom of each image
You are not allowed to download and post the published electronic version of your chapter,

nor may you scan the printed edition to create an electronic version.
Central Storage: This license does not include permission for a scanned version of the material to be stored in a central repository such as that provided by Heron/XanEdu.

19. **Website** (regular and for author): A hyper-text must be included to the Homepage of the journal from which you are licensing at http://www.sciencedirect.com/science/journal/xxxxx. or for books to the Elsevier homepage at http://www.elsevier.com

20. **Thesis/Dissertation**: If your license is for use in a thesis/dissertation your thesis may be submitted to your institution in either print or electronic form. Should your thesis be published commercially, please reapply for permission. These requirements include permission for the Library and Archives of Canada to supply single copies, on demand, of the complete thesis and include permission for UMI to supply single copies, on demand, of the complete thesis. Should your thesis be published commercially, please reapply for permission.

21. **Other Conditions**:

v1.6

Gratis licenses (referencing $0 in the Total field) are free. Please retain this printable license for your reference. No payment is required.

If you would like to pay for this license now, please remit this license along with your payment made payable to "COPYRIGHT CLEARANCE CENTER" otherwise you will be invoiced within 48 hours of the license date. Payment should be in the form of a check or money order referencing your account number and this invoice number RLNK11049518.
Once you receive your invoice for this order, you may pay your invoice by credit card. Please follow instructions provided at that time.

Make Payment To:
Copyright Clearance Center
Dept 001
P.O. Box 843006
Boston, MA 02284-3006

For suggestions or comments regarding this order, contact Rightslink Customer Support: customercare@copyright.com or +1-877-622-5543 (toll free in the US) or +1-978-646-2777.

WOLTERS KLUWER HEALTH LICENSE TERMS AND CONDITIONS

Sep 14, 2011

This is a License Agreement between Sarah M Schumacher ("You") and Wolters Kluwer Health ("Wolters Kluwer Health") provided by Copyright Clearance Center ("CCC"). The license consists of your order details, the terms and conditions provided by Wolters Kluwer Health, and the payment terms and conditions.

All payments must be made in full to CCC. For payment instructions, please see information listed at the bottom of this form.

License Number	2743121493608
License date	Sep 06, 2011
Licensed content publisher	Wolters Kluwer Health
Licensed content publication	Circulation Research
Licensed content title	Antiarrhythmic Drug-Induced Internalization of the Atrial-Specific K Channel Kv1.5
Licensed content author	Sarah M. Schumacher, Dyke P. McEwen, Lian Zhang, Kristin L. Arendt, Kristin M. Van Genderen, Jeffrey R. Martens
Licensed content date	Jun 19, 2009
Volume Number	104
Issue Number	12
Type of Use	Dissertation/Thesis
Requestor type	Individual
Title of your thesis / dissertation	Mechanisms Controlling Kv Channel Surface Density in Cardiac Myocytes
Expected completion date	Sep 2011
Estimated size(pages)	140
Billing Type	Invoice
Billing Address	Department of Pharmacology University of Michigan Medical School Ann Arbor, MI 48109 United States
Customer reference info	
Total	0.00 USD
Terms and Conditions	

Terms and Conditions

1. A credit line will be prominently placed and include: for books - the author(s), title of book, editor, copyright holder, year of publication; For journals - the author(s), title of article, title of journal, volume number, issue number and inclusive pages.
2. The requestor warrants that the material shall not be used in any manner which may be

considered derogatory to the title, content, or authors of the material, or to Wolters Kluwer/Lippincott, Williams & Wilkins.

3. Permission is granted for one time use only as specified in your correspondence. Rights herein do not apply to future reproductions, editions, revisions, or other derivative works. Once term has expired, permission to renew must be made in writing.
4. Permission granted is non-exclusive, and is valid throughout the world in the English language and the languages specified in your original request.
5. Wolters Kluwer Health/ Lippincott, Williams & Wilkins, cannot supply the requestor with the original artwork or a "clean copy."
6. The requestor agrees to secure written permission from the author (for book material only).
7. Permission is valid if the borrowed material is original to a LWW imprint (Lippincott-Raven Publishers, Williams & Wilkins, Lea & Febiger, Harwal, Igaku-Shoin, Rapid Science, Little Brown & Company, Harper & Row Medical, American Journal of Nursing Co, and Urban & Schwarzenberg - English Language).
8. If you opt not to use the material requested above, please notify Rightslink within 90 days of the original invoice date.
9. Other Terms and Conditions:

v1.0

Gratis licenses (referencing $0 in the Total field) are free. Please retain this printable license for your reference. No payment is required.

If you would like to pay for this license now, please remit this license along with your payment made payable to "COPYRIGHT CLEARANCE CENTER" otherwise you will be invoiced within 48 hours of the license date. Payment should be in the form of a check or money order referencing your account number and this invoice number RLNK11048094.
Once you receive your invoice for this order, you may pay your invoice by credit card. Please follow instructions provided at that time.

Make Payment To:
Copyright Clearance Center
Dept 001
P.O. Box 843006
Boston, MA 02284-3006

For suggestions or comments regarding this order, contact Rightslink Customer Support: customercare@copyright.com or +1-877-622-5543 (toll free in the US) or +1-978-646-2777.

BIBLIOGRAPHY

1. Go AS, Hylek EM, Phillips KA, Chang Y, Henault LE, Selby JV, Singer DE. Prevalence of diagnosed atrial fibrillation in adults: National implications for rhythm management and stroke prevention: The anticoagulation and risk factors in atrial fibrillation (atria) study. *Jama*. 2001;285:2370-2375

2. Calkins H, Brugada J, Packer DL, Cappato R, Chen SA, Crijns HJ, Damiano RJ, Jr., Davies DW, Haines DE, Haissaguerre M, Iesaka Y, Jackman W, Jais P, Kottkamp H, Kuck KH, Lindsay BD, Marchlinski FE, McCarthy PM, Mont JL, Morady F, Nademanee K, Natale A, Pappone C, Prystowsky E, Raviele A, Ruskin JN, Shemin RJ. Hrs/ehra/ecas expert consensus statement on catheter and surgical ablation of atrial fibrillation: Recommendations for personnel, policy, procedures and follow-up. A report of the heart rhythm society (hrs) task force on catheter and surgical ablation of atrial fibrillation. *Heart Rhythm*. 2007;4:816-861

3. Feinberg WM, Blackshear JL, Laupacis A, Kronmal R, Hart RG. Prevalence, age distribution, and gender of patients with atrial fibrillation. Analysis and implications. *Archives of internal medicine*. 1995;155:469-473

4. Wattigney WA, Mensah GA, Croft JB. Increased atrial fibrillation mortality: United states, 1980-1998. *American journal of epidemiology*. 2002;155:819-826

5. Brand FN, Abbott RD, Kannel WB, Wolf PA. Characteristics and prognosis of lone atrial fibrillation. 30-year follow-up in the framingham study. *Jama*. 1985;254:3449-3453

6. Wolf PA, Abbott RD, Kannel WB. Atrial fibrillation as an independent risk factor for stroke: The framingham study. *Stroke; a journal of cerebral circulation*. 1991;22:983-988

7. Casella L, Abelmann WH, Ellis LB. Patients with mitral stenosis and systemic emboli; hemodynamic and clinical observations. *Archives of internal medicine*. 1964;114:773-781

8. Gage BF, Waterman AD, Shannon W, Boechler M, Rich MW, Radford MJ. Validation of clinical classification schemes for predicting stroke: Results from the national registry of atrial fibrillation. *Jama*. 2001;285:2864-2870

9. Crandall MA, Bradley DJ, Packer DL, Asirvatham SJ. Contemporary management of atrial fibrillation: Update on anticoagulation and invasive management strategies. *Mayo Clinic proceedings*. 2009;84:643-662

10. Roy D, Talajic M, Nattel S, Wyse DG, Dorian P, Lee KL, Bourassa MG, Arnold JM, Buxton AE, Camm AJ, Connolly SJ, Dubuc M, Ducharme A, Guerra PG, Hohnloser SH, Lambert J, Le Heuzey JY, O'Hara G, Pedersen OD, Rouleau JL, Singh BN, Stevenson LW, Stevenson WG, Thibault B, Waldo AL. Rhythm control versus rate control for atrial fibrillation and heart failure. *The New England journal of medicine*. 2008;358:2667-2677

11. Karch MR, Zrenner B, Deisenhofer I, Schreieck J, Ndrepepa G, Dong J, Lamprecht K, Barthel P, Luciani E, Schomig A, Schmitt C. Freedom from atrial tachyarrhythmias after catheter ablation of atrial fibrillation: A randomized comparison between 2 current ablation strategies. *Circulation*. 2005;111:2875-2880

12. Nilsson B, Chen X, Pehrson S, Kober L, Hilden J, Svendsen JH. Recurrence of pulmonary vein conduction and atrial fibrillation after pulmonary vein isolation for atrial fibrillation: A randomized trial of the ostial versus the extraostial ablation strategy. *American heart journal*. 2006;152:537 e531-538

13. Oral H, Veerareddy S, Good E, Hall B, Cheung P, Tamirisa K, Han J, Fortino J, Chugh A, Bogun F, Pelosi F, Jr., Morady F. Prevalence of asymptomatic recurrences of atrial fibrillation after successful radiofrequency catheter ablation. *Journal of cardiovascular electrophysiology*. 2004;15:920-924

14. Cappato R, Calkins H, Chen SA, Davies W, Iesaka Y, Kalman J, Kim YH, Klein G, Packer D, Skanes A. Worldwide survey on the methods, efficacy, and safety of catheter ablation for human atrial fibrillation. *Circulation*. 2005;111:1100-1105

15. d'Avila A, Ruskin JN. Nonpharmacologic strategies: The evolving story of ablation and hybrid therapy. *The American journal of cardiology*. 2008;102:20H-24H

16. Packer DL, Asirvatham S, Munger TM. Progress in nonpharmacologic therapy of atrial fibrillation. *Journal of cardiovascular electrophysiology*. 2003;14:S296-309

17. Amos GJ, Wettwer E, Metzger F, Li Q, Himmel HM, Ravens U. Differences between outward currents of human atrial and subepicardial ventricular myocytes. *The Journal of physiology*. 1996;491 (Pt 1):31-50

18. Camm AJ. Safety considerations in the pharmacological management of atrial fibrillation. *International journal of cardiology*. 2008;127:299-306

19. Camm AJ, Savelieva I. Advances in antiarrhythmic drug treatment of atrial fibrillation: Where do we stand now? *Heart Rhythm*. 2004;1:244-246

20. Mays DJ, Foose JM, Philipson LH, Tamkun MM. Localization of the kv1.5 k+ channel protein in explanted cardiac tissue. *The Journal of clinical investigation*. 1995;96:282-292

21. Kim SS, Knight BP. Electrical and pharmacologic cardioversion for atrial fibrillation. *The Medical clinics of North America*. 2008;92:101-120, xi

22. Fuster V, Ryden LE, Cannom DS, Crijns HJ, Curtis AB, Ellenbogen KA, Halperin JL, Le Heuzey JY, Kay GN, Lowe JE, Olsson SB, Prystowsky EN, Tamargo JL, Wann S, Priori SG, Blanc JJ, Budaj A, Camm AJ, Dean V, Deckers JW, Despres C, Dickstein K, Lekakis J, McGregor K, Metra M, Morais J, Osterspey A, Zamorano JL, Smith SC, Jr., Jacobs AK, Adams CD, Anderson JL, Antman EM, Hunt SA, Nishimura R, Ornato JP, Page RL, Riegel B. [acc/aha/esc 2006 guidelines for the management of patients with atrial fibrillation--excutive summary]. *Rev Port Cardiol*. 2007;26:383-446

23. Nerbonne JM, Kass RS. Molecular physiology of cardiac repolarization. *Physiol Rev*. 2005;85:1205-1253

24. Nattel S. New ideas about atrial fibrillation 50 years on. *Nature*. 2002;415:219-226

25. Allessie MA, Boyden PA, Camm AJ, Kleber AG, Lab MJ, Legato MJ, Rosen MR, Schwartz PJ, Spooner PM, Van Wagoner DR, Waldo AL. Pathophysiology and prevention of atrial fibrillation. *Circulation*. 2001;103:769-777

26. Sun H, Chartier D, Leblanc N, Nattel S. Intracellular calcium changes and tachycardia-induced contractile dysfunction in canine atrial myocytes. *Cardiovasc Res*. 2001;49:751-761

27. Courtemanche M, Ramirez RJ, Nattel S. Ionic mechanisms underlying human atrial action potential properties: Insights from a mathematical model. *The American journal of physiology*. 1998;275:H301-321

28. Ausma J, Wijffels M, Thone F, Wouters L, Allessie M, Borgers M. Structural changes of atrial myocardium due to sustained atrial fibrillation in the goat. *Circulation*. 1997;96:3157-3163

29. Ausma J, Wijffels M, van Eys G, Koide M, Ramaekers F, Allessie M, Borgers M. Dedifferentiation of atrial cardiomyocytes as a result of chronic atrial fibrillation. *Am J Pathol*. 1997;151:985-997

30. Brundel BJ, Henning RH, Kampinga HH, Van Gelder IC, Crijns HJ. Molecular mechanisms of remodeling in human atrial fibrillation. *Cardiovasc Res*. 2002;54:315-324

31. Brundel BJ, Kampinga HH, Henning RH. Calpain inhibition prevents pacing-induced cellular remodeling in a hl-1 myocyte model for atrial fibrillation. *Cardiovasc Res*. 2004;62:521-528

32. Ford JW, Milnes JT. New drugs targeting the cardiac ultra-rapid delayed-rectifier current (i kur): Rationale, pharmacology and evidence for potential therapeutic value. *Journal of cardiovascular pharmacology*. 2008;52:105-120

33. Vassallo P, Trohman RG. Prescribing amiodarone: An evidence-based review of clinical indications. *JAMA*. 2007;298:1312-1322

34. Brendel J, Peukert S. Blockers of the kv1.5 channel for the treatment of atrial arrhythmias. *Curr Med Chem Cardiovasc Hematol Agents*. 2003;1:273-287

35. Wang Z, Fermini B, Nattel S. Sustained depolarization-induced outward current in human atrial myocytes. Evidence for a novel delayed rectifier k+ current similar to kv1.5 cloned channel currents. *Circ Res*. 1993;73:1061-1076

36. Ravens U. Potassium channels in atrial fibrillation: Targets for atrial and pathology-specific therapy? *Heart Rhythm*. 2008;5:758-759

37. Brundel BJ, Van Gelder IC, Henning RH, Tuinenburg AE, Wietses M, Grandjean JG, Wilde AA, Van Gilst WH, Crijns HJ. Alterations in potassium channel gene expression in atria of patients with persistent and paroxysmal atrial fibrillation: Differential regulation of protein and mrna levels for k+ channels. *Journal of the American College of Cardiology*. 2001;37:926-932

38. Michelakis ED, Weir EK. The pathobiology of pulmonary hypertension. Smooth muscle cells and ion channels. *Clinics in chest medicine*. 2001;22:419-432

39. Sweeney M, Yuan JX. Hypoxic pulmonary vasoconstriction: Role of voltage-gated potassium channels. *Respiratory research*. 2000;1:40-48

40. Nattel S, Carlsson L. Innovative approaches to anti-arrhythmic drug therapy. *Nature reviews*. 2006;5:1034-1049

41. Waldo AL. A perspective on antiarrhythmic drug therapy to treat atrial fibrillation: There remains an unmet need. *American heart journal*. 2006;151:771-778

42. Decher N, Kumar P, Gonzalez T, Pirard B, Sanguinetti MC. Binding site of a novel kv1.5 blocker: A "foot in the door" against atrial fibrillation. *Molecular pharmacology*. 2006;70:1204-1211

43. Schram G, Pourrier M, Melnyk P, Nattel S. Differential distribution of cardiac ion channel expression as a basis for regional specialization in electrical function. *Circulation research*. 2002;90:939-950

44. Gogelein H, Brendel J, Steinmeyer K, Strubing C, Picard N, Rampe D, Kopp K, Busch AE, Bleich M. Effects of the atrial antiarrhythmic drug ave0118 on cardiac ion channels. *Naunyn Schmiedebergs Arch Pharmacol*. 2004;370:183-192

45. Gross MF, Beaudoin S, McNaughton-Smith G, Amato GS, Castle NA, Huang C, Zou A, Yu W. Aryl sulfonamido indane inhibitors of the kv1.5 ion channel. *Bioorg Med Chem Lett*. 2007;17:2849-2853

46. Eldstrom J, Wang Z, Xu H, Pourrier M, Ezrin A, Gibson K, Fedida D. The molecular basis of high-affinity binding of the antiarrhythmic compound vernakalant (rsd1235) to kv1.5 channels. *Molecular pharmacology*. 2007;72:1522-1534

47. Fedida D. Vernakalant (rsd1235): A novel, atrial-selective antifibrillatory agent. *Expert Opin Investig Drugs*. 2007;16:519-532

48. Fedida D, Orth PM, Chen JY, Lin S, Plouvier B, Jung G, Ezrin AM, Beatch GN. The mechanism of atrial antiarrhythmic action of rsd1235. *J Cardiovasc Electrophysiol*. 2005;16:1227-1238

49. Mao ZL, Wheeler JJ, Clohs L, Beatch GN, Keirns J. Pharmacokinetics of novel atrial-selective antiarrhythmic agent vernakalant hydrochloride injection (rsd1235): Influence of cyp2d6 expression and other factors. *J Clin Pharmacol*. 2009;49:17-29

50. Schumacher SM, McEwen DP, Zhang L, Arendt KL, Van Genderen KM, Martens JR. Antiarrhythmic drug-induced internalization of the atrial-specific k+ channel kv1.5. *Circulation research*. 2009;104:1390-1398

51. van der Heyden MA, Smits ME, Vos MA. Drugs and trafficking of ion channels: A new pro-arrhythmic threat on the horizon? *British journal of pharmacology*. 2008;153:406-409

52. Dennis A, Wang L, Wan X, Ficker E. Herg channel trafficking: Novel targets in drug-induced long qt syndrome. *Biochemical Society transactions*. 2007;35:1060-1063

53. Rajamani S, Eckhardt LL, Valdivia CR, Klemens CA, Gillman BM, Anderson CL, Holzem KM, Delisle BP, Anson BD, Makielski JC, January CT. Drug-induced long qt syndrome: Herg k+ channel block and disruption of protein trafficking by fluoxetine and norfluoxetine. *British journal of pharmacology*. 2006;149:481-489

54. Takemasa H, Nagatomo T, Abe H, Kawakami K, Igarashi T, Tsurugi T, Kabashima N, Tamura M, Okazaki M, Delisle BP, January CT, Otsuji Y. Coexistence of herg current block and disruption of protein trafficking in ketoconazole-induced long qt syndrome. *British journal of pharmacology*. 2008;153:439-447

55. Yeung KS, Meanwell NA. Inhibition of herg channel trafficking: An under-explored mechanism for drug-induced qt prolongation. *ChemMedChem*. 2008;3:1501-1502

56. Cordes JS, Sun Z, Lloyd DB, Bradley JA, Opsahl AC, Tengowski MW, Chen X, Zhou J. Pentamidine reduces herg expression to prolong the qt interval. *British journal of pharmacology*. 2005;145:15-23

57. Guo J, Massaeli H, Li W, Xu J, Luo T, Shaw J, Kirshenbaum LA, Zhang S. Identification of ikr and its trafficking disruption induced by probucol in cultured neonatal rat cardiomyocytes. *The Journal of pharmacology and experimental therapeutics*. 2007;321:911-920

58. Kuryshev YA, Ficker E, Wang L, Hawryluk P, Dennis AT, Wible BA, Brown AM, Kang J, Chen XL, Sawamura K, Reynolds W, Rampe D. Pentamidine-induced long qt syndrome and block of herg trafficking. *The Journal of pharmacology and experimental therapeutics*. 2005;312:316-323

59. Ficker E, Dennis A, Kuryshev Y, Wible BA, Brown AM. Herg channel trafficking. *Novartis Foundation symposium*. 2005;266:57-69; discussion 70-54, 95-59

60. Walker VE, Atanasiu R, Lam H, Shrier A. Co-chaperone fkbp38 promotes herg trafficking. *The Journal of biological chemistry*. 2007;282:23509-23516

61. Ficker E, Obejero-Paz CA, Zhao S, Brown AM. The binding site for channel blockers that rescue misprocessed human long qt syndrome type 2 ether-a-gogo-related gene (herg) mutations. *The Journal of biological chemistry*. 2002;277:4989-4998

62. Ficker E, Dennis AT, Wang L, Brown AM. Role of the cytosolic chaperones hsp70 and hsp90 in maturation of the cardiac potassium channel herg. *Circ Res*. 2003;92:e87-100

63. Ficker E, Kuryshev YA, Dennis AT, Obejero-Paz C, Wang L, Hawryluk P, Wible BA, Brown AM. Mechanisms of arsenic-induced prolongation of cardiac repolarization. *Molecular pharmacology*. 2004;66:33-44

64. Drolet B, Simard C, Roden DM. Unusual effects of a qt-prolonging drug, arsenic trioxide, on cardiac potassium currents. *Circulation*. 2004;109:26-29

65. Smyth JW, Hong TT, Gao D, Vogan JM, Jensen BC, Fong TS, Simpson PC, Stainier DY, Chi NC, Shaw RM. Limited forward trafficking of connexin 43 reduces cell-cell coupling in stressed human and mouse myocardium. *J Clin Invest*. 2010;120:266-279

66. Ellgaard L, Helenius A. Quality control in the endoplasmic reticulum. *Nature reviews*. 2003;4:181-191

67. Olson TM, Alekseev AE, Liu XK, Park S, Zingman LV, Bienengraeber M, Sattiraju S, Ballew JD, Jahangir A, Terzic A. Kv1.5 channelopathy due to kcna5 loss-of-function mutation causes human atrial fibrillation. *Human molecular genetics*. 2006;15:2185-2191

68. London B, Guo W, Pan X, Lee JS, Shusterman V, Rocco CJ, Logothetis DA, Nerbonne JM, Hill JA. Targeted replacement of kv1.5 in the mouse leads to loss of the 4-aminopyridine-sensitive component of i(k,slow) and resistance to drug-induced qt prolongation. *Circ Res*. 2001;88:940-946

69. Marks DL, Pagano RE. Endocytosis and sorting of glycosphingolipids in sphingolipid storage disease. *Trends Cell Biol.* 2002;12:605-613

70. Maxfield FR, McGraw TE. Endocytic recycling. *Nat.Rev.Mol.Cell Biol.* 2004;5:121-132

71. Prekeris R. Rabs, rips, fips, and endocytic membrane traffic. *ScientificWorldJournal.* 2003;3:870-880

72. Brown SS. Cooperation between microtubule- and actin-based motor proteins. *Annu.Rev.Cell Dev.Biol.* 1999;15:63-80

73. Dantzig JA, Liu TY, Goldman YE. Functional studies of individual myosin molecules. *Ann.N.Y.Acad.Sci.* 2006;1080:1-18:1-18

74. Langford GM. Myosin-v, a versatile motor for short-range vesicle transport. *Traffic.* 2002;3:859-865

75. Seabra MC, Coudrier E. Rab gtpases and myosin motors in organelle motility. *Traffic.* 2004;5:393-399

76. Steele DF, Eldstrom J, Fedida D. Mechanisms of cardiac potassium channel trafficking. *The Journal of physiology*. 2007;582:17-26

77. Steele DF, Zadeh AD, Loewen ME, Fedida D. Localization and trafficking of cardiac voltage-gated potassium channels. *Biochemical Society transactions*. 2007;35:1069-1073

78. Deutsch C. The birth of a channel. *Neuron*. 2003;40:265-276

79. Deutsch C. Potassium channel ontogeny. *Annual review of physiology*. 2002;64:19-46

80. Staudacher I, Schweizer PA, Katus HA, Thomas D. Herg: Protein trafficking and potential for therapy and drug side effects. *Current opinion in drug discovery & development*.13:23-30

81. Robinson JM, Deutsch C. Coupled tertiary folding and oligomerization of the t1 domain of kv channels. *Neuron*. 2005;45:223-232

82. Babila T, Moscucci A, Wang H, Weaver FE, Koren G. Assembly of mammalian voltage-gated potassium channels: Evidence for an important role of the first transmembrane segment. *Neuron*. 1994;12:615-626

83. Levitan ES, Takimoto K. Surface expression of kv1 voltage-gated k+ channels is governed by a c-terminal motif. *Trends in cardiovascular medicine*. 2000;10:317-320

84. Li D, Takimoto K, Levitan ES. Surface expression of kv1 channels is governed by a c-terminal motif. *The Journal of biological chemistry*. 2000;275:11597-11602

85. Wible BA, Yang Q, Kuryshev YA, Accili EA, Brown AM. Cloning and expression of a novel k+ channel regulatory protein, kchap. *The Journal of biological chemistry*. 1998;273:11745-11751

86. Jindal HK, Folco EJ, Liu GX, Koren G. Posttranslational modification of voltage-dependent potassium channel kv1.5: Cooh-terminal palmitoylation modulates its biological properties. *Am J Physiol Heart Circ Physiol*. 2008;294:H2012-2021

87. Zhang L, Foster K, Li Q, Martens JR. S-acylation regulates kv1.5 channel surface expression. *Am J Physiol Cell Physiol*. 2007;293:C152-161

88. England SK, Uebele VN, Kodali J, Bennett PB, Tamkun MM. A novel k+ channel beta-subunit (hkv beta 1.3) is produced via alternative mrna splicing. *The Journal of biological chemistry*. 1995;270:28531-28534

89. Gonzalez T, Navarro-Polanco R, Arias C, Caballero R, Moreno I, Delpon E, Tamargo J, Tamkun MM, Valenzuela C. Assembly with the kvbeta1.3 subunit modulates drug block of hkv1.5 channels. *Molecular pharmacology*. 2002;62:1456-1463

90. Kwak YG, Hu N, Wei J, George AL, Jr., Grobaski TD, Tamkun MM, Murray KT. Protein kinase a phosphorylation alters kvbeta1.3 subunit-mediated inactivation of the kv1.5 potassium channel. *The Journal of biological chemistry*. 1999;274:13928-13932

91. Kwak YG, Navarro-Polanco RA, Grobaski T, Gallagher DJ, Tamkun MM. Phosphorylation is required for alteration of kv1.5 k(+) channel function by the kvbeta1.3 subunit. *The Journal of biological chemistry*. 1999;274:25355-25361

92. Uebele VN, England SK, Chaudhary A, Tamkun MM, Snyders DJ. Functional differences in kv1.5 currents expressed in mammalian cell lines are due to the presence of endogenous kv beta 2.1 subunits. *The Journal of biological chemistry*. 1996;271:2406-2412

93. Uebele VN, England SK, Gallagher DJ, Snyders DJ, Bennett PB, Tamkun MM. Distinct domains of the voltage-gated k+ channel kv beta 1.3 beta-subunit affect voltage-dependent gating. *The American journal of physiology*. 1998;274:C1485-1495

94. Mason HS, Latten MJ, Godoy LD, Horowitz B, Kenyon JL. Modulation of kv1.5 currents by protein kinase a, tyrosine kinase, and protein tyrosine phosphatase requires an intact cytoskeleton. *Molecular pharmacology*. 2002;61:285-293

95. Williams CP, Hu N, Shen W, Mashburn AB, Murray KT. Modulation of the human kv1.5 channel by protein kinase c activation: Role of the kvbeta1.2 subunit. *The Journal of pharmacology and experimental therapeutics*. 2002;302:545-550

96. Holmes TC, Fadool DA, Ren R, Levitan IB. Association of src tyrosine kinase with a human potassium channel mediated by sh3 domain. *Science (New York, N.Y.* 1996;274:2089-2091

97. Philipson LH, Hice RE, Schaefer K, LaMendola J, Bell GI, Nelson DJ, Steiner DF. Sequence and functional expression in xenopus oocytes of a human insulinoma and islet potassium channel. *Proceedings of the National Academy of Sciences of the United States of America*. 1991;88:53-57

98. Folco EJ, Liu GX, Koren G. Caveolin-3 and sap97 form a scaffolding protein complex that regulates the voltage-gated potassium channel kv1.5. *Am J Physiol Heart Circ Physiol*. 2004;287:H681-690

99. Abi-Char J, El-Haou S, Balse E, Neyroud N, Vranckx R, Coulombe A, Hatem SN. The anchoring protein sap97 retains kv1.5 channels in the plasma membrane of cardiac myocytes. *Am J Physiol Heart Circ Physiol*. 2008;294:H1851-1861

100. Abi-Char J, Maguy A, Coulombe A, Balse E, Ratajczak P, Samuel JL, Nattel S, Hatem SN. Membrane cholesterol modulates kv1.5 potassium channel distribution and function in rat cardiomyocytes. *The Journal of physiology*. 2007;582:1205-1217

101. Eldstrom J, Choi WS, Steele DF, Fedida D. Sap97 increases kv1.5 currents through an indirect n-terminal mechanism. *FEBS letters*. 2003;547:205-211

102. Martens JR, Sakamoto N, Sullivan SA, Grobaski TD, Tamkun MM. Isoform-specific localization of voltage-gated k+ channels to distinct lipid raft populations. Targeting of kv1.5 to caveolae. *The Journal of biological chemistry*. 2001;276:8409-8414

103. Maruoka ND, Steele DF, Au BP, Dan P, Zhang X, Moore ED, Fedida D. Alpha-actinin-2 couples to cardiac kv1.5 channels, regulating current density and channel localization in hek cells. *FEBS letters*. 2000;473:188-194

104. Mathur R, Choi WS, Eldstrom J, Wang Z, Kim J, Steele DF, Fedida D. A specific n-terminal residue in kv1.5 is required for upregulation of the channel by sap97. *Biochemical and biophysical research communications*. 2006;342:1-8

105. McEwen DP, Li Q, Jackson S, Jenkins PM, Martens JR. Caveolin regulates kv1.5 trafficking to cholesterol-rich membrane microdomains. *Molecular pharmacology*. 2008;73:678-685

106. Leonoudakis D, Conti LR, Anderson S, Radeke CM, McGuire LM, Adams ME, Froehner SC, Yates JR, 3rd, Vandenberg CA. Protein trafficking and anchoring

complexes revealed by proteomic analysis of inward rectifier potassium channel (kir2.X)-associated proteins. *The Journal of biological chemistry*. 2004;279:22331-22346

107. Murata M, Buckett PD, Zhou J, Brunner M, Folco E, Koren G. Sap97 interacts with kv1.5 in heterologous expression systems. *Am J Physiol Heart Circ Physiol*. 2001;281:H2575-2584

108. Tiffany AM, Manganas LN, Kim E, Hsueh YP, Sheng M, Trimmer JS. Psd-95 and sap97 exhibit distinct mechanisms for regulating k(+) channel surface expression and clustering. *The Journal of cell biology*. 2000;148:147-158

109. Eldstrom J, Doerksen KW, Steele DF, Fedida D. N-terminal pdz-binding domain in kv1 potassium channels. *FEBS letters*. 2002;531:529-537

110. Cukovic D, Lu GW, Wible B, Steele DF, Fedida D. A discrete amino terminal domain of kv1.5 and kv1.4 potassium channels interacts with the spectrin repeats of alpha-actinin-2. *FEBS letters*. 2001;498:87-92

111. McEwen DP, Schumacher SM, Li Q, Benson MD, Iniguez-Lluhi JA, Van Genderen KM, Martens JR. Rab-gtpase-dependent endocytic recycling of kv1.5 in atrial myocytes. *The Journal of biological chemistry*. 2007;282:29612-29620

112. Choi WS, Khurana A, Mathur R, Viswanathan V, Steele DF, Fedida D. Kv1.5 surface expression is modulated by retrograde trafficking of newly endocytosed channels by the dynein motor. *Circulation research*. 2005;97:363-371

113. Balse E, El-Haou S, Dillanian G, Dauphin A, Eldstrom J, Fedida D, Coulombe A, Hatem SN. Cholesterol modulates the recruitment of kv1.5 channels from rab11-associated recycling endosome in native atrial myocytes. *Proceedings of the National Academy of Sciences of the United States of America*. 2009;106:14681-14686

114. Benson MD, Li QJ, Kieckhafer K, Dudek D, Whorton MR, Sunahara RK, Iniguez-Lluhi JA, Martens JR. Sumo modification regulates inactivation of the voltage-gated potassium channel kv1.5. *Proceedings of the National Academy of Sciences of the United States of America*. 2007;104:1805-1810

115. Boehmer C, Laufer J, Jeyaraj S, Klaus F, Lindner R, Lang F, Palmada M. Modulation of the voltage-gated potassium channel kv1.5 by the sgk1 protein kinase involves inhibition of channel ubiquitination. *Cell Physiol Biochem*. 2008;22:591-600

116. Kato M, Ogura K, Miake J, Sasaki N, Taniguchi S, Igawa O, Yoshida A, Hoshikawa Y, Murata M, Nanba E, Kurata Y, Kawata Y, Ninomiya H, Morisaki T, Kitakaze M, Hisatome I. Evidence for proteasomal degradation of kv1.5 channel protein. *Biochemical and biophysical research communications*. 2005;337:343-348

117. Lafuente-Lafuente C, Mouly S, Longas-Tejero MA, Bergmann JF. Antiarrhythmics for maintaining sinus rhythm after cardioversion of atrial fibrillation. *Cochrane database of systematic reviews (Online)*. 2007:CD005049

118. Lafuente-Lafuente C, Mouly S, Longas-Tejero MA, Mahe I, Bergmann JF. Antiarrhythmic drugs for maintaining sinus rhythm after cardioversion of atrial fibrillation: A systematic review of randomized controlled trials. *Archives of internal medicine*. 2006;166:719-728

119. Feng J, Wible B, Li GR, Wang Z, Nattel S. Antisense oligodeoxynucleotides directed against kv1.5 mrna specifically inhibit ultrarapid delayed rectifier k+ current in cultured adult human atrial myocytes. *Circulation research*. 1997;80:572-579

120. Wible BA, Hawryluk P, Ficker E, Kuryshev YA, Kirsch G, Brown AM. Herg-lite: A novel comprehensive high-throughput screen for drug-induced herg risk. *Journal of pharmacological and toxicological methods*. 2005;52:136-145

121. Snyders J, Knoth KM, Roberds SL, Tamkun MM. Time-, voltage-, and state-dependent block by quinidine of a cloned human cardiac potassium channel. *Molecular pharmacology*. 1992;41:322-330

122. Miesenbock G, De Angelis DA, Rothman JE. Visualizing secretion and synaptic transmission with ph-sensitive green fluorescent proteins. *Nature*. 1998;394:192-195

123. Caballero R, Pourrier M, Schram G, Delpon E, Tamargo J, Nattel S. Effects of flecainide and quinidine on kv4.2 currents: Voltage dependence and role of s6 valines. *British journal of pharmacology*. 2003;138:1475-1484

124. Yang T, Snyders DJ, Roden DM. Inhibition of cardiac potassium currents by the vesnarinone analog opc-18790: Comparison with quinidine and dofetilide. *The Journal of pharmacology and experimental therapeutics*. 1997;280:1170-1175

125. O'Connell KM, Whitesell JD, Tamkun MM. Localization and mobility of the delayed-rectifer k+ channel kv2.1 in adult cardiomyocytes. *Am J Physiol Heart Circ Physiol*. 2008;294:H229-237

126. Chen FS, Steele D, Fedida D. Allosteric effects of permeating cations on gating currents during k+ channel deactivation. *The Journal of general physiology*. 1997;110:87-100

127. White NJ. Cardiotoxicity of antimalarial drugs. *The Lancet infectious diseases*. 2007;7:549-558

128. Snyders DJ, Yeola SW. Determinants of antiarrhythmic drug action. Electrostatic and hydrophobic components of block of the human cardiac hkv1.5 channel. *Circ Res*. 1995;77:575-583

129. Decher N, Pirard B, Bundis F, Peukert S, Baringhaus KH, Busch AE, Steinmeyer K, Sanguinetti MC. Molecular basis for kv1.5 channel block: Conservation of drug binding sites among voltage-gated k+ channels. *The Journal of biological chemistry*. 2004;279:394-400

130. Drolet B, Simard C, Mizoue L, Roden DM. Human cardiac potassium channel DNA polymorphism modulates access to drug-binding site and causes drug resistance. *The Journal of clinical investigation*. 2005;115:2209-2213

131. Macia E, Ehrlich M, Massol R, Boucrot E, Brunner C, Kirchhausen T. Dynasore, a cell-permeable inhibitor of dynamin. *Developmental cell*. 2006;10:839-850

132. Kirchhausen T, Macia E, Pelish HE. Use of dynasore, the small molecule inhibitor of dynamin, in the regulation of endocytosis. *Methods in enzymology*. 2008;438:77-93

133. Newton AJ, Kirchhausen T, Murthy VN. Inhibition of dynamin completely blocks compensatory synaptic vesicle endocytosis. *Proceedings of the National Academy of Sciences of the United States of America*. 2006;103:17955-17960

134. King SJ, Brown CL, Maier KC, Quintyne NJ, Schroer TA. Analysis of the dynein-dynactin interaction in vitro and in vivo. *Molecular biology of the cell*. 2003;14:5089-5097

135. Melkonian KA, Maier KC, Godfrey JE, Rodgers M, Schroer TA. Mechanism of dynamitin-mediated disruption of dynactin. *The Journal of biological chemistry*. 2007;282:19355-19364

136. Smillie KJ, Cousin MA. Dynamin i phosphorylation and the control of synaptic vesicle endocytosis. *Biochemical Society symposium*. 2005:87-97

137. Steinbeck G, Remp T, Hoffmann E. Effects of class i drugs on atrial fibrillation. *Journal of cardiovascular electrophysiology*. 1998;9:S104-108

138. Colatsky TJ, Follmer CH, Starmer CF. Channel specificity in antiarrhythmic drug action. Mechanism of potassium channel block and its role in suppressing and aggravating cardiac arrhythmias. *Circulation*. 1990;82:2235-2242

139. Siddoway LA, Roden DM, Woosley RL. Clinical pharmacology of old and new antiarrhythmic drugs. *Cardiovascular clinics*. 1985;15:199-248

140. Colatsky TJ. Mechanisms of action of lidocaine and quinidine on action potential duration in rabbit cardiac purkinje fibers. An effect on steady state sodium currents? *Circ Res*. 1982;50:17-27

141. Slawsky MT, Castle NA. K+ channel blocking actions of flecainide compared with those of propafenone and quinidine in adult rat ventricular myocytes. *The Journal of pharmacology and experimental therapeutics*. 1994;269:66-74

142. Martens JR, Navarro-Polanco R, Coppock EA, Nishiyama A, Parshley L, Grobaski TD, Tamkun MM. Differential targeting of shaker-like potassium channels to lipid rafts. *The Journal of biological chemistry*. 2000;275:7443-7446

143. Zlochiver S, Munoz V, Vikstrom KL, Taffet SM, Berenfeld O, Jalife J. Electrotonic myofibroblast-to-myocyte coupling increases propensity to reentrant arrhythmias in two-dimensional cardiac monolayers. *Biophysical journal*. 2008;95:4469-4480

144. Van Wagoner DR, Pond AL, McCarthy PM, Trimmer JS, Nerbonne JM. Outward k+ current densities and kv1.5 expression are reduced in chronic human atrial fibrillation. *Circulation research*. 1997;80:772-781

145. Christ T, Wettwer E, Voigt N, Hala O, Radicke S, Matschke K, Varro A, Dobrev D, Ravens U. Pathology-specific effects of the ikur/ito/ik,ach blocker ave0118 on ion channels in human chronic atrial fibrillation. *British journal of pharmacology*. 2008;154:1619-1630

146. Ausma J, Litjens N, Lenders MH, Duimel H, Mast F, Wouters L, Ramaekers F, Allessie M, Borgers M. Time course of atrial fibrillation-induced cellular structural remodeling in atria of the goat. *Journal of molecular and cellular cardiology*. 2001;33:2083-2094

147. Thijssen VL, Ausma J, Liu GS, Allessie MA, van Eys GJ, Borgers M. Structural changes of atrial myocardium during chronic atrial fibrillation. *Cardiovasc Pathol*. 2000;9:17-28

148. Goette A, Honeycutt C, Langberg JJ. Electrical remodeling in atrial fibrillation. Time course and mechanisms. *Circulation*. 1996;94:2968-2974

149. Cai D, McEwen DP, Martens JR, Meyhofer E, Verhey KJ. Single molecule imaging reveals differences in microtubule track selection between kinesin motors. *PLoS Biol*. 2009;7:e1000216

150. Zadeh AD, Cheng Y, Xu H, Wong N, Wang Z, Goonasekara C, Steele DF, Fedida D. Kif5b is an essential forward trafficking motor for the kv1.5 cardiac potassium channel. *The Journal of physiology*. 2009;587:4565-4574

151. Desnos C, Huet S, Darchen F. 'Should i stay or should i go?': Myosin v function in organelle trafficking. *Biol Cell*. 2007;99:411-423

152. Dantzig JA, Liu TY, Goldman YE. Functional studies of individual myosin molecules. *Annals of the New York Academy of Sciences*. 2006;1080:1-18

153. Zhao LP, Koslovsky JS, Reinhard J, Bahler M, Witt AE, Provance DW, Jr., Mercer JA. Cloning and characterization of myr 6, an unconventional myosin of the dilute/myosin-v family. *Proceedings of the National Academy of Sciences of the United States of America*. 1996;93:10826-10831

154. Correia SS, Bassani S, Brown TC, Lise MF, Backos DS, El-Husseini A, Passafaro M, Esteban JA. Motor protein-dependent transport of ampa receptors into spines during long-term potentiation. *Nat Neurosci*. 2008;11:457-466

155. Pierobon P, Achouri S, Courty S, Dunn AR, Spudich JA, Dahan M, Cappello G. Velocity, processivity, and individual steps of single myosin v molecules in live cells. *Biophys J*. 2009;96:4268-4275

156. Yildiz A, Forkey JN, McKinney SA, Ha T, Goldman YE, Selvin PR. Myosin v walks hand-over-hand: Single fluorophore imaging with 1.5-nm localization. *Science (New York, N.Y*. 2003;300:2061-2065

157. Mehta AD, Rock RS, Rief M, Spudich JA, Mooseker MS, Cheney RE. Myosin-v is a processive actin-based motor. *Nature*. 1999;400:590-593

158. Vale RD, Milligan RA. The way things move: Looking under the hood of molecular motor proteins. *Science (New York, N.Y*. 2000;288:88-95

159. Baker JE, Krementsova EB, Kennedy GG, Armstrong A, Trybus KM, Warshaw DM. Myosin v processivity: Multiple kinetic pathways for head-to-head coordination. *Proceedings of the National Academy of Sciences of the United States of America*. 2004;101:5542-5546

160. Rudolf R, Kogel T, Kuznetsov SA, Salm T, Schlicker O, Hellwig A, Hammer JA, 3rd, Gerdes HH. Myosin va facilitates the distribution of secretory granules in the f-actin rich cortex of pc12 cells. *J Cell Sci*. 2003;116:1339-1348

161. Wu X, Rao K, Bowers MB, Copeland NG, Jenkins NA, Hammer JA, 3rd. Rab27a enables myosin va-dependent melanosome capture by recruiting the myosin to the organelle. *J Cell Sci*. 2001;114:1091-1100

162. Tabb JS, Molyneaux BJ, Cohen DL, Kuznetsov SA, Langford GM. Transport of er vesicles on actin filaments in neurons by myosin v. *J Cell Sci*. 1998;111 (Pt 21):3221-3234

163. Wang Z, Edwards JG, Riley N, Provance DW, Jr., Karcher R, Li XD, Davison IG, Ikebe M, Mercer JA, Kauer JA, Ehlers MD. Myosin vb mobilizes recycling endosomes and ampa receptors for postsynaptic plasticity. *Cell*. 2008;135:535-548

164. Volpicelli LA, Lah JJ, Fang G, Goldenring JR, Levey AI. Rab11a and myosin vb regulate recycling of the m4 muscarinic acetylcholine receptor. *J Neurosci*. 2002;22:9776-9784

165. Nedvetsky PI, Stefan E, Frische S, Santamaria K, Wiesner B, Valenti G, Hammer JA, 3rd, Nielsen S, Goldenring JR, Rosenthal W, Klussmann E. A role of myosin vb and rab11-fip2 in the aquaporin-2 shuttle. *Traffic*. 2007;8:110-123

166. Lapierre LA, Kumar R, Hales CM, Navarre J, Bhartur SG, Burnette JO, Provance DW, Jr., Mercer JA, Bahler M, Goldenring JR. Myosin vb is associated with plasma membrane recycling systems. *Mol Biol Cell*. 2001;12:1843-1857

167. Swiatecka-Urban A, Talebian L, Kanno E, Moreau-Marquis S, Coutermarsh B, Hansen K, Karlson KH, Barnaby R, Cheney RE, Langford GM, Fukuda M, Stanton BA. Myosin vb is required for trafficking of the cystic fibrosis transmembrane conductance regulator in rab11a-specific apical recycling endosomes in polarized human airway epithelial cells. *The Journal of biological chemistry*. 2007;282:23725-23736

168. Song BD, Leonard M, Schmid SL. Dynamin gtpase domain mutants that differentially affect gtp binding, gtp hydrolysis, and clathrin-mediated endocytosis. *The Journal of biological chemistry*. 2004;279:40431-40436

169. Jordens I, Marsman M, Kuijl C, Neefjes J. Rab proteins, connecting transport and vesicle fusion. *Traffic*. 2005;6:1070-1077

170. Roland JT, Bryant DM, Datta A, Itzen A, Mostov KE, Goldenring JR. Rab gtpase-myo5b complexes control membrane recycling and epithelial polarization. *Proceedings of the National Academy of Sciences of the United States of America*. 2011;108:2789-2794

171. Loewen ME, Wang Z, Eldstrom J, Dehghani Zadeh A, Khurana A, Steele DF, Fedida D. Shared requirement for dynein function and intact microtubule cytoskeleton for normal surface expression of cardiac potassium channels. *Am J Physiol Heart Circ Physiol*. 2009;296:H71-83

172. Leonoudakis D, Conti LR, Radeke CM, McGuire LM, Vandenberg CA. A multiprotein trafficking complex composed of sap97, cask, veli, and mint1 is associated with inward rectifier kir2 potassium channels. *The Journal of biological chemistry*. 2004;279:19051-19063

173. Petrecca K, Miller DM, Shrier A. Localization and enhanced current density of the kv4.2 potassium channel by interaction with the actin-binding protein filamin. *J Neurosci*. 2000;20:8736-8744

174. Hattan D, Nesti E, Cachero TG, Morielli AD. Tyrosine phosphorylation of kv1.2 modulates its interaction with the actin-binding protein cortactin. *The Journal of biological chemistry*. 2002;277:38596-38606

175. Kuznetsov SA, Langford GM, Weiss DG. Actin-dependent organelle movement in squid axoplasm. *Nature*. 1992;356:722-725

176. Fath KR, Trimbur GM, Burgess DR. Molecular motors are differentially distributed on golgi membranes from polarized epithelial cells. *The Journal of cell biology*. 1994;126:661-675

177. Atkinson SJ, Doberstein SK, Pollard TD. Moving off the beaten track. *Curr Biol*. 1992;2:326-328

178. Gurkan C, Lapp H, Alory C, Su AI, Hogenesch JB, Balch WE. Large-scale profiling of rab gtpase trafficking networks: The membrome. *Mol Biol Cell*. 2005;16:3847-3864

179. Brundel BJ, Ausma J, van Gelder IC, Van der Want JJ, van Gilst WH, Crijns HJ, Henning RH. Activation of proteolysis by calpains and structural changes in human paroxysmal and persistent atrial fibrillation. *Cardiovasc Res*. 2002;54:380-389

180. Schafler AE, Friedl R, Hekmat K, Hannekum A, Kirmanoglou K. Chronic atrial fibrillation: Decreased actin expression in patients with chronic atrial fibrillation. *J Cardiovasc Surg (Torino)*. 2008;49:83-86

181. Van Eyk JE, Powers F, Law W, Larue C, Hodges RS, Solaro RJ. Breakdown and release of myofilament proteins during ischemia and ischemia/reperfusion in rat hearts: Identification of degradation products and effects on the pca-force relation. *Circulation research*. 1998;82:261-271

182. Matsumura Y, Saeki E, Inoue M, Hori M, Kamada T, Kusuoka H. Inhomogeneous disappearance of myofilament-related cytoskeletal proteins in stunned myocardium of guinea pig. *Circulation research*. 1996;79:447-454

183. Goll DE, Dayton WR, Singh I, Robson RM. Studies of the alpha-actinin/actin interaction in the z-disk by using calpain. *The Journal of biological chemistry*. 1991;266:8501-8510

184. Barta J, Toth A, Edes I, Vaszily M, Papp JG, Varro A, Papp Z. Calpain-1-sensitive myofibrillar proteins of the human myocardium. *Mol Cell Biochem*. 2005;278:1-8

185. Westfall MV, Rust EM, Metzger JM. Slow skeletal troponin i gene transfer, expression, and myofilament incorporation enhances adult cardiac myocyte contractile function. *Proc Natl Acad Sci U S A*. 1997;94:5444-5449

186. Yatani A, Wakamori M, Mikala G, Bahinski A. Block of transient outward-type cloned cardiac k+ channel currents by quinidine. *Circulation research*. 1993;73:351-359

187. Barrows B, Cheung K, Bialobrzeski T, Foster J, Schulze J, Miller A. Extracellular potassium dependency of block of herg by quinidine and cisapride is primarily determined by the permeant ion and not by inactivation. *Channels (Austin)*. 2009;3:239-248

188. Du YM, Zhang XX, Tu DN, Zhao N, Liu YJ, Xiao H, Sanguinetti MC, Zou A, Liao YH. Molecular determinants of kv1.5 channel block by diphenyl phosphine oxide-1. *Journal of molecular and cellular cardiology*. 2010;48:1111-1120

189. Avdeef A, Bendels S, Di L, Faller B, Kansy M, Sugano K, Yamauchi Y. Pampa--critical factors for better predictions of absorption. *J Pharm Sci*. 2007;96:2893-2909

190. Schumacher SM, McEwen DP, Zhang L, Arendt KL, Van Genderen KM, Martens JR. Antiarrhythmic drug-induced internalization of the atrial-specific k+ channel kv1.5. *Circ Res*. 2009

191. Keller GA, Ponte ML, Di Girolamo G. Other drugs acting on nervous system associated with qt-interval prolongation. *Current drug safety*. 2009

192. Sewing S, Roeper J, Pongs O. Kv beta 1 subunit binding specific for shaker-related potassium channel alpha subunits. *Neuron*. 1996;16:455-463

193. Martens JR, Kwak YG, Tamkun MM. Modulation of kv channel alpha/beta subunit interactions. *Trends in cardiovascular medicine*. 1999;9:253-258

194. Coleman SK, Newcombe J, Pryke J, Dolly JO. Subunit composition of kv1 channels in human cns. *J Neurochem*. 1999;73:849-858

195. England SK, Uebele VN, Shear H, Kodali J, Bennett PB, Tamkun MM. Characterization of a voltage-gated k+ channel beta subunit expressed in human heart. *Proceedings of the National Academy of Sciences of the United States of America*. 1995;92:6309-6313

196. Rettig J, Heinemann SH, Wunder F, Lorra C, Parcej DN, Dolly JO, Pongs O. Inactivation properties of voltage-gated k+ channels altered by presence of beta-subunit. *Nature*. 1994;369:289-294

197. Scott VE, Rettig J, Parcej DN, Keen JN, Findlay JB, Pongs O, Dolly JO. Primary structure of a beta subunit of alpha-dendrotoxin-sensitive k+ channels from bovine brain. *Proceedings of the National Academy of Sciences of the United States of America*. 1994;91:1637-1641

198. Morales MJ, Castellino RC, Crews AL, Rasmusson RL, Strauss HC. A novel beta subunit increases rate of inactivation of specific voltage-gated potassium channel alpha subunits. *The Journal of biological chemistry*. 1995;270:6272-6277

199. Majumder K, De Biasi M, Wang Z, Wible BA. Molecular cloning and functional expression of a novel potassium channel beta-subunit from human atrium. *FEBS letters*. 1995;361:13-16

200. Chouinard SW, Wilson GF, Schlimgen AK, Ganetzky B. A potassium channel beta subunit related to the aldo-keto reductase superfamily is encoded by the drosophila hyperkinetic locus. *Proceedings of the National Academy of Sciences of the United States of America*. 1995;92:6763-6767

201. McCormack K, McCormack T, Tanouye M, Rudy B, Stuhmer W. Alternative splicing of the human shaker k+ channel beta 1 gene and functional expression of the beta 2 gene product. *FEBS letters*. 1995;370:32-36

202. Wang Z, Kiehn J, Yang Q, Brown AM, Wible BA. Comparison of binding and block produced by alternatively spliced kvbeta1 subunits. *The Journal of biological chemistry*. 1996;271:28311-28317

203. Heinemann SH, Rettig J, Graack HR, Pongs O. Functional characterization of kv channel beta-subunits from rat brain. *The Journal of physiology*. 1996;493 (Pt 3):625-633

204. Decher N, Kumar P, Gonzalez T, Renigunta V, Sanguinetti MC. Structural basis for competition between drug binding and kvbeta 1.3 accessory subunit-induced n-type inactivation of kv1.5 channels. *Molecular pharmacology*. 2005;68:995-1005

205. Arias C, Guizy M, David M, Marzian S, Gonzalez T, Decher N, Valenzuela C. Kvbeta1.3 reduces the degree of stereoselective bupivacaine block of kv1.5 channels. *Anesthesiology*. 2007;107:641-651

206. Po S, Roberds S, Snyders DJ, Tamkun MM, Bennett PB. Heteromultimeric assembly of human potassium channels. Molecular basis of a transient outward current? *Circulation research*. 1993;72:1326-1336

207. Jenkins PM, McIntyre JC, Zhang L, Anantharam A, Vesely ED, Arendt KL, Carruthers CJ, Kerppola TK, Iniguez-Lluhi JA, Holz RW, Sutton MA, Martens JR. Subunit-dependent axonal trafficking of distinct {alpha} heteromeric potassium channel complexes. *J Neurosci*. 2011;31:13224-13235

208. Xu C, Lu Y, Tang G, Wang R. Expression of voltage-dependent k(+) channel genes in mesenteric artery smooth muscle cells. *The American journal of physiology*. 1999;277:G1055-1063

209. Yuan XJ, Wang J, Juhaszova M, Golovina VA, Rubin LJ. Molecular basis and function of voltage-gated k+ channels in pulmonary arterial smooth muscle cells. *The American journal of physiology*. 1998;274:L621-635

210. Plane F, Johnson R, Kerr P, Wiehler W, Thorneloe K, Ishii K, Chen T, Cole W. Heteromultimeric kv1 channels contribute to myogenic control of arterial diameter. *Circulation research*. 2005;96:216-224

211. Wang J, Juhaszova M, Rubin LJ, Yuan XJ. Hypoxia inhibits gene expression of voltage-gated k+ channel alpha subunits in pulmonary artery smooth muscle cells. *J Clin Invest*. 1997;100:2347-2353

212. Zadeh AD, Xu H, Loewen ME, Noble GP, Steele DF, Fedida D. Internalized kv1.5 traffics via rab-dependent pathways. *The Journal of physiology*. 2008;586:4793-4813

213. Kim SJ, Choi WS, Han JS, Warnock G, Fedida D, McIntosh CH. A novel mechanism for the suppression of a voltage-gated potassium channel by glucose-

dependent insulinotropic polypeptide: Protein kinase a-dependent endocytosis. *The Journal of biological chemistry*. 2005;280:28692-28700